



DIPLOMARBEIT

Simulation of Supercritical Carbon Dioxide Cycles for Electrothermal Energy Storage

Ausgeführt am Institut für

Energietechnik und Thermodynamik
der Technischen Universität Wien

unter der Anleitung von Prof. Dr. Andreas Werner

durch

Stylios Flegkas
0727275

Nattergasse 23/4
1170 Wien

Datum

Unterschrift

Abstract

An up to date synopsis of the existing electrothermal energy storage systems is presented in this thesis. Further a brief overview of thermodynamic power cycles and the advantages of carbon dioxide as a working fluid are described. Also the used thermal energy storage system is presented. A plethora of electrothermal energy storage systems are calculated in the process simulation software *IPSEpro*. First simulations feature simple Brayton and re-compression cycles, while also the utilization of waste heat and the usage of an isothermal expander are proposed. Furthermore the integration of a carbon dioxide transcritical organic Rankine cycle to improve the efficiency of the system is examined. Main findings include that the best round trip efficiency is provided by systems with an isothermal expander which are site-independent, while the usage of waste heat provides high efficiency values but also makes the plant site-dependent.

Contents

Abstract	i
1 Introduction	1
1.1 Energy Storage	1
1.2 Goals of the Thesis	4
2 Electrothermal Energy Storage	5
2.1 Working Principle	5
2.1.1 Roundtrip Efficiency Calculation	6
2.2 Introducing Studies	8
2.3 Recent Studies	10
2.3.1 Working Fluid Argon	10
2.3.2 Working Fluid Carbon Dioxide	15
2.3.3 Working Fluid Water - CHEST	25
3 Theoretical Background	27
3.1 Thermodynamic Cycles for Electricity Production	27
3.1.1 Steam Rankine Cycle	27
3.1.2 Organic Rankine Cycle	30
3.1.3 Comparison of the Organic Rankine Cycle with the Steam Rankine Cycle	31
3.1.4 Gas Power Cycle	33
3.2 Thermodynamic Cycles with CO_2 as Working Fluid	36
3.2.1 Properties of CO_2	37
3.3 SandTES	39
4 Simulation	42
4.1 Software	42
4.1.1 IPSEpro	42
4.1.2 EES	44
4.1.3 REFPROP	44
4.1.4 CAPE-OPEN	44
4.2 <i>ETES</i> Utilizing Supercritical CO_2 Cycles	45
4.2.1 Simple Heat Pump and Brayton Cycle Configuration	46
4.2.2 Implementation of a Second Turbine in the Charge Cycle	51
4.2.3 Supercritical <i>ETES</i> with an Isothermal Expansion	54
4.3 Combined Heat and Energy Storage	58
4.3.1 Utilizing Waste Heat in Addition to the Two SandTES Units	59
4.3.2 Replacement of the <i>LT-SandTES</i> Unit with Waste Heat	59
4.3.3 Comparison with an Independent <i>ETES</i> System	59

4.4 Improvements through the Addition of a Transcritical CO_2 Cycle 60

4.5 Summary and Outlook 61

List of Figures 63

List of Tables 66

Chapter 1

Introduction

1.1 Energy Storage

Latest predictions, summarized in Fig. (1.1) state that carbon dioxide (CO_2) emissions related to the combustion of fossil fuels will increase from 31.2 billion metric tons (*bmt*) in 2010 to 36.4 *bmt* in 2020 and 45.5 *bmt* in 2040 [1]. Although most of the growth in emissions is attributed to the developing non-OECD nations that continue to rely heavily on fossil fuels, six European Union Member States, amongst them Austria, will not be able to decrease their emissions below the respective 2020 target set by the Effort Sharing Decision of the European Parliament [2]. This situation amplifies the necessity of the development and expansion of clean energy sources.

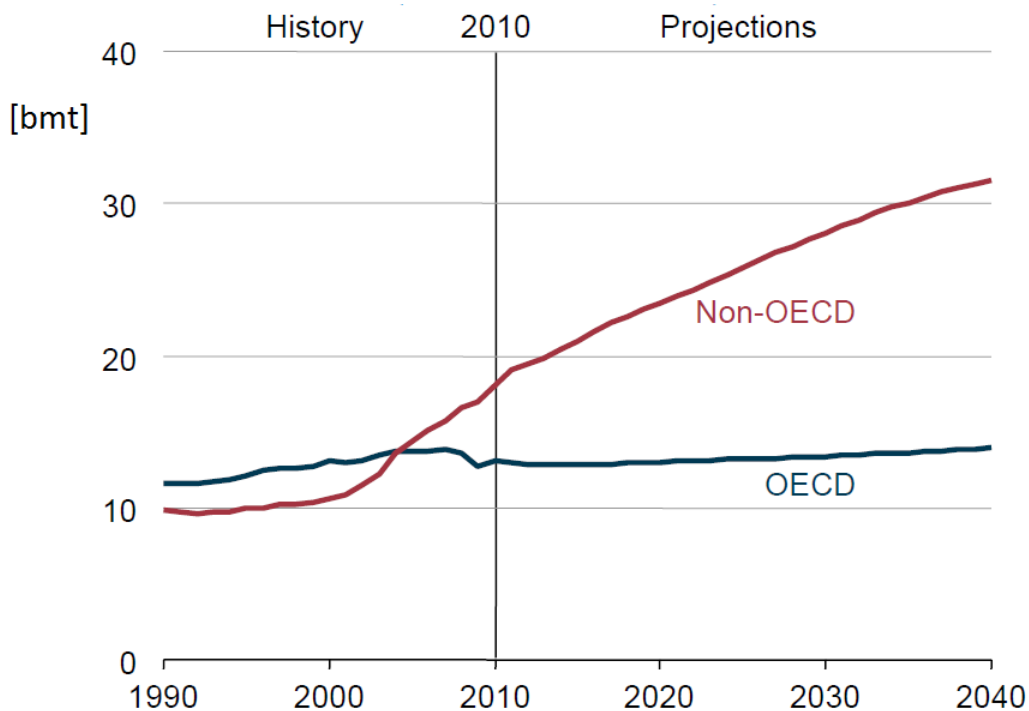


Figure 1.1: World energy-related carbon dioxide emissions, 1990-2040 (billion metric tons) [1].

Due to the volatile nature of renewable energy types and specially of aeolic and solar sources, the interest in storage methods in order to match the intermittent output with costumer demand has increased rapidly. Numerous energy storage technologies exist, which differ in terms of power quality and discharge time. Fig. (1.2) gives an overview of the various energy storage

types currently at use.

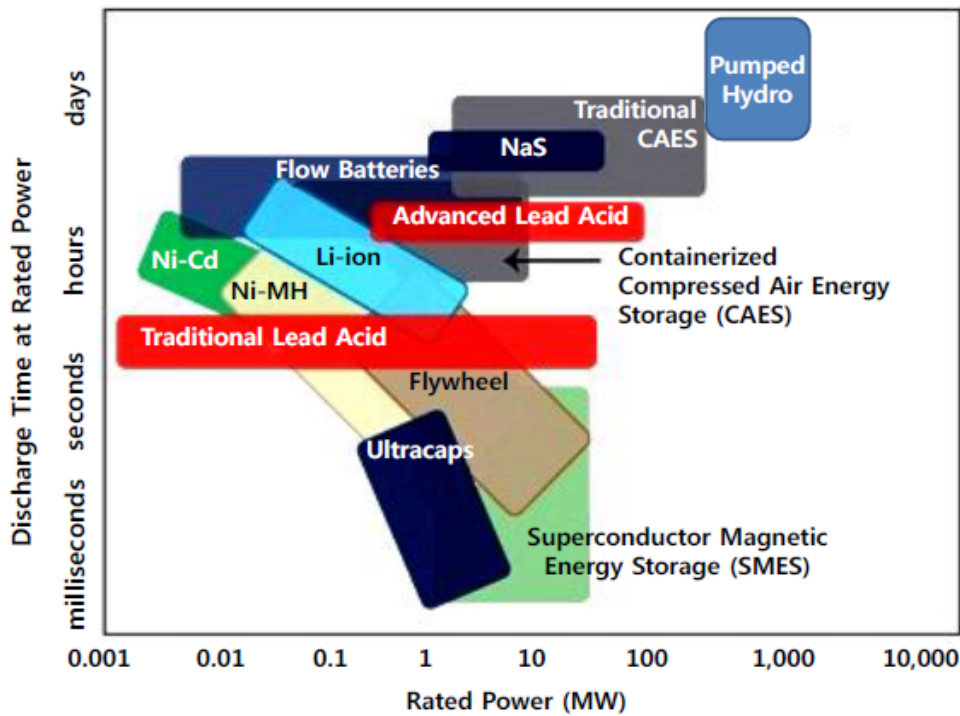


Figure 1.2: Comparison of various energy storage technologies in terms of power capacity and discharge time [3].

Technologies that meet the need to assure the continuity and quality of power and regulation of its frequency for only seconds or less include flywheels, superconducting magnetic energy storage (*SMES*), lead acid batteries, lithium ion batteries, flow batteries, and ultracapacitors. Technologies to be considered for load leveling for large-scale energy systems, typically in the range of hours to days of discharge time are, sodium sulfur (*NaS*) batteries, advanced absorbent glass mat lead acid batteries, and flow batteries. High efficiencies can be achieved by batteries, however their lifetime and number of charge cycles is limited [3].

In contrast, mechanical storage systems like Pumped Hydroelectric Storage (*PHS*) and Compressed Air Energy Storage (*CAES*), have significant advantages concerning both factors and are based on mature technologies. *PHS* consists in elevating water to an upper reservoir, allows the storage of several *GWh*. *CAES* systems use a cavern to store pressurized air and offer a capacity in the region of hundreds of *MWh*.

In addition to these energy storage types, thermal energy storage (*TES*) has obtained growing importance and interest. The technology can be distinguished into three main types:

- sensible,
- latent,
- thermochemical storage.

In sensible storage, a temperature change in the storage material allows the storage of heat whilst in latent storage, the heat storage results from a phase change in the storage material. In thermochemical storage, the heat of charging and discharging is converted into

reaction enthalpies of reversible chemical reactions. Especially at higher temperature levels thermal energy storage can be used to improve the flexibility and to decrease the net electricity production of fossil-fuel power plants which have to operate in a highly volatile electricity market. Thermodynamic processes for electric energy storage that are based on the storage of high temperature heat are, Adiabatic Compressed Energy Storage (*ACAES*), cold Liquefied Air Energy Storage (*LAES*) or Electrothermal Energy Storage (*ETES*) [4].

ETES is a novel type of bulk electricity storage which is especially suited for the integration of renewable intermittent energy sources such as wind into the electricity grid in a sustainable way. The concept is based on heat pump and heat engine technologies utilizing transcritical or supercritical CO_2 cycles [5]. The main advantages of *ETES* systems are their high energy density and independence from geological formations, which is the biggest drawback of *CAES* and *PHS* systems.

Another possible application of the still developing *ETES* technology is the reduction of the potential energy loss during the curtailment of wind turbines. Curtailment means reducing generation at a facility below what it could be capable of producing. The most common reasons for curtailment are insufficient transmissions, local congestion and excessive supply during low load periods.

Approximately *\$1.6 billion* or *20 million MWh* of electricity were lost in the Chinese power sector in 2012 according to the secretary general of the Chinese Wind Energy Association due to curtailment. The curtailment of 2012 almost doubled since 2011. A major contributing element was that China's power generation capacity rose considerably in 2012, and wind gave way to thermal and nuclear power. The government curtailment forced 10 – 20 % of the wind turbines to a standstill on average across the country [6]. Loses of the same order have been reported in the US as well. Roughly *292,000 MWh* of wind power were curtailed by the Midcontinent Independent System Operator of the USA in 2009, in 2010 that figure increased to about *824,000 MWh*. Considering that the average price of *1kWh* in the US during that period was about *\$0.07* the cost for one system's generation capacity losses in 2010 was *\$57 million* and *\$20 million* respectively in 2009 [7, 8]. Even in the energy generation market those are big numbers and the rate at which they are increasing is intimidating for the wind industry. *ETES* offers the potential to better utilize the curtailed potential.

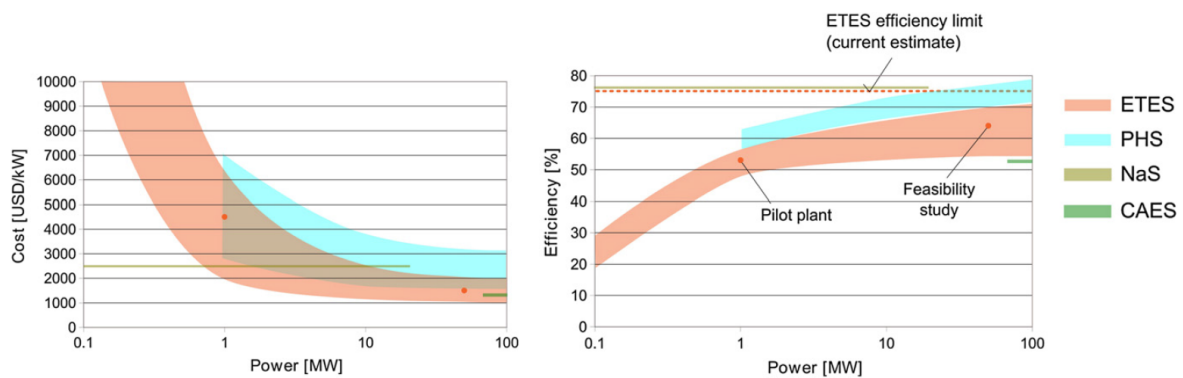


Figure 1.3: Efficiency and cost bands of the proposed *ETES* system as a function of power rating [5].

Figure (1.3) shows a general cost vs. efficiency evaluation of all bulk electricity storage types, without taking into account location dependencies. The modest roundtrip efficiency estimates of *ETES*, when combined with attractive capital cost estimates, indicate that *ETES* can become the bulk electricity storage technology of choice. This is without considering the

cost of storage in terms of \$/kWh, where *ETES* has an even more attractive standing and also without considering its environmentally benign and site independent nature. These facts lead to the conclusion that *ETES* systems in general hold a potential to become a future bulk electricity storage technology [5].

1.2 Goals of the Thesis

The purpose of this work is first of all to give a comprehensive and widespread overview of all energy storage types that rely on the use of alternating heat pump/heat engine systems coupled with thermal energy storage.

Then the theoretical background of thermodynamic power cycles is provided. Carbon dioxide is presented as a working fluid for gas power cycles. Its properties analyzed and its advantage over other working fluids, like water, helium or organic are presented.

Finally a plethora of electrothermal energy storage systems utilizing carbon dioxide as the working fluid are suggested.

Chapter 2

Electrothermal Energy Storage

2.1 Working Principle

The main components of an *ETES* system are a compressor, an expander and two thermal storage units, one hot and one cold. The compressor and the expander may be either turbomachinery-based or reciprocating devices. They are mechanically coupled and linked to a motor or a generator.

The working principle of an *ETES* system is that during periods of excess electricity generation an electric driven motor is used to drive the compressor of the working fluid. The heat from the compressed working fluid is transferred to the hot storage system. Then, the fluid is expanded and the produced power might be used to reduce compression power. Finally the cold expanded fluid is used to remove heat from the cold storage system. The process is illustrated in Fig. (2.1). The system operates as a high temperature ratio heat pump, using electrical energy to extract heat from the cold storage and heat the hot storage.

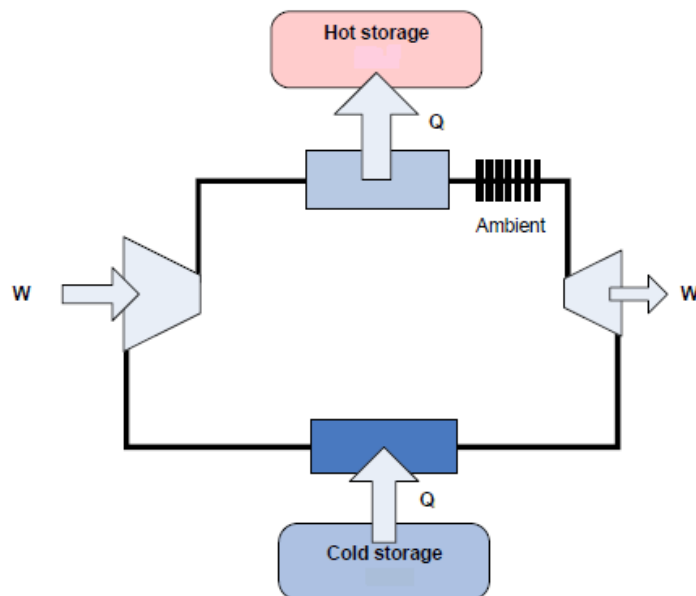


Figure 2.1: Working principle of a electrothermal energy storage system during charging mode [3].

While in discharging mode, shown in Fig. (2.2), the process is the reverse of the previously explained charging mode. The cold working fluid cooled by the cold storage system is

compressed. Then, it is heated by the hot storage system and is expanded in a suited turbine producing power. The device operates as a heat engine, the heat is returned from the hot to the cold store and electrical energy is retrieved.

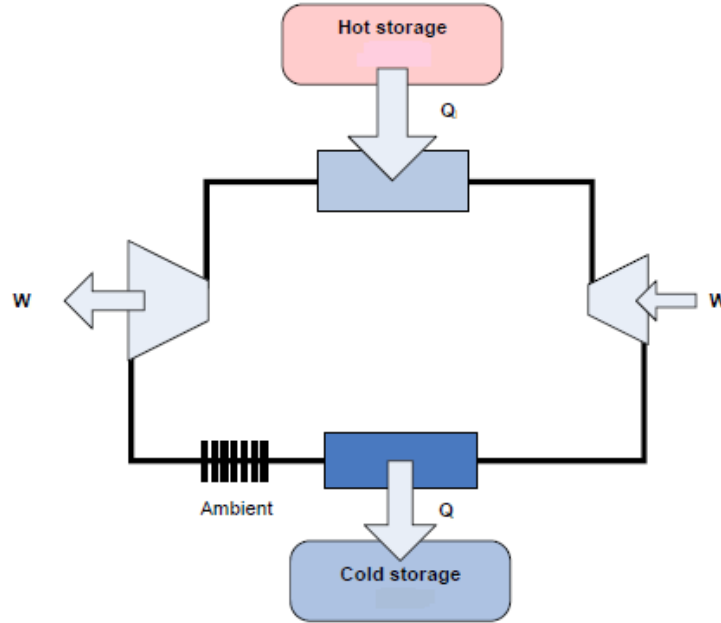


Figure 2.2: Working principle of a electrothermal energy storage system during discharging mode [3].

Conceptually any thermodynamic cycle that can be made to run backwards can be used for *ETES* design. The currently proposed cycles are: a transcritical Rankine cycle where the working fluid undergoes a phase change or a transcritical or supercritical Brayton cycle, where no phase change occurs. Nevertheless the following points ought to be taken into account when choosing the proper cycle. *ETES* should use a cycle that can run as reversibly as possible in the heat pump and heat engine mode and that closely matches the heat sources and sinks with which it interacts, also environmental benign materials should be used.

The major drawback of this concept is the limited roundtrip efficiency (η_{RT}), which relates the generated electricity ($W_{discharge}$) delivered during the discharge mode, to the electricity needed to charge the system (W_{charge}):

$$\eta_{RT} = \frac{W_{discharge}}{W_{charge}} \quad (2.1)$$

Even the ideal process is limited by the Carnot efficiency η_{Carnot} depending on the temperatures of the cold T_{cold} and hot T_{hot} reservoirs:

$$\eta_{Carnot} = 1 - \frac{T_{cold}}{T_{hot}} \quad (2.2)$$

2.1.1 Roundtrip Efficiency Calculation

The roundtrip efficiency of an *ETES* system can be defined as the ratio of electric output power during the discharging mode to electric input power during charging mode. In the charging mode, the actual compressor and expander work for the working fluid are determined using an isentropic efficiency defined as:

$$\eta_{C1} = \frac{W_{C1}^s}{W_{C1}} \quad (2.3)$$

$$\eta_{E1} = \frac{W_{E1}}{W_{E1}^s} \quad (2.4)$$

Where (s) denotes an isentropic change of state. The back work ratio (r_{bw1}) for the charging mode is defined as the ratio of ideal expansion work to ideal compression work as:

$$r_{bw1} = \frac{W_{E1}^s}{W_{C1}^s} \quad (2.5)$$

In a similar manner, for the discharging mode, the actual compressor and expander powers for the working fluid are determined using an isentropic efficiency defined as:

$$\eta_{C2} = \frac{W_{C2}^s}{W_{C2}} \quad (2.6)$$

$$\eta_{E2} = \frac{W_{E2}}{W_{E2}^s} \quad (2.7)$$

The back work ratio for the discharging mode (r_{bw2}) is defined as the ratio of isentropic compression work to isentropic expansion work as:

$$r_{bw2} = \frac{W_{C2}^s}{W_{E2}^s} \quad (2.8)$$

The roundtrip efficiency of the TEES system can be obtained as:

$$\eta_{RT} = \frac{W_{net2}}{W_{net1}} = \frac{W_{E2} - W_{C2}}{W_{C1} - W_{E1}} = \frac{\eta_{E2}W_{E2}^s - (r_{bw2}W_{E2}^s)/\eta_{C2}}{W_{C1}^s/\eta_{C1} - \eta_{E1}(r_{bw1}W_{C1}^s)} = \frac{\eta_{C1}}{\eta_{C2}} \frac{\eta_{C2}\eta_{E2} - r_{bw2}}{1 - \eta_{C1}\eta_{E1}r_{bw1}} \frac{W_{E2}^s}{W_{C1}^s} \quad (2.9)$$

where the subscript *net* denotes net power [9].

The roundtrip efficiency of an *ETES* system can be degraded due to the exergy losses of the system. Because a minimum temperature difference is required for heat transfer to/from the thermal storage, the temperature difference between the high and low operating temperatures of the heat engine is less than that of the heat pump. This means that the thermodynamic cycle of the *ETES* is not perfectly reversible.

It can be shown that regardless of the hot storage temperature and the heat sink temperature, the roundtrip efficiency is equal to 1 if the heat transfer takes place over an infinitely small difference. A closer fit of the two thermodynamic cycles of the charging and discharging modes, a better matching of the selected cycle to the heat sources and heat sinks with the cycle interacts, is necessary to get a higher roundtrip efficiency [5].

In the *ETES* system with the good thermal-matching, since the exergy losses occurring in the turbomachinery have a greater impact on the roundtrip efficiency compared to the exergy losses in the heat exchangers, another maximum roundtrip efficiency by assuming an infinitely small temperature difference for heat transfer is useful to be described. If the exergy losses in the heat exchangers are neglected in equation (2.9), W_{E2}^s is equal to W_{C1}^s , and r_{bw2} is equal to r_{bw1} . Then, the maximum roundtrip efficiency, neglecting the exergy losses in the heat exchangers, can be obtained as:

$$\eta_{RT,max} = \frac{\eta_{C1}}{\eta_{C2}} \frac{\eta_{C2}\eta_{E2} - r_{bw}}{1 - \eta_{C1}\eta_{E1}r_{bw}} \quad (2.10)$$

For simplicity, if it is assumed that η_{C1} , η_{E1} , η_{C2} , and η_{E2} are equal to η and r_{bw1} , r_{bw2} equal to r_{bw} then equation (2.10) can be revised as:

$$\eta_{RTmax} = \frac{\eta^2 - r_{bw}}{1 - \eta^2 r_{bw}} \quad (2.11)$$

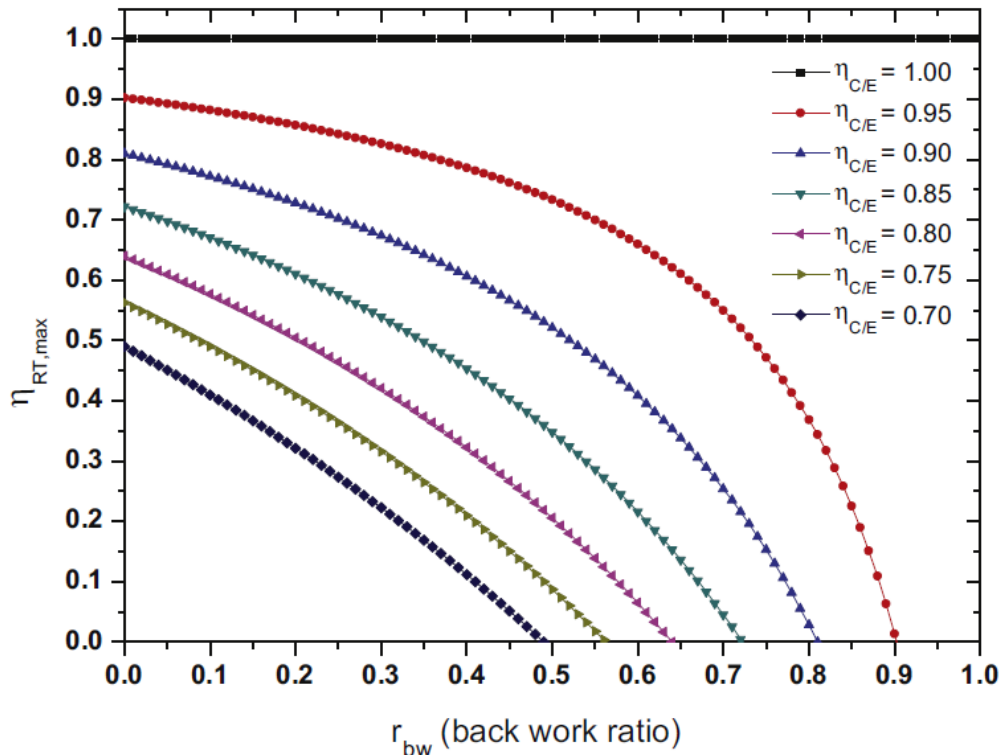


Figure 2.3: Maximum roundtrip efficiency of a *ETES* system as a function of r_{bw} and $\eta_{C/E}$ [9].

Fig. (2.3) shows the maximum roundtrip efficiency as a function of the r_{bw} and the efficiency of the compressor/expander $\eta_{C/E}$. For a given $\eta_{C/E}$, the maximum roundtrip efficiency decreases rapidly with an increase in the r_{bw} . This means that it is very important to minimize the r_{bw} of the reference thermodynamic cycle to optimize the *ETES* system [9].

2.2 Introducing Studies

The concept of using mechanical heat transformation in combination with thermal storage was first introduced by Marguerre in 1922 [10]. In the proposed system, electricity drives an axial steam compressor and the energy is stored in a pressurized water tank. A theoretical analysis of a *ETES* system using a Brayton cycle is presented by Weissenbach in [11].

The first publication about the exclusive storage of electrical energy in the form of heat for back conversion to electricity is presented by Cahn in a patent application from 1978 [12]. Cahn describes a method for storing the off-peak electrical output of an electricity generating plant in the form of heat, by using it to raise the temperature level of a quantity of stored heat retention material.

Particularly hot water is drawn from a hot water storage and is cooled by flashing it at successively lower pressures. The cold condensate is sent to a cold water storage while the

various flash vapors are fed to appropriate stages of a steam compressor driven by excess power. The compressed steam is directed to the heat exchangers where it is used to heat a Low Vapor Pressure (*LVP*) thermal energy retention material flowing from cold to hot storage through the heat exchangers. The prescribed temperature levels of the *LVP* material for this invention are approximately 90 – 150 °C for the cold storage temperature and approximately 230 – 315 °C for the hot storage temperature tanks. The hot *LVP* material is stored at atmospheric pressure preferably under an inert gas atmosphere.

During periods of peak power demand the heat is recalled in the form of electrical power. The whole process is reversed and the hot *LVP* material is used to generate steam which runs a turbine thereby producing electrical power from a generator. The processes of charging as well as discharging are illustrated in Fig. (2.4).

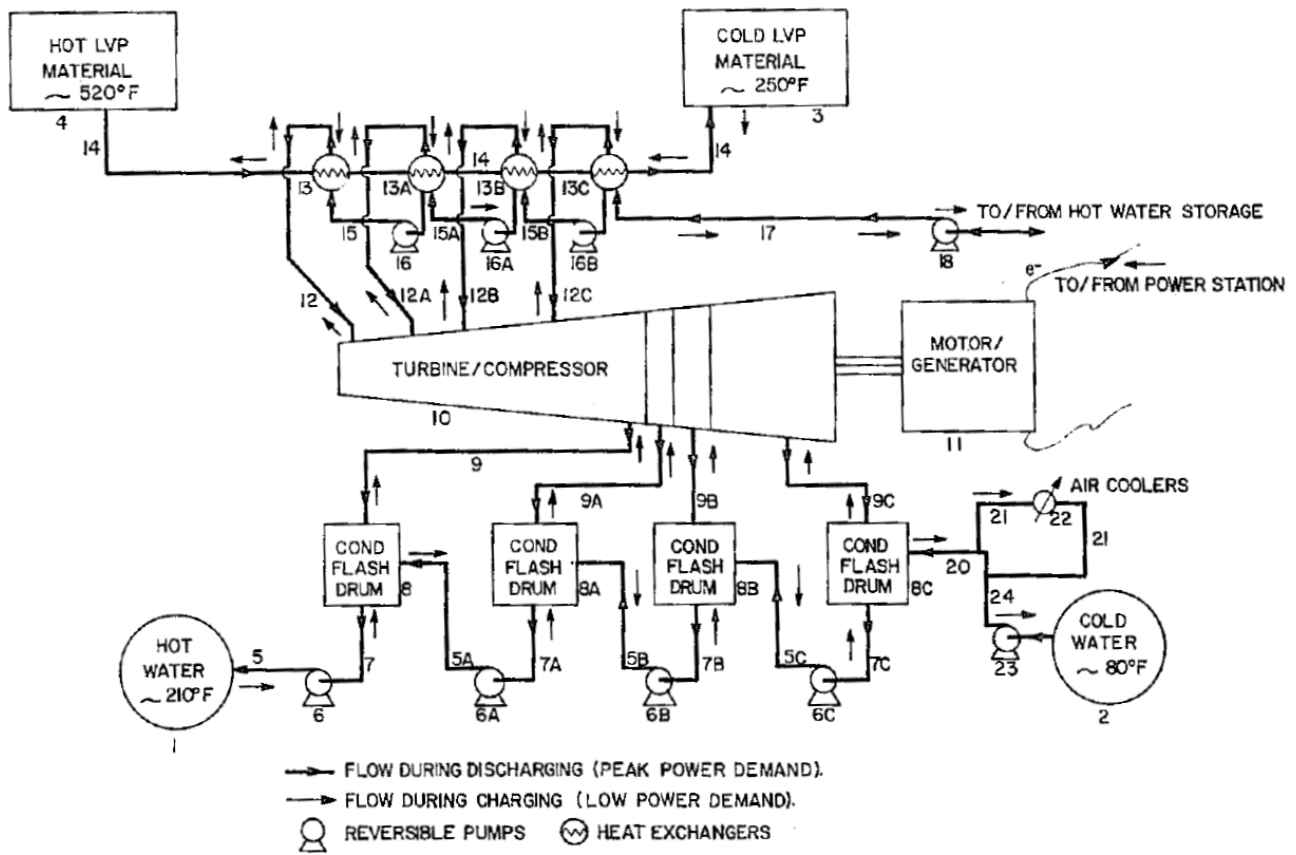


Figure 2.4: Flow diagram during charging and discharging of Cahns proposed system [12].

In a patent issued in 2007 [13], Wolf proposed a procedure where electrical energy originating from solar, wind or industrial sources, that due to the momentarily lack in demand couldn't be utilized, is stored and transformed back into technical work or electricity. The goal is to store the local arising energy and return it to the network in times of high demand.

During the loading cycle, the system works like a heat pump, while during discharge the cycle reverses in order to generate electricity. The chosen working fluid is CO_2 while pressurized water is used as storage material. Further on two examples are presented.

The first example featuring the power supply of a single-family house is shown in Fig. (2.5). The excess energy of the solar collector and wind turbine is stored in a battery which intends to compensate the momentarily differences between production and demand. The spare energy that wasn't stored in the battery is fed via a motor, which drives a compressor, to the

thermodynamic cycle. The working fluid is compressed from 39,8 to 120 *bar* and 155°C. Also geothermal energy is used to evaporate the CO_2 isothermally before it is heated in an recuperator from 10°C to 50°C. The pressurized water in the tank is heated up to 155°C and the working fluid cooled to 55°C. The second example describes another application of the invention in combination with an 2 MW_{el} wind power plant.

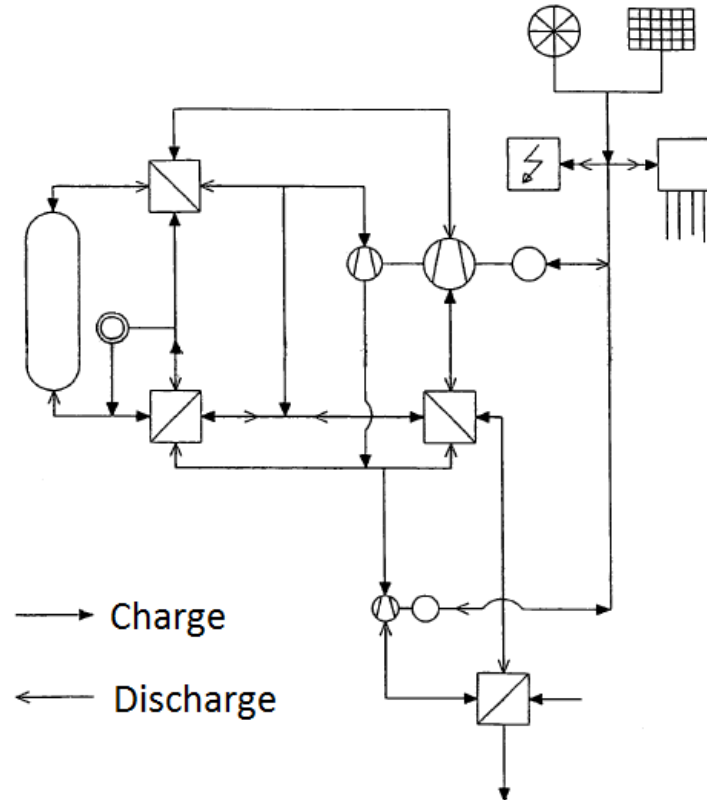


Figure 2.5: Flow diagram during charging and discharging of Wolfs proposed system [12].

2.3 Recent Studies

This section is divided into three subsections according to the working fluid that is used in each process.

2.3.1 Working Fluid Argon

Two companies, SAIPEM-SA [14] and Isentropic Ltd. [15] working independently from each other, developed a very similar approach to *ETES* called Pumped Thermal Electricity Storage (*PTES*) or Pumped Heat Electricity Storage (*PHES*).

Argon (*Ar*) was chosen as the heat-transfer fluid for this application. The properties of *Ar* depend heavily on temperature. For instance, the thermal conductivity, as well as the dynamic viscosity of *Ar* vary by a factor of 3 between ambient temperature and 1000°C, as shown in Fig. (2.6).

In general, the roundtrip efficiency and storage density increase with the compressor pressure ratio. That high ratio leads to high costs for the hot reservoir that is used as thermal energy

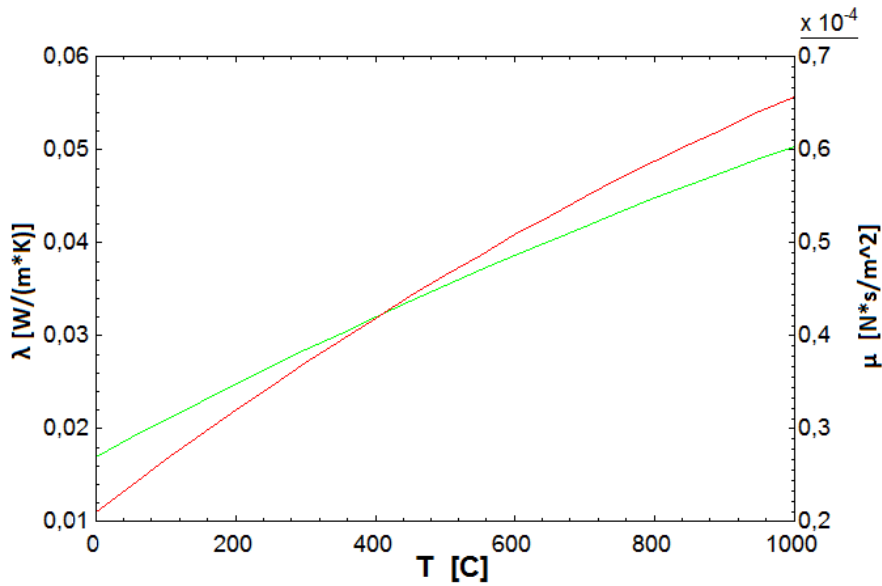


Figure 2.6: Thermal conductivity (green) and dynamic viscosity (red) of Argon over temperature (Source: Engineering Equation Software, F-Chart Software).

storage unit. The compression ratio to reach a given temperature with *Ar* as the working fluid is low because of its monoatomic nature, therefore all needed vessels are less expensive. *Ar* also has a better effect on equipment in comparison to other considered gases like Nitrogen. It also has a higher density, hence the peripheral velocity of the rotors is lower and the stresses are about 30 % lower as well. Finally the equipment is easier to fabricate and lasts longer while the oxidation of the metallic components is avoided because of *Ar* being an inert gas [14].

SAIPEM

Desrues et al. [16, 17] presented a concept based on a high temperature heat pump cycle which transforms electrical energy into thermal energy and stores it inside two large regenerators, followed by a thermal engine cycle transforming the stored thermal energy back into electricity.

The system consists of a high pressure tank and a low pressure tank, four turbomachines, one compressor-turbine pair used during the charging period, and another one during discharge and two heat exchangers. The tanks are regenerators, made of refractory material which will alternatively store or deliver heat. One tank is operating at high pressure (*HP*) and the other at low pressure (*LP*). The turbomachines allow the circulation of a gas (Argon) in the tanks, following a closed thermodynamic Brayton cycle. Both processes are depicted in Fig. (2.7).

During the charging cycle, the *HP* tank refractory material initially at T_0 is slowly heated by the hot gas entering at T_1 , while the *LP* tank material initially at T_2 is slowly cooled by the cold gas entering at T_3 . This generates two transient thermal fronts, progressing upward in the *LP* tank and downward in the *HP* tank. When the thermal fronts approaches the ends of the tanks, the *HP* tank temperature T_0 will suddenly increase while the *LP* tank temperature T_2 decreases. The loading is stopped when the temperature differences between one tank's outlet and its prescribed nominal temperature exceeds a given relative threshold.

Following the same principal during the discharge period, the *LP* tank refractory material at T_3 is slowly heated by the expanded gas at T_2 , while the *HP* tank material at T_1 is slowly cooled by gas at ambient temperature T_0 . Anew two transient thermal fronts are generated. The charging period is again stopped when the relative temperature differences between one

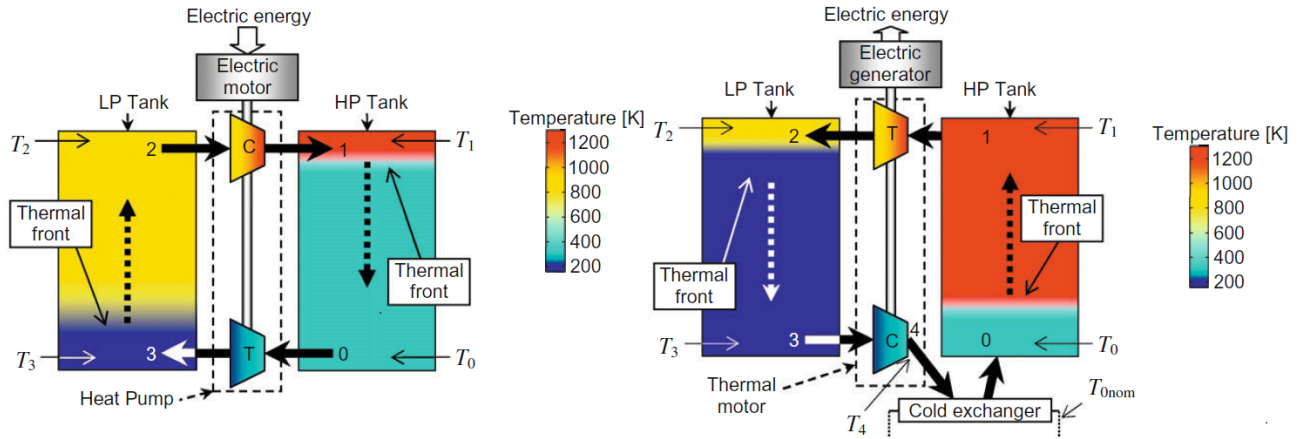


Figure 2.7: Overview of the storage principle proposed by Desrues et al. during charging mode (left) and discharging mode (right) [16].

tank outlet and its prescribed nominal temperature exceeds the given threshold.

In order to keep the inlet turbomachine temperatures at their nominal values, two heat exchangers, both located just before the tank entry, are necessary. They avoid the rise of the temperatures after each cycle keeping T_2 and T_0 constant, and evacuate the additional heat produced from the turbomachine's irreversibility. However, given that cooling a gas at high temperatures is not convenient, it is preferable to keep T_2 constant, and perform all necessary cooling at the ambient temperature T_0 .

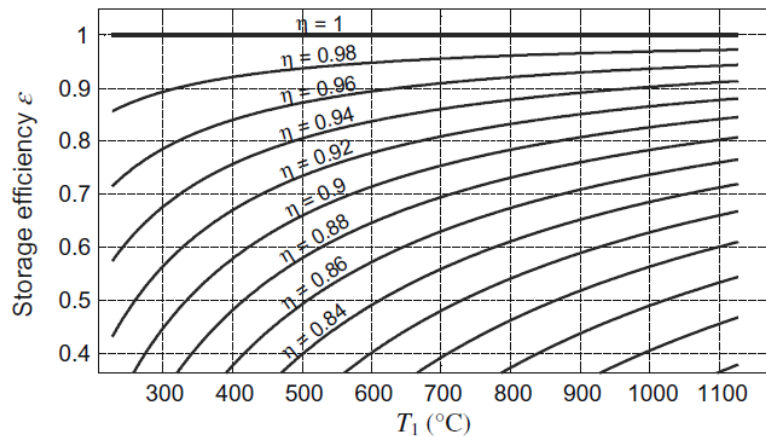


Figure 2.8: Storage efficiency as a function of T_1 , the polytropic efficiency η at ambient temperature and at a thermal compression ratio of 1.55 [16].

Neglecting head losses in the flow, and assuming the system is adiabatic Desrues et al. deduced in [16] the global storage efficiency of the proposed energy storage system. Under the assumption that the same mass of gas passes through the turbomachines during both the charging and the discharging cycles, Fig. (2.8) depicting the storage efficiency as a function of T_1 , occurred. In order to conclude to a reasonable global storage efficiency of 70 %, which is reached by a *PHS* system two approaches can be considered. First, T_1 may be low with a high polytropic efficiency η (for example, $\eta \approx 0.94$ and $T_1 \approx 320^\circ\text{C}$), or T_1 may be high, with a low η (for example $\eta \approx 0.84$ and $T_1 \approx 1050^\circ\text{C}$).

Isentropic Ltd.

According to Howes, the origins of *PHEES* lie within an aviation problem namely, the extension of the interthermal glide of a glider of modest performance by storage of energy during a thermal climb [18]. Outgoing from this aeronautical problem Isentropic Ltd. [15] developed a concept of *PHEES* similar to the previous approach of SAIPEM.

The developed system consists of a highly reversible reciprocating gas cycle machine, instead of a turbine-compressor pair, that works as both an engine and a heat pump and stores electrical energy as heat and cold in stores filled with crushed rocks or gravel. A simplified schematic of such an energy storage system is illustrated in Fig. (2.9).

In a charging cycle the system takes electricity from the grid and uses it to drive the pistons of the heat pump. The cycle starts with the compression of the gas (Argon) from the top of the cold store which is at ambient temperature and 1 *bar* in the cylinders to 12 *bar*. Due to the compression the gas is heated up to 500 °C. The hot gas then enters the top of the hot store where it permeates the storage medium, heating it. At the beginning of the process the upper zone of the hot store is at 500 °C while the lower zone is at ambient temperature. The hot thermal front in between moves downward as more of the storage material is heated. At the bottom of the hot store, where the gas is still at 12 *bar* but at ambient temperature it exits the store and flows into the expanders which expand it back to 1 *bar*. The expansion cools the gas to -160 °C where it is much denser. Then it flows into the cold store where it again permeates the storage medium, this time warming the gas and cooling the medium. The bottom zone of the cold tank is at -160 °C while the zone at the top is at ambient temperature. In between a cold thermal front which moves upward as more of the storage material is cooled exists. The gas moves to the top of the cold store, at its original position and the process is repeated [15].

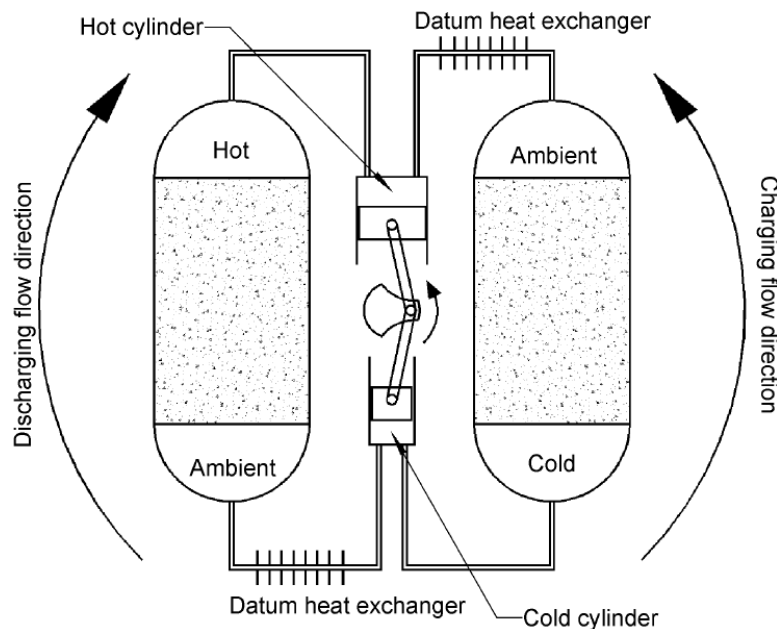


Figure 2.9: Simplified schematic of the *PHEES* system developed by Isentropic Ltd. [18].

The system can be reversed at any time during the charging cycle, releasing the stored energy. During the discharge cycle the engine continues to turn in the same direction but the valve timings change so that the gas begins to flow in the opposite direction. This process takes only about one second. When the gas circulates in reverse the system accesses a heat engine to drive the generators and convert the energy back to the grid as electricity. As the energy is

released the thermal fronts in the tanks move in the opposite directions as during the charging process.

The overall roundtrip efficiency of *PHES* is estimated in the order of 72%. Which is comparable to existing *PHS* values. The technology is designed for power ranges from 2-5 MW per unit with up to 8 hours of stored energy. These facts make it an exceptional compliment to wind and solar applications.

Thermodynamic analysis of *PTES* systems

White et al. discuss in [19] the thermodynamic aspects of *PTES*, including energy and power density, the various sources of irreversibility, and their impact on roundtrip efficiency. It is shown that the roundtrip efficiency and storage density increase with the compressor pressure ratio. Although, for given compression and expansion efficiencies, the ratio between the highest and lowest temperatures in each of the reservoirs and not the compression pressure ratio determines the performance. Especially for a turbomachinery-based *PTES* system, the effects of compression and expansion irreversibility can be mitigated by reducing the ratio between hot and cold store discharge temperatures, which also has the advantage of increasing the energy and power densities.

McTigue et al. present in [20] the thermodynamic features of *PTES* based on steady flow analysis of the compression and expansion devices coupled with a Schumann-style model of the hot and cold thermal stores. The sources of exergetic loss have been considered in detail in order to obtain the maximum roundtrip efficiency. A parametric analysis reveals that optimum values for some design variables of *PTES* exist, that either lead to a trade-off between efficiency and energy density or improve both qualities simultaneously. Furthermore, multi-objective optimisation was applied to generate trade-off surfaces. These result that curves of roundtrip efficiency vs. energy density are relatively flat over a considerable range, so that high energy density can be attained with only a modest efficiency penalty. It was also shown that, since the losses associated with pressure drop and irreversible heat transfer in the stores are only a few percent, the success of *PTES* systems depends on the compressor and expander performance. With reasonable estimates for mechanical and electrical losses, an overall roundtrip efficiency of just under 70% is expected, while with an optimistic set of parameters the roundtrip efficiency could exceed 85% with reciprocating devices.

Thess in [21] attempts to formulate a simple thermodynamic model that predicts the efficiency of *PHES* as a function of the temperature of the thermal energy storage at maximum output power. Predictions state that for storage temperatures above 400 °C *PHES* has a higher efficiency than existing *CAES* and that it can even compete with the efficiencies predicted for advanced-adiabatic *CAES*.

Also a thermodynamically identical variant to *PHES* referred to as Pumped Cryogenic Electricity Storage (*PCES*) is presented. In *PCES* the electrical energy is used to drive a refrigeration cycle which extracts thermal energy from a cryogenic energy source. When electricity is required, a thermal power cycle operating between cold storage and the environment converts the cold back to electricity. An overview of the roundtrip efficiency of *PHES* and *PCES* is presented on Fig. (2.10).

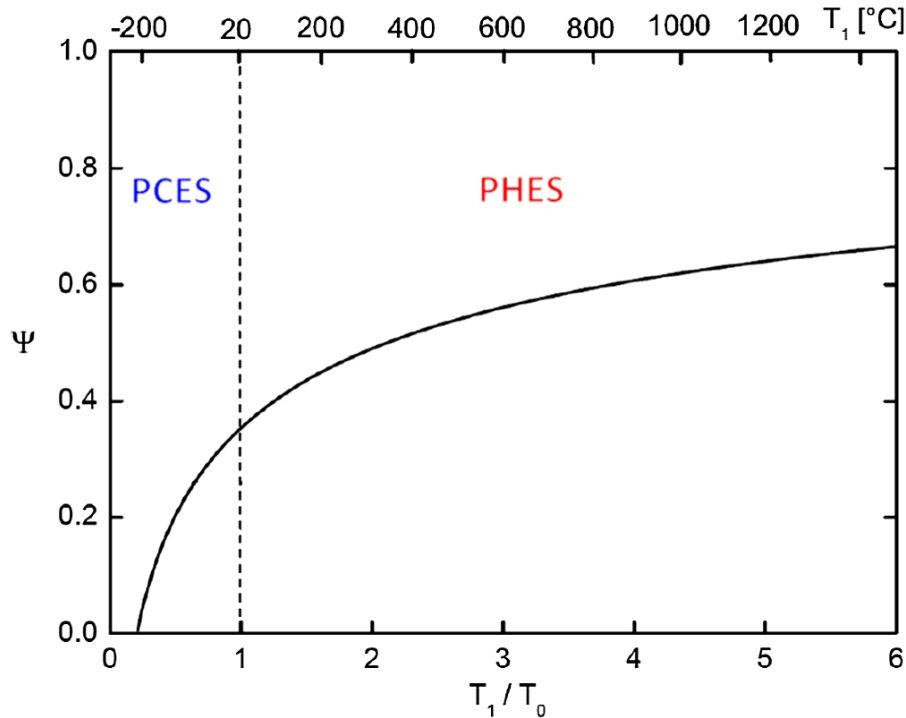


Figure 2.10: Thermodynamic efficiency of *PHES* and *PCES*. Roundtrip efficiency as a function of the storage temperature. The lower abscissa represents the nondimensional temperature ratio, the upper abscissa represents dimensional temperature for the case of an ambient temperature of $T_0 = 20^\circ\text{C}$. T_1 is the temperature of the hot storage and Ψ the roundtrip efficiency calculated according to [21].

2.3.2 Working Fluid Carbon Dioxide

The first concept utilizing CO_2 (critical pressure at 73.8 bar and critical temperature at 31°C) as the working fluid was by Wolf [13] described in section (2.2). ABB Corporate Research [5, 22] also makes use of CO_2 in their proposed *ETES* system as well as Kim et al. [23, 9].

Due to issues of ozone layer protection and global warming prevention and mainly because of its thermo-physical properties, CO_2 or *R 744*, seems to be a promising working fluid for *ETES*. It is characterized by its very low critical temperature, its excellent thermal properties, while it offers a very high power density. It is also environmental-friendly, and it is non-flammable and non-toxic, however it is a suffocating gas. CO_2 has a low surface tension, which leads to reduced effects of cavitation in the machinery, thereby allowing for compression and expansion closer to the saturation curve. Furthermore, only small compression ratios are required in the vicinity of the critical point, which lead to high efficiency of the machinery. The high density of CO_2 near the critical region results in a large power density and subsequently to compact equipment.

The biggest drawback is the high absolute pressure of the supercritical CO_2 . However, the high pressure level that occurs, is due to the requirement of supercritical operation, rather than the properties of CO_2 itself. Compared with other working fluids, the pressure of CO_2 is actually among the lowest in the supercritical region [5].

ABB

According to Mercangöz et al. [5] a big challenge in the implementation of *ETES* is to match the cycle temperature profiles with those of the thermal storage materials. Currently two concepts of thermal storage that would be appropriate for an *ETES* application exist.

On the other hand two tank fluid thermal storage, with water or an emulsion like molten salt would result into a non-isothermal temperature profile during heat exchange with the working fluids used in *ETES*. The biggest advantage would be the possibility to use high efficiency heat exchangers. This concept can be limited due to the storage material reaching its boiling or freezing points. The other option would be the usage of Phase Change Materials (*PCM*) that result in an isothermal temperature profile during heat exchange with *ETES* working fluids, like water.

Figure (2.11) illustrates the issue of matching the selected cycle to the heat sources and heat sinks with which the cycle interacts. Two examples of possible mismatches are given in the upper frames, in the left case, the cycle delivers and retrieves heat from a medium that stores the heat at constant temperature (as latent heat in a *PCM*), but uses a working fluid the temperature of which varies during the heat exchange i.e. the working fluid exchanges the heat in sensible form. In order to transfer the heat from the working fluid to the storage medium during charging, the working fluid temperature must be above the storage temperature during the whole heat transfer process and the cycle therefore must follow the black arrows. To discharge the stored heat, the working fluid must receive the heat from the storage and therefore its temperature must be below the phase change temperature of the storage material. If these conditions aren't met, a significant reduction of the work output compared with the work input occurs.

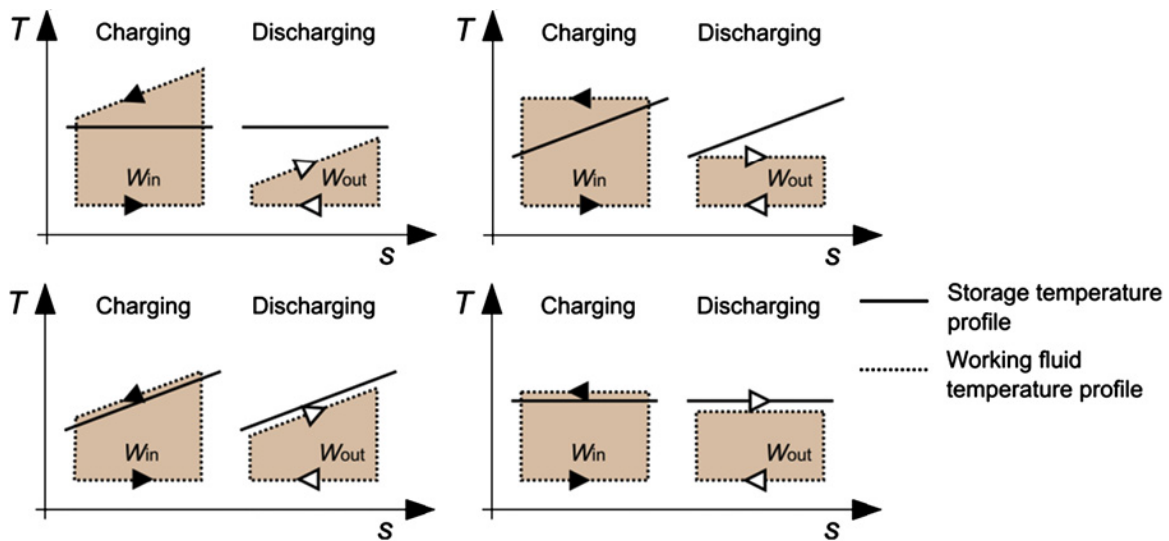


Figure 2.11: Bad and good match between the cycle and heat sources/sinks. Bad match (upper two cases) reduces the roundtrip efficiency. Good match is on the lower two frames for sensible heat storage (left) and latent heat storage (right) [5].

On the hot storage side two or more tanks at different temperatures, filled with water, are used. In order to avoid boiling, the tanks are pressurized. Liquid water has a very high heat capacity, which results in a high energy density of the storage in both volume and mass. Furthermore it has excellent heat transfer and transport properties while it is environmental friendly, highly available, inflammable, and non-corrosive. A disadvantage is that it offers a

relatively narrow temperature range, since it freezes at 0°C and boils at 100°C at ambient pressure. These limits can only partially be mitigated by additives that lower the freezing point and pressurization to allow storage at higher temperatures.

An ice slurry storage system is used at the low temperature side of the cycle. The advantages of this configuration are, increased site independence with minimum interaction with the environment, reduction of backwork, increased temperature potential and therefore increased storage utilization factor.

The presence of an ice storage unit does not eliminate the need for interacting with an external heat sink to discharge the initial electrical energy that cannot be back converted. The method chosen to discharge this heat is an additional balancing ice making cycle, which will operate during periods of low electricity demand when the charging cycle is running and when the ice storage is being replenished. Preferably operating with ammonia as the working fluid and containing a multi stage intercooled compressor, which eventually discharges at its condenser the residual heat corresponding to the exergy losses into an external heat sink such as cooling water or air. The cycle configuration is presented in Fig. (2.12).

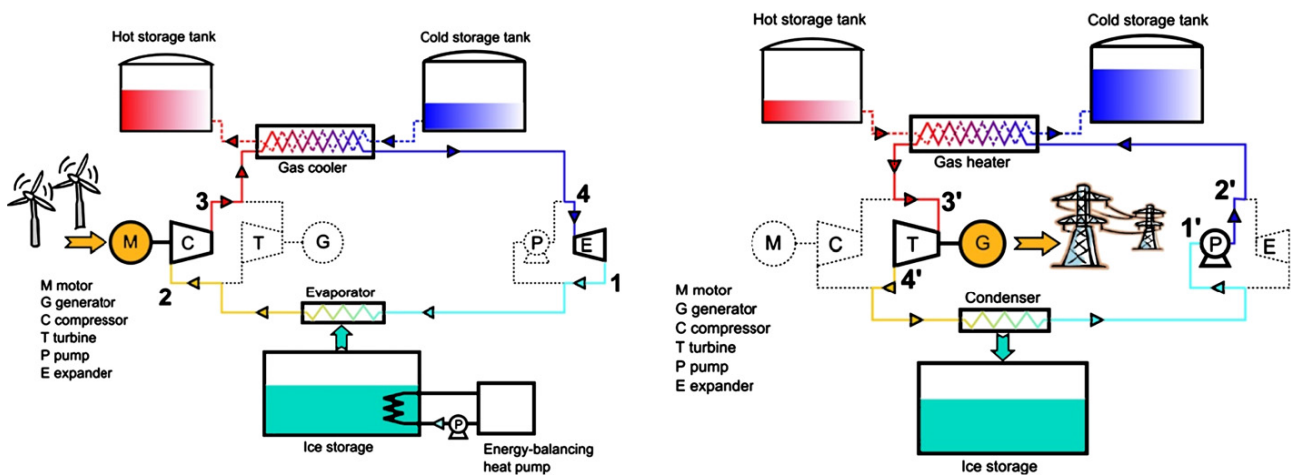


Figure 2.12: Schematic of the charging (left) and discharging (right) configuration of an *ETES* system [5].

Morandin et al. introduce in [24] a methodology for the synthesis and conceptual design of a *ETES* system based on the analysis of the thermal integration between charging and discharging cycles using pinch-analysis tools. This method states that the heat exchanger network, the temperatures and volumes of the storage tanks are not defined a priori but are determined after the cycle parameters are optimized. The study resulted in the base case *ETES* plant flowsheet shown in Fig. (2.13).

The system is based on hot water storage, salt-water ice storage and a supercritical CO_2 Rankine cycle. An additional ammonia based refrigeration cycle, operating between 2 bar and 14.5 bar, during charging cycles was implemented, in order to improve the thermal integration at low temperatures. The heat pump cycle operates at $p_1 = 18 \text{ bar}$ and $p_2 = 188.7 \text{ bar}$ with $T_3 = 277 \text{ K}$ while the thermal engine cycle operates at $p_5 = 20.8 \text{ bar}$ and $p_6 = 174.2 \text{ bar}$ with $T_7 = 450 \text{ K}$. It is also shown that an *ETES* system cannot run in steady state conditions only by operating the heat pump and thermal engine cycles, therefore the thermal imbalances generated by the irreversibilities occurring in the system during charge and discharge must be rejected to the environment. A bigger mass flow during charging or a longer period cycle are used to balance the thermal engine requirement at the cold storage side, while the extra

heat available above the pinch point is balanced by air-cooling. As a result, a greater work must be spent during charge to store the same thermal energy required during discharge. This configuration yields a maximum roundtrip efficiency of 60 %.

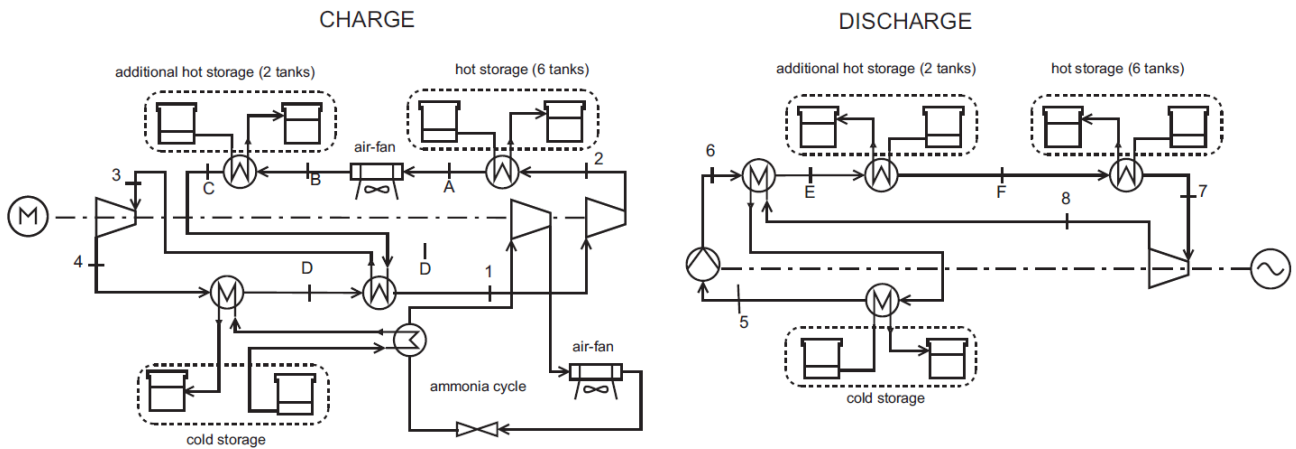


Figure 2.13: Process flow diagram of the base case configuration design of an *ETES* plant [24].

In a paired paper [25], Morandin et al. generated different system configurations, by modifying the base case configuration, which were optimized separately following the objective of maximum roundtrip efficiency only.

Further optimizations were also performed on the base case configuration, shown in Fig. (2.13) in order to elucidate the impact of superheating before the heat pump compression, on the maximum roundtrip efficiency. In the improved configuration the lower end-portion of the heat pump supercritical profile is used to superheat the working fluid before the compression thus obtaining higher temperatures at the compressor outlet, allowing for higher hot storage temperatures, Fig. (2.14). This allows reaching higher thermal engine maximum temperatures and higher expansion work which compensate the slight increase in compression work at the heat pump side. After the optimization the ammonia refrigeration cycle is no longer necessary. The maximum roundtrip efficiency obtained is 2.3 % higher than in the base case scenario. The major reason behind the increase in roundtrip efficiency is the better thermal integration obtained with high degree of internal heat recovery in both cycles.

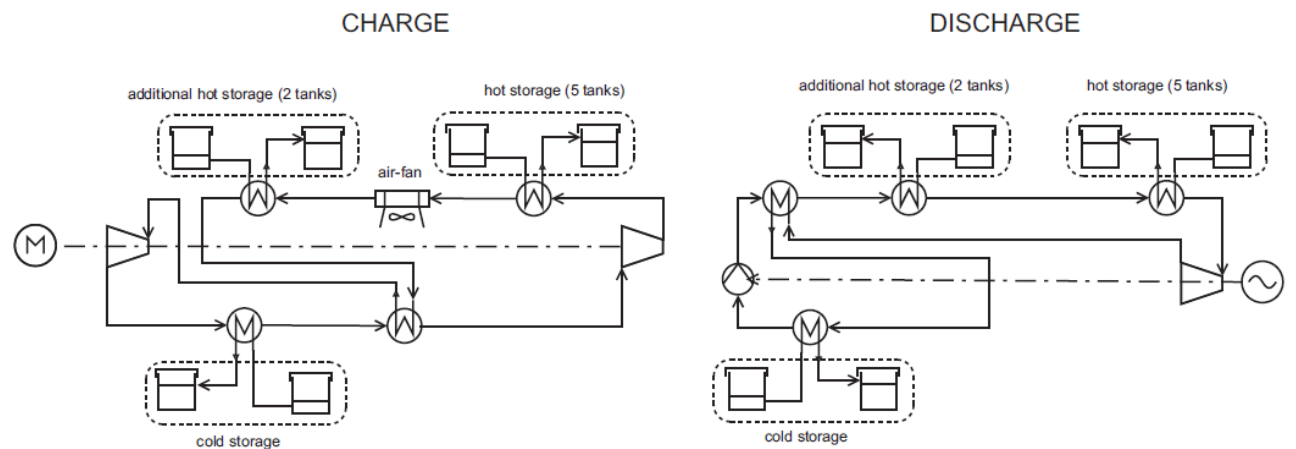


Figure 2.14: Process flow diagram of the optimum design *ETES* plant with the maximum roundtrip efficiency [25].

The first modification of the base case basic plant configuration consisted in opening thermal cuts between two compression stages in the charging cycle and two expansion stages in the discharging cycle for inter-cooling, by means of air-cooling and reheating purposes. The thermodynamic effects of inter-cooling or reheating between stages of hydraulic turbomachinery are negligible compared to the effects obtained at the vapour side of the cycles since liquid thermal properties do not vary significantly in a wide range of pressure and temperatures. The results of the optimization showed that such additional heat sinks and heat sources do not lead to a significant increase in heat integration opportunities compared to the base case scenario.

A simple system with only inter-cooling between thermal engine turbine stages, shown in Fig. (2.15) which provides a maximum roundtrip efficiency of 56.4% was calculated. Here the entire heat produced by irreversibilities is removed from the system by inter-cooling the thermal engine turbine stages. A portion of the available heat from such inter-cooling is recovered within the thermal discharging cycle by preheating the CO_2 in supercritical conditions.

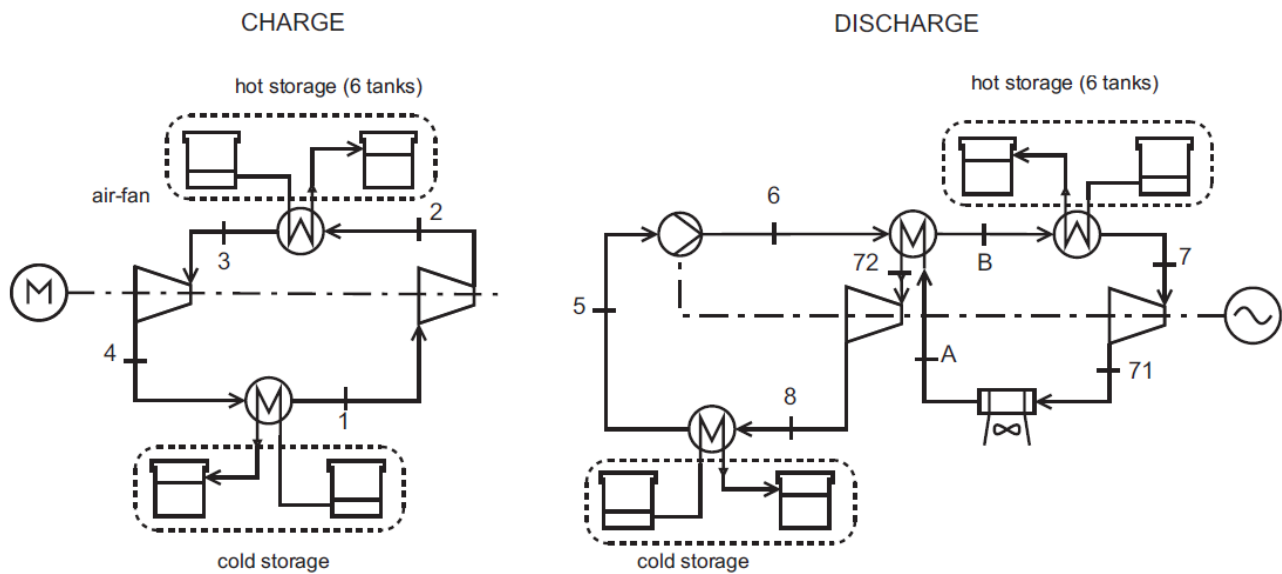


Figure 2.15: Process flow diagram of a design solution with inter-cooling between thermal engine turbine stages [25].

On another approach the possibility of adding splitters and mixers to allow the extraction or injection of working fluid at an intermediate pressure between turbomachinery stages was examined. For this to be feasible, multi-stage hydraulic turbomachinery must be used that can accommodate the different mass flow rates that occur. Almost the same value of maximum roundtrip efficiency as in the base case scenario was obtained, therefore it can be concluded that the modifications to the basic cycle configurations introduced at this step do not improve the system thermal integration and result in a highly complex system structure which appears unnecessary compared to the base case.

In a final approach, throttling valves are used instead of the hydraulic expander in the charging cycle and a flash drum is added to separate the vapour at the outlet of the first throttling stage, which is sent directly to the high pressure compression stage. The discharge cycle is modified by adding a vapour draw-off and a mixing drum that allows preheating the liquid CO_2 through direct mixing with superheated vapour. For given low and high cycle pressures, the combination of throttling valves with intermediate vapour separation reduces the entropy losses of the expansion. In parallel, the saturated vapour obtained at the top of the flash drum is injected into an intermediate compression stage so that an inter-cooling effect

is obtained which helps reducing the compression work. These two effects counterbalance the reduced specific refrigeration effect associated with a low amount of refrigerant flowing through the low-pressure side of the cycle, therefore higher heat pump performances can be reached. A maximum value of the roundtrip efficiency equal to 48.1 % was found for this configuration.

The loss in performance with respect to the base case must be attributed to the use of throttling valves instead of hydraulic expanders, which show that the work-recovery hydraulic expander in the charging cycle is crucial if high roundtrip efficiencies are to be met.

In a final paper Morandin et al. [22], make a thermoeconomic analysis of the previously described topologies. The optimal trade-off between thermodynamic performance and investment costs of an *ETES* system based on CO_2 transcritical cycles was investigated and the obtained results were presented. Three optimization case studies were performed and the resulting optimal Pareto fronts are shown in Fig. (2.16). The Pareto efficiency is a state of allocation of resources in which it is impossible to make any one individual property better, without making at least one individual worse [26].

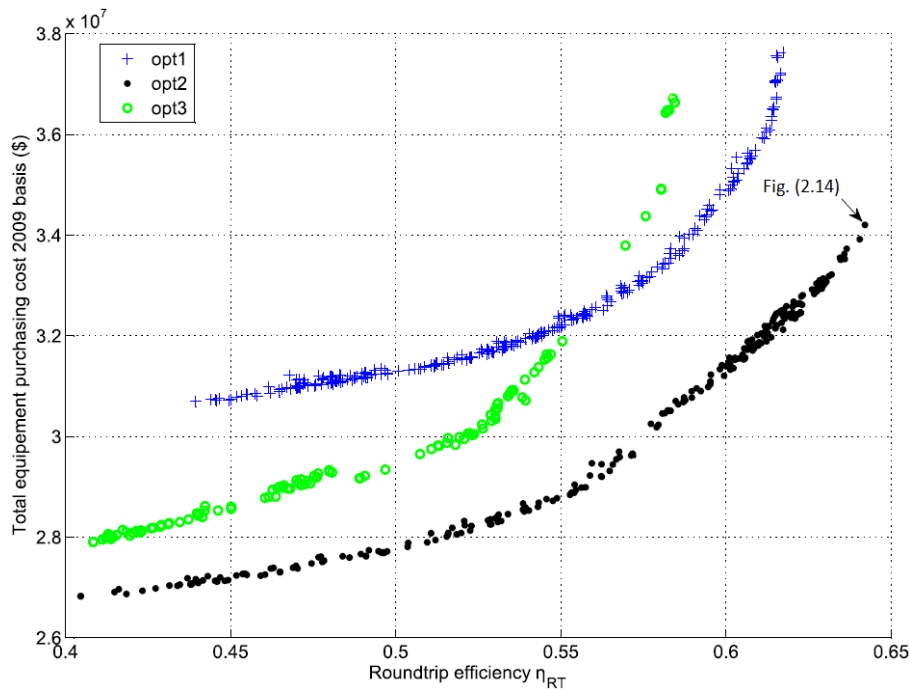


Figure 2.16: Optimal Pareto fronts according to [22].

The first option consists of the base case configuration without superheating before the CO_2 pump compressor (opt1), leading to a maximum roundtrip efficiency of 62 %. For this configuration two independent hot storage systems are required, since the heat of the lower end part of the CO_2 heat pump supercritical profile below the ambient temperature cannot be used for internal heat recovery, it has to be stored in an additional pair of water tanks. For the second option, a recuperator to superheat the CO_2 before the pump compressor was implemented. The opportunity of internal heat recovery, makes the additional ammonia cycle unnecessary. The final option considered is similar to the second option but utilizes an additional air-fan in the heat engine expansion. Although a significant loss in performance is introduced by the intercooled expansion, only one intermediate tank is needed at the hot water storage side.

Wright et al. present in [27] the control concept of an *ETES* plant and discuss several

issues specific to the plants design and operation. The report describes the major control characteristics of the plant together with methods, tools, and results of the model. Main findings include the fact that, in order for the plant to operate continuously, both the water thermal storage and ice storage must be returned to their initial conditions after every 24 hour period. Otherwise, small changes in the thermal environment during waste heat rejection or performance variations of internal components cause the storage system to drift from its designed operating temperature, pressure and energy storage capability, challenging its ability to operate.

In a companion paper, Fuller et al. [28] analyse the particular requirements from the perspective of the CO_2 turbomachinery that are needed for the storage plant. A selection of turbomachinery types and their shaft arrangement that is suitable for *ETES* is presented. Also the expected performance, main design features and challenges are discussed, together with questions related to the scalability of the turbomachines towards high power targets. Furthermore impacts of the turbomachinery designs on the *ETES* system performance, such as the sensitivity of the system roundtrip efficiency on the turbomachinery efficiency are discussed.

A pilot project in the city of Zurich, which aims at demonstrating the concept of *ETES* is presented in [29]. The paper shows that the project of *ETES Auwiesen* is feasible and presents a spectrum of possible applications of *ETES* technology with a focus on urban networks. The first tests are estimated to start in 2015. Also, the integration of the *ETES* design concept within district energy services is discussed in [30].

Trans- and supercritical CO_2 cycles and isothermal *ETES*

Kim et al. analyse in [23] transcritical and supercritical CO_2 cycles and the difference in the specific heat of the high-pressure side in comparison to the low-pressure side. Also a hybrid system of a transcritical CO_2 cycle combined with an *ETES* system is proposed.

CO_2 Brayton cycles with high-temperature heat sources are considered to be promising because they cause a reduction in the large internal irreversibility in the recuperator due to the higher specific heat of the high-pressure side than that of the low-pressure side. On the other hand, transcritical CO_2 (tCO_2) Rankine cycles exhibit a large internal irreversibility in the recuperator, because of heat transfer from the turbine exhaust stream with a low specific heat to the pump exit stream with a high specific heat.

In the case of the tCO_2 Rankine cycle for high temperature heat conversion, although the compression work is significantly reduced, the outlet temperature of CO_2 heated through the recuperator is much lower than that in the CO_2 Brayton cycle. This is because at temperatures below $150^\circ C$, especially below $120^\circ C$, the isobaric specific heat of CO_2 in the high-pressure side is considerably higher than that in the low-pressure side, as illustrated in Fig. (2.17). The operation of CO_2 Brayton cycles can escape from this temperature range, and therefore, the outlet temperature of CO_2 heated through the recuperator in this cycle is much higher than that in the tCO_2 Rankine cycle. However, if heat, which is used to compensate for the difference in the specific heats of CO_2 between the two sides, is available in this low-temperature range, the tCO_2 Rankine cycle will be more effective than the Brayton cycle. This is because less compression work is required, while the same outlet temperature of CO_2 heated through the recuperator is obtained. The concept of a CO_2 cycle using both the low- and high-temperature heat sources can also be applied to the Brayton cycle.

In this study the maximum cycle temperature was assumed to be $600^\circ C$ operating between 200 bar and 57.3 bar. *ETES* systems can be combined with a cycle that utilises both low- and high temperature sources. The schematic and reference cycle of this system are shown in

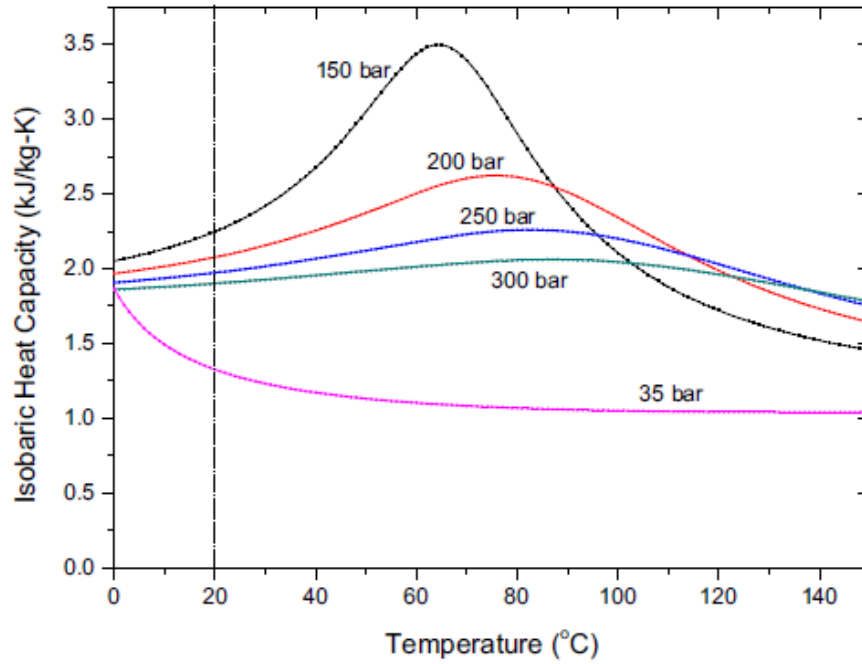


Figure 2.17: Variation in the isobaric specific heat of CO_2 in the operating temperature range depending on the CO_2 pressure [9].

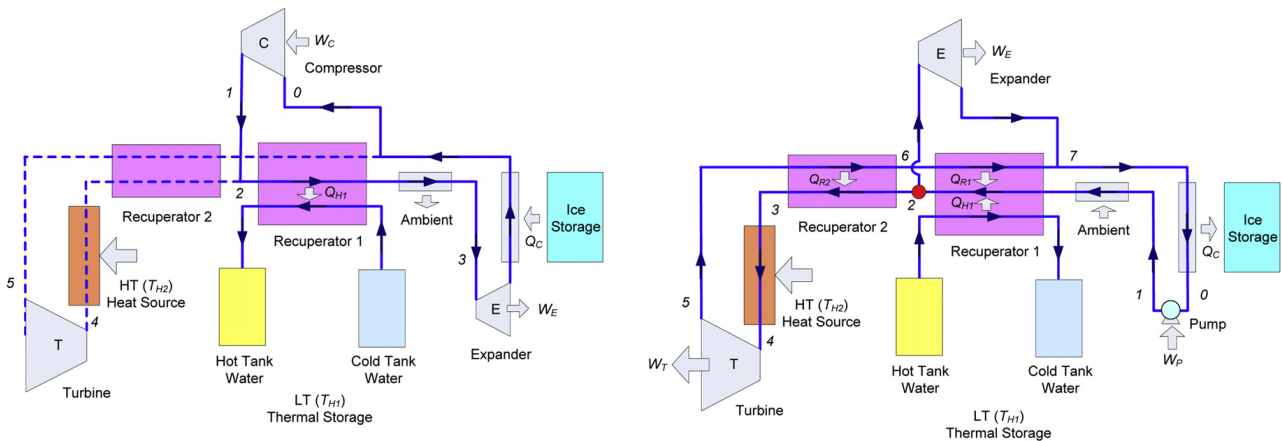


Figure 2.18: Schematic of *ETES* cycle during charging mode utilising both low- and high-temperature sources, charging mode (left) and discharging mode (right) [23].

figures (2.18) and (2.19) respectively. The charging mode is similar to the process described earlier in this section. However, during the discharging mode, the high-pressure CO_2 heated by the low-temperature (LT) source (the *TES* unit) is divided by two parts by a split ratio y , which is controlled according to the demand for electricity. One portion y , of the gas is sent to the high-temperature (HT) heater and the other portion $(1 - y)$, is sent to the low-temperature expander. The expanded hot gas from the HT turbine transfers its heat to the compressed gas through the HT recuperator, where it is cooled down and combined with the expanded gas from the LT expander. The combined, expanded CO_2 transfers its heat to the compressed gas through the LT recuperator.

The presented *ETES* cycle is able to produce approximately 45% more power than the Brayton cycle by reducing the compression work and improve the cycle efficiency by approxi-

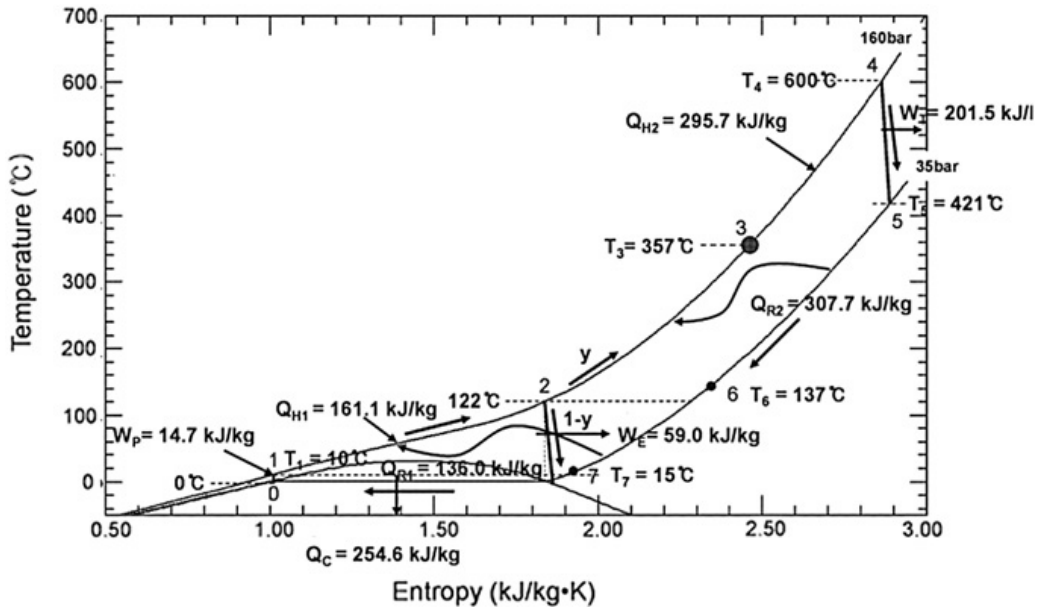


Figure 2.19: T-s diagram of an *ETES* system utilising both low- and high-temperature sources, generation mode [23].

mately 19% at 600 °C with the same heat input from the high-temperature source.

An *ETES* system with isothermal compression and expansion processes with transcritical CO_2 cycles is proposed by Kim et al. in [9]. The system layout is shown in Fig. (2.20), while the $T - s$ diagram of the base reference cycle is shown in Fig. (2.21). During the isothermal expansion of CO_2 in the heat engine mode, the gas can do more expansion work by absorbing heat directly from the hot storage, resulting in a higher roundtrip efficiency than in the isentropic *ETES* system because of its lower back work ratio. The hot water from the hot storage tank is used by the pump/motor to compress/expand the supercritical CO_2 as a liquid piston, and a portion of the water is sprayed to cool/heat the supercritical CO_2 via a circulation pump. The isothermal cycle increases the maximum roundtrip efficiency to 68.8% from 64.8% in the isentropic case.

Since water is used by the pump/motor to compress/expand the supercritical CO_2 , the CO_2 may dissolve into the water, which can cause internal corrosion in the pipelines, water pump/motor, and heat exchangers. In addition, the presence of water in CO_2 flows might also cause corrosion.

In order to solve the corrosion problem caused by the mixture of CO_2 and water, the refrigeration oil for the CO_2 compressor can be used by the pump/motor to compress/expand the supercritical CO_2 as a liquid piston while the heat of the refrigeration oil is transferred to/from the water into the hot tank by the heat exchanger.

During the isothermal expansion, much heat is supplied directly from the hot tank. Therefore, the temperature of the hot tank decreases slightly with time during the discharging mode, resulting in a varying condition and performance of the system. In order to compensate this phenomenon the usage of a larger storage tank with a greater initial mass of water is advisable. This would result into a higher roundtrip efficiency due to smaller temperature drops in the tank.

One of the difficulties in *ETES* systems with transcritical CO_2 cycles is to match the thermal capacity of water with that of CO_2 to allow the best possible thermal integration. Fig. (2.17)

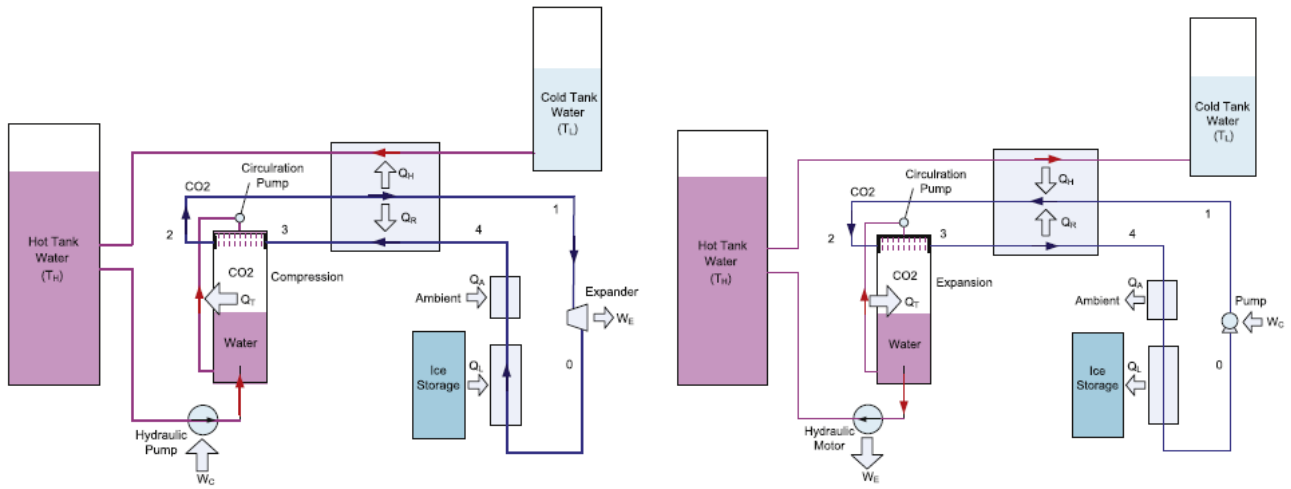


Figure 2.20: Schematic of an isothermal *ETES* system with a transcritical CO_2 cycle, charging mode (left) and discharging mode (right) [9].

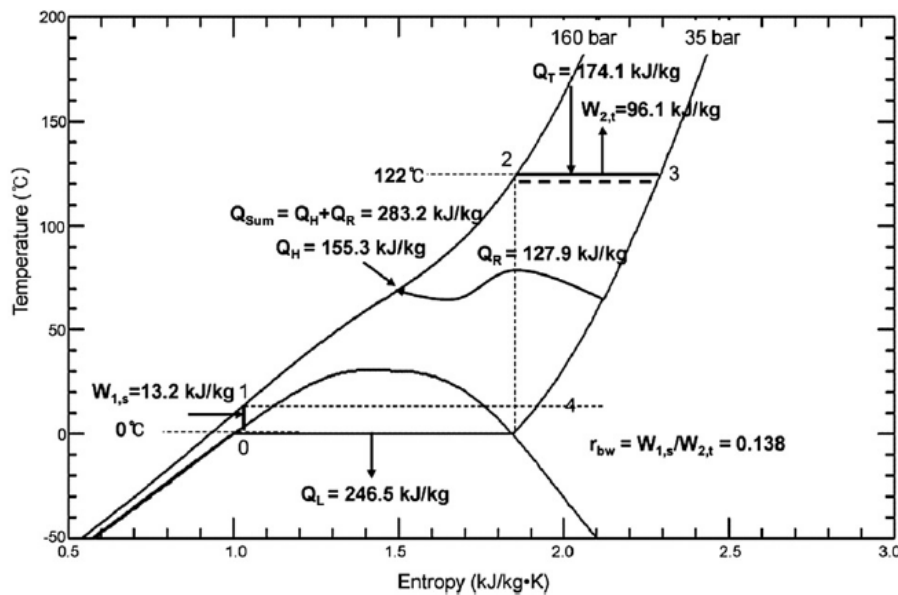


Figure 2.21: Base reference cycle of isothermal *ETES* systems with a transcritical CO_2 cycle [9].

shows that the isobaric specific heat of CO_2 in the high-pressure side changes significantly in the operating temperature range, while that of water is almost constant. Although it is possible to reduce the variation in the isobaric specific heat of CO_2 by increasing the maximum CO_2 pressure, in the case of isentropic *ETES* this would result into an increase of the maximum operating temperature of CO_2 , because of the high-pressure ratio. Thus the pressure of the water tank must be greatly increased to prevent the boiling of water. On the other hand, in an isothermal *ETES* system it is possible to limit the maximum operating temperature freely despite the high-pressure ratio.

2.3.3 Working Fluid Water - CHEST

Steinmann in [31] presents a concept of Compressed Heat Energy STorage *CHEST* based on a medium temperature conventional Rankine cycle with steam combined with a thermal storage unit. The concept attains an efficiency of 70 % while the maximum temperature stays below 400 °C. Also an option to integrate heat provided by low temperature sources during the charging process is implemented.

During the charging mode, low pressure water is evaporated using heat from the environment. After compression, the high pressure steam releases its energy in a thermal storage unit. There, the steam is condensed and the condensate is cooled down to the saturation temperature of the evaporation process. During discharge, heat released by the storage system is used to generate steam for running a steam turbine. After expansion, the steam is condensed. The cycle is closed by the condensate entering the preheating section of the storage unit.

For the implementation of the *CHEST* concept, a Rankine cycle with a maximum temperature of 400 °C was chosen. A Brayton cycle was also considered, but due to the large volumetric flow rate and high working temperature, a Rankine cycle was preferred. Due to the fact that the *CHEST* concept is based on a medium pressure Rankine cycle the storage system must include both sensible and latent heat storage in order to minimize entropy generation resulting from temperature differences during charging and discharging.

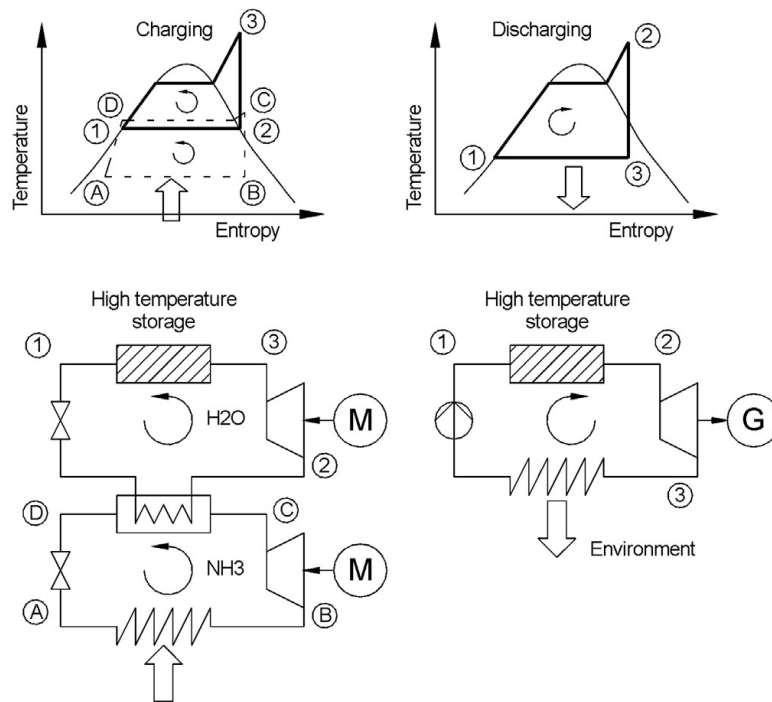


Figure 2.22: Cascaded system for charging with an ammonia cycle for low temperature compression and water as the working fluid for high temperature compression. Single fluid (water) Rankine cycle for discharging [31].

Furthermore an exemplary implementation of the *CHEST* concept is presented. It consists of a cascaded system with a low temperature stage using ammonia as the working fluid and water as the working fluid for the high temperature stage. The layout is depicted in Fig. (2.22). With the assumption of an adiabatic system, and that no pressure losses in pipes or the storage system occur, a roundtrip efficiency of 72.8 % was determined.

The *CHEST* concept also allows the integration of low temperature heat sources, such as

waste heat from industrial processes, geothermal heat or solar energy. If heat at low temperatures above the ambient temperature is available, the compression work needed during the charging of the storage system is reduced, while the work provided during discharge remains the same. As a result, the difference between the electrical energy that is needed to charge the storage and the electrical work provided during the discharge process can be reduced. It is even possible that the electric work delivered during discharge outweighs the work needed during the charging process.

Chapter 3

Theoretical Background

The fundamental thermodynamic cycles for energy production will be presented and explained in this section. Also important properties of the working fluid CO_2 will be presented elucidating why it makes a very good medium for an *ETES* system. Finally the *SandTES* unit will be introduced along with its basic characteristics and working principle.

3.1 Thermodynamic Cycles for Electricity Production

3.1.1 Steam Rankine Cycle

The schematic and the $T - s$ diagram of a simple steam Rankine cycle power plant is shown in Fig. (3.1). The boiler feedwater pump increases the pressure level of the water. Afterwards the water is heated isobarically. The working fluid evaporates and increases in volume. The following turbine expands the steam while producing work. Finally the cooler is used as a heat sink to dissipate the heat to the environment and bring back the working fluid to its original state.

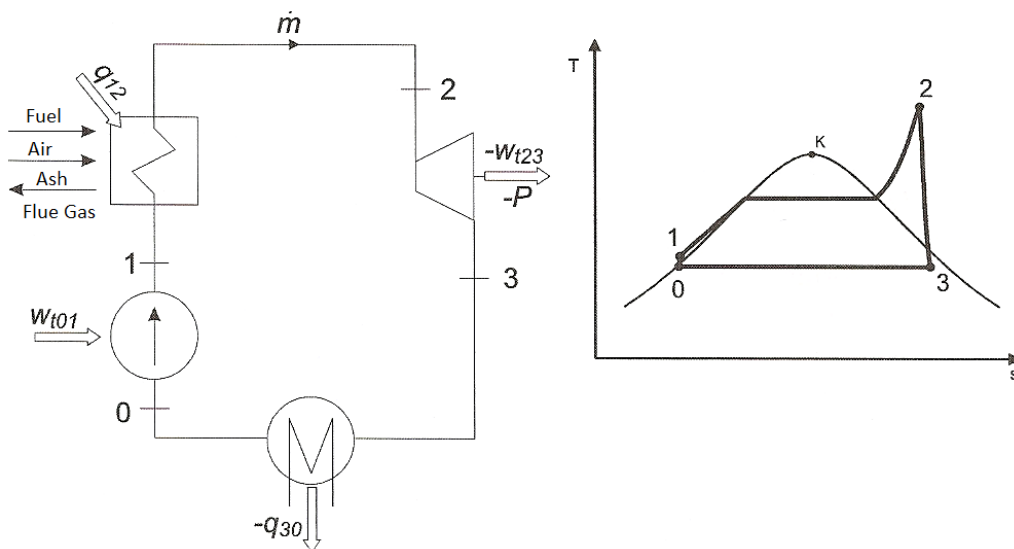


Figure 3.1: Schematic and $T - s$ diagram of a simple steam power plant. The working fluid (water) passes through the two phase area, this means that it can absorb high amounts of heat at very low temperature differences [32].

The ideal Rankine cycle undergoes the following changes of state:

- 0 – 1 : Isentropic pressure boosting through the boiler feedwater pump.
- 1 – 2 : Isobaric heat supply in order to warm up and evaporate the liquid water and further superheat the steam.
- 2 – 3 : Isentropic expansion of the steam in the turbine.
- 3 – 0 : Isobaric heat discharge condensating the working fluid in the cooler.

Applying the first law of thermodynamics the specific useful work done w_N can be calculated as:

$$-w_N = | w_{T23} - w_{P01} | \quad (3.1)$$

The specific work that is needed for the isentropic change of state in the boiler feedwater pump is:

$$w_{P01} = h_1 - h_0 = \frac{h_{1^s} - h_0}{\eta_{sP}} \quad (3.2)$$

Where η_{sP} is the isentropic efficiency of the feedwater pump. The produced work in the turbine can be calculated as:

$$-w_{T23} = h_2 - h_3 = \eta_{sT}(h_2 - h_{3^s}) \quad (3.3)$$

In the previous equation, η_{sT} is the isentropic efficiency of the turbine. Finally the thermal efficiency η_{th} of the cycle is defined as:

$$\eta_{th} = \frac{-w_N}{q_{12}} = \frac{-w_N}{h_2 - h_1} \quad (3.4)$$

Whereby q_{12} is the specific heat input provided by the boiler.

Several procedures exist that help to improve the efficiency of the cycle, the most important are re-heating and feedwater pre-heating. Both try to increase the thermodynamic mean temperature of the cycle. This can be achieved by increasing the pressure of the cycle and/or increasing the inlet temperature of the turbine. A limiting factor is the erosion that occurs if the steam mass fraction is about below $\chi = 90\%$ at the turbine outlet. In that case water drops would hit the turbine blades causing erosive wear.

Re-Heating

Reheating enables the ability to increase the pressure in the boiler without risking to expand the working fluid in to the two phase area. Fig. (3.2) shows the schematic of an Rankine cycle improved via a second turbine stage.

After the steam is expanded in the high pressure turbine it is heated again to the same temperature level as before and then enters the low pressure turbine. This procedure leads to the shift of the $T - s$ diagram to the right which means that it is more likely to not expand into the critical region. The overall improvement of a re-heater in a steam power cycle is about 10%.

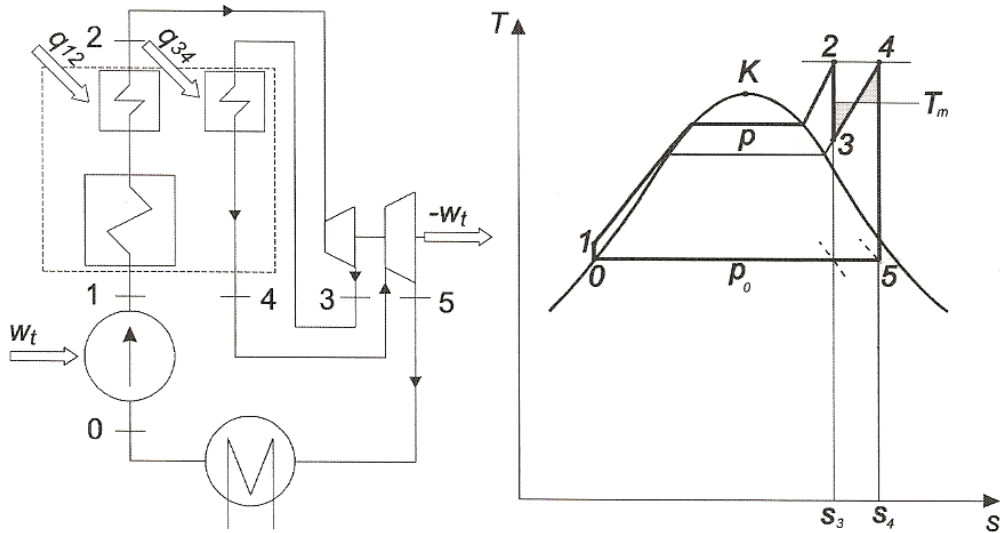


Figure 3.2: Schematic and $T - s$ diagram of an improved simple steam power Rankine cycle through re-heating [32].

Feedwater Pre-Heating

At a system with feedwater pre-heating, a portion of the mass flow is split from the turbine and used to warm up the feedwater. After the heat exchange, the split mass flow is throttled to the low pressure level of the cycle. The schematic and $T - s$ diagram of such a system are illustrated in Fig. (3.3).

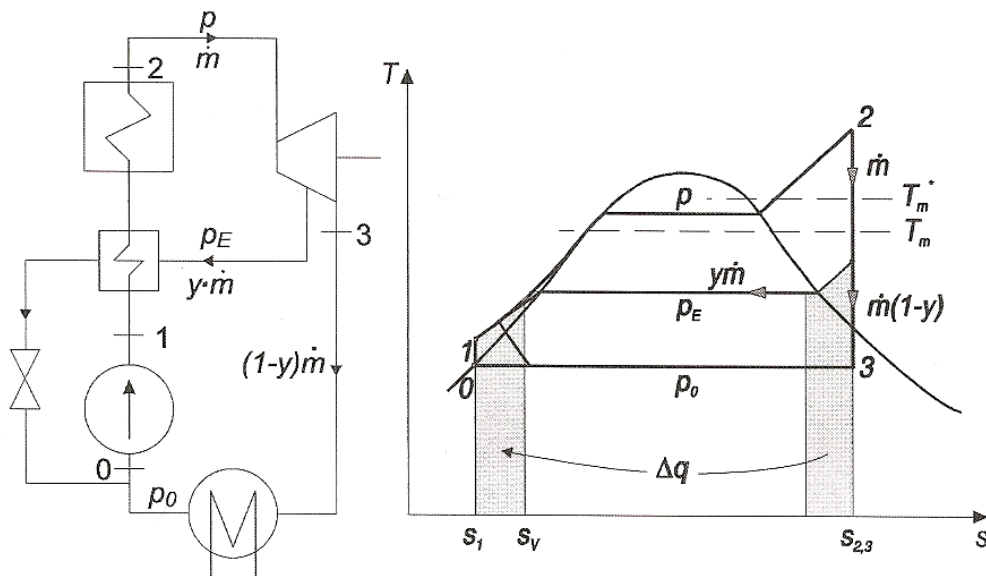


Figure 3.3: Schematic and $T - s$ diagram of the improved steam Rankine power cycle through feedwater preheating via mass flow splitting [32].

Through this configuration, a portion of the heat is transferred from the steam side of the cycle to the water side thus increasing the mean thermodynamic temperature and the thermal efficiency of the cycle.

3.1.2 Organic Rankine Cycle

The particularity of the Organic Rankine Cycle (*ORC*) over the traditional Rankine cycle lays in the working fluid: an organic component is used instead of water. The boiling point of these fluids is lower than that of water, which allows recovering heat at a lower temperature than in the traditional steam Rankine cycle. Its thermophysical properties differ from that of water in a number of aspects, which has practical implications on the design of the *ORC*.

The layout of an *ORC* is somewhat simpler than that of the steam Rankine cycle: there is no water-steam drum connected to the boiler, and one single heat exchanger can be used to perform the three evaporation phases: preheating, vaporization and superheating. The variations on the cycle architecture are also more limited: reheating and turbine bleeding are generally not suitable for the *ORC*, but a recuperator can be installed as a liquid preheater between the pump outlet and the expander outlet, as illustrated in Fig. (3.4).

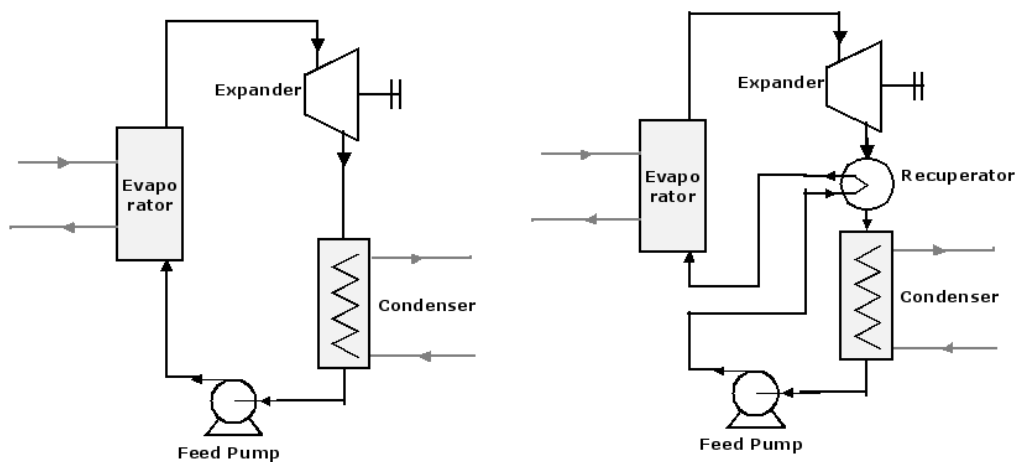


Figure 3.4: Working principle of an *ORC* with (right) and without (left) recuperator [33].

The basic cycle is very similar to the traditional steam cycle: the organic working fluid is successively pumped, vaporized, expanded and then condensed. The cycle with recuperator takes advantage of the residual heat after the expansion to preheat the liquid after the pump. This operation allows reducing the amount of heat needed to vaporize the fluid in the evaporator.

The main applications of organic Rankine cycles are:

- Biomass combined heat and power.
- Geothermal energy.
- Solar power plants.
- Heat recovery on internal combustion engines.
- Heat recovery on mechanical equipment and industry processes.

The last point is of significant importance for this work. Many applications in manufacturing industry reject heat at relatively low temperature. In large-scale plants, this heat is usually overabundant and cannot be reused on-site or for applications such as district heating. It is therefore rejected to the atmosphere. This causes two types of pollution:

- The pollutants (CO_2 , NO_x , SO_x , HC) contained in the flue gases can generate at higher temperature levels higher health or environmental risk.
- The heat rejection can perturb aquatic equilibrium and have a negative effect on biodiversity.

Recovering this waste heat can mitigate these two types of pollution. It can moreover generate electricity to be consumed on-site or sent back to the grid. In such a system, the waste heat is usually recovered by an intermediate heat transfer loop and used to evaporate the working fluid of the *ORC*. A potential of 750 MW is estimated for power generation from industrial waste heat source in the US.

Some industries present a particularly high potential for waste heat recovery. Among them, the cement industry, in which 40 % of the heat is lost in flue gases. These flue gases are located after the limestone preheater or in the clinker cooler, with a temperature varying between 215 – 315 °C. The CO_2 emissions from cement industry amount for 5 % of the total world CO_2 emissions, and half of it is due to the combustion of fossil fuels in the kilns. Other possible industries include the iron and steel industries (10 % of the CO_2 emission in China), refineries or chemical industries [33].

3.1.3 Comparison of the Organic Rankine Cycle with the Steam Rankine Cycle

Fig. (3.5) shows in the $T-s$ diagram the saturation curves of water and of a few typical organic fluids in *ORC* applications. Two main differences can be stated:

1. The slope of the saturated vapor curve is negative for water, while the curve is much more vertical for organic fluids. As a consequence, the limitation of the vapor quality at the end of the expansion process disappears in an *ORC* cycle, and there is no need to superheat the vapor before the turbine inlet.
2. The entropy difference between saturated liquid and saturated vapor is much smaller for organic fluids. This also involves that the enthalpy of vaporization is smaller. Therefore, for the same thermal power through the evaporator, the organic working fluid mass flow rate must be much higher than that of water, leading to a higher pump consumption.

Other differences between the cycles can be summed up in the following points:

Superheating. As previously stated, organic fluids usually remain superheated at the end of the expansion. Therefore, there is no need for superheating in *ORC*, contrary to steam cycles. The absence of condensation also reduces the risk of corrosion on the turbine blade, and increases its lifetime up to 30 years instead of 15-20 for steam turbines.

Low temperature heat recovery. Due to the lower boiling point of the organic working fluids, heat can be recovered at a much lower temperature.

Components size. The size of the components is very dependent on the volume flow rate of the working fluid because pressure drops increase with the square of the fluid velocity. This leads to the necessity of increasing the heat exchangers hydraulic diameter and the pipe diameter to reduce this velocity. The turbine size is roughly proportional to the volume flow rate.

Turbine inlet temperature. In steam Rankine cycles, due to the superheating constraint, a temperature higher than 450 °C is required at the turbine inlet to avoid droplets formation

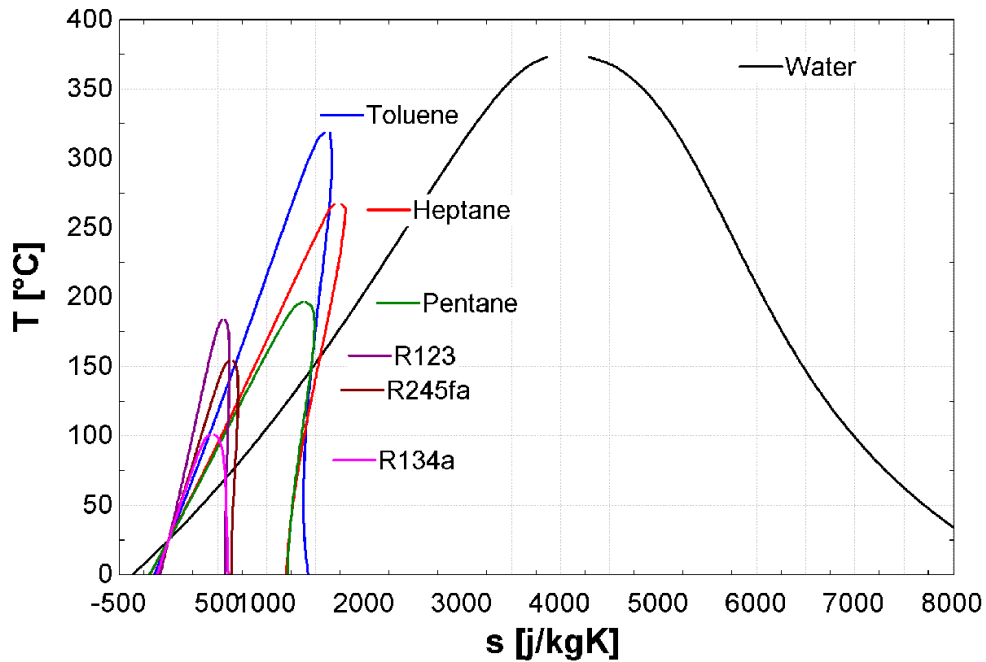


Figure 3.5: $T - s$ diagram of a few typical organic fluids and of water [33].

during the expansion. This leads to higher thermal stresses in the boiler and on the turbine blades and to higher cost.

Pump consumption. Pump consumption is proportional to the liquid volume flow rate and to the pressure difference between outlet and inlet. It can be evaluated by the Back Work Ratio (BWR), which is defined as the pump consumption divided by the turbine output power. In a steam Rankine cycle, the water flow rate is relatively low and the BWR is typically 0.4%. Generally, the lower the critical temperature, the higher the BWR .

High pressure. In a steam cycle, pressures of about 60 – 70 bar and thermal stresses increase the complexity and the cost of the steam boiler. In an *ORC*, pressure generally does not exceed 30 bar. Moreover, the working fluid is not evaporated directly at the heat source but by the intermediary of a heat transfer loop. This makes the heat recovery easier since thermal oil is at ambient pressure, and avoids the necessity of an on-site steam boiler operator.

Condensing Pressure. In order to avoid air infiltrations in the cycle, high condensing pressures are advisable. It is not the case for water, whose condensing pressure is generally lower than 100 mbar absolute. Low temperature organic fluids meet this requirement since they condense at a pressure higher than the atmospheric pressure. However, fluids with a higher critical temperature are subatmospheric at ambient temperature.

Fluid characteristics. Water as working fluid is very convenient compared to organic fluids. Its main advantages are:

- Cost-effectiveness and availability.
- Non-toxicity.
- Non-flammability.
- Environment friendly: low Global Warming Potential, null Ozone Depleting Potential.
- Chemical stability: no working fluid deterioration in case of hot spot in the evaporator.

- Low viscosity: lower friction losses, higher heat exchange coefficients.

However, steam cycles are generally not fully tight. Water is lost as a result of leaks, drainage or boiler blow down. Therefore, a water-treatment system must be integrated to the power plant to feed the cycle with high-purity deionised water.

Turbine design. In steam cycles, the pressure ratio and the enthalpy drop on the turbine are both very high. This involves using turbines with several expansion stages. In *ORC* cycles the enthalpy drop is much lower, and single or two-stage turbines are usually used, which reduces their cost.

Additional effects of the low enthalpy drop include lower rotating speeds and lower tip speed. The lower rotating speed allows direct drive of the electric generator without reduction gear (this is especially advantageous for low power-range plants), while the low tip speed decreases the stress on the turbine blade and makes their design easier.

Efficiency. The efficiency of current high temperature *ORC* does not exceed 24%. Typical steam Rankine cycles show a thermal efficiency higher than 30%, but with a more complex cycle design (in terms of number of components or size). The same trend is stated for low temperature heat sources: steam Rankine cycles remain more efficient than *ORC* cycles.

Advantages of <i>ORC</i>	Advantages of steam cycles
No superheating	Fluid characteristics
Lower turbine inlet temperature	High efficiency
Compactness (higher fluid density)	Pump consumption
Lower evaporation pressure	
Higher condensation pressure	
No water-treatment system	
Turbine design	
Low temperature heat recovery	

Table 3.1: Advantages of organic Rankine cycles and steam Rankine cycles

The advantages of both cycles are summarized in Table (3.1). As a consequence, the *ORC* cycle is more profitable in the low to medium power range (typically less than a few *MW*), since small-scale power plants cannot afford an on-site operator, and require simple and easy to manufacture components and design. For high power ranges, the steam cycle is generally preferred, except for low temperature heat sources [33].

3.1.4 Gas Power Cycle

Gas power cycles are subdivided into open and closed cycles, both are illustrated in Fig. (3.6). In these cycles the working fluid only undergoes state changes in the gaseous phase.

At the open gas power cycle flue gas is the working fluid. This cycle has the advantage of a simpler plant configuration, but the disadvantage that the turbine is polluted by the flue gas. On the other hand, the working fluid can be freely chosen in a closed power cycle. The main problem of this system is the choice of the gas boiler material because of the high temperature levels that arise.

If the mechanical friction losses from the compressor and the turbine are neglected, then the useful work done w_t is:

$$-w_t = \eta_m(-w_{t23} - w_{t01}) \quad (3.5)$$

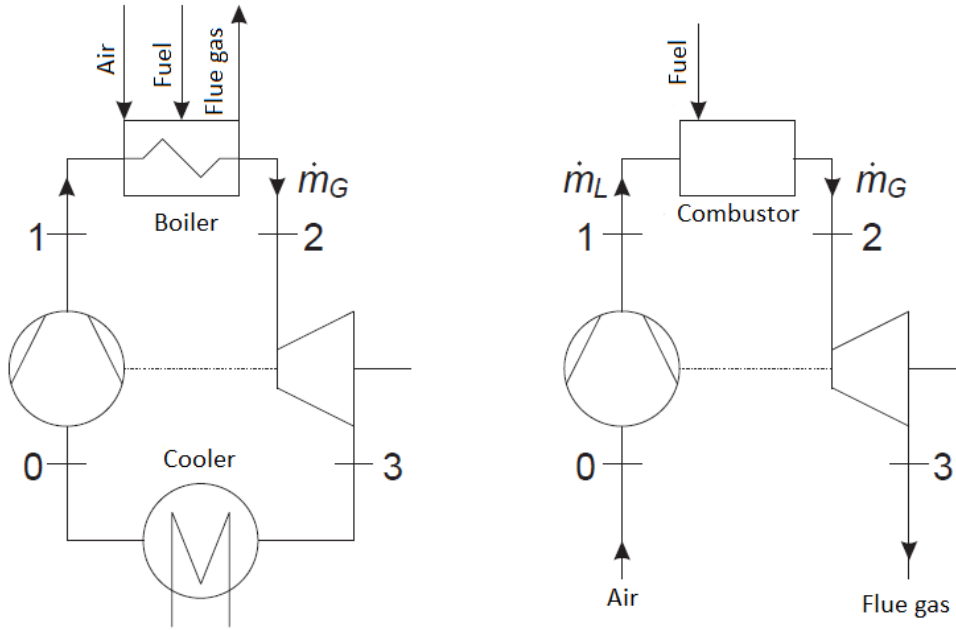


Figure 3.6: Schematic of a closed (left) and an open (right) gas power cycle [32].

The turbine and the compressor are assumed to work adiabatically. The first law of thermodynamics, with the efficiencies for the turbomachinery η_{sT} , η_{sC} and for the mechanical losses η_m states that :

$$-w_t = \eta_m(h_2 - h_3) - (h_1 - h_0) = \eta_m \eta_{sT}(h_2 - h_{3s}) \frac{h_{1s} - h_0}{\eta_{sC}} \quad (3.6)$$

The exergetic process efficiency defined as:

$$\zeta_P = \frac{-w_t}{e_2 - e_1} \quad (3.7)$$

In comparison to the steam power cycle, the exergetic efficiency of the gas power cycle is much lower. This is because in the steam cycle the temperature level at the cooling side of the cycle is much closer to the ambient temperature (T_u), meaning that the exergy loss in the cooler is much smaller than in this cycle. The exergy losses can be visualised in the $T - s$ diagram of Fig. (3.7).

The gas power cycle can be improved either by the addition of a recuperator or by additional compressor and turbine stages.

Recuperator

The gas power cycle can be improved through the addition of a recuperator. In this way a portion of the lost heat on the low pressure side of the cycle is used to heat the working fluid at the exit point of the compressor. Fig. (3.8) shows the schematic and the $T - s$ diagram of an open gas power cycle with such a configuration.

A minimum temperature difference must be set so that the recuperator does not get too big. The recuperator efficiency is defined as:

$$\eta_R = \frac{T_{1^*} - T_1}{T_3 - T_1} \quad (3.8)$$

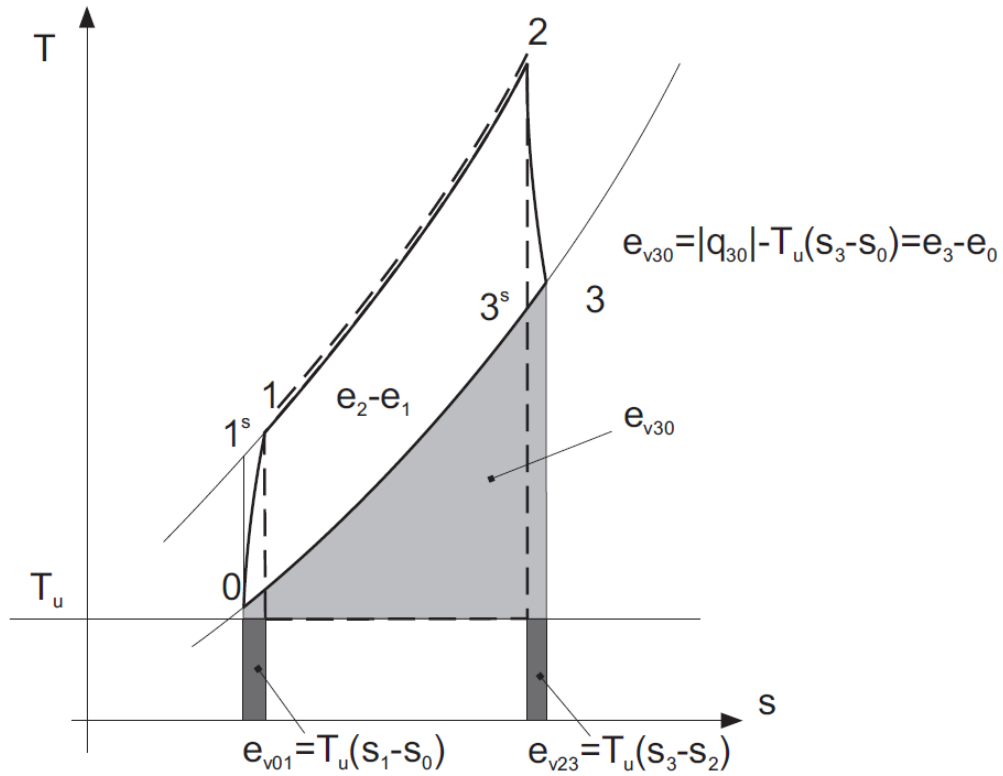


Figure 3.7: Exergy losses in a gas power cycle. The entropy increases in the two adiabatic machines due to the irreversibility of the processes. The exergy difference from point 3 to point 0 is waste, because the heat is released to the environment [32].

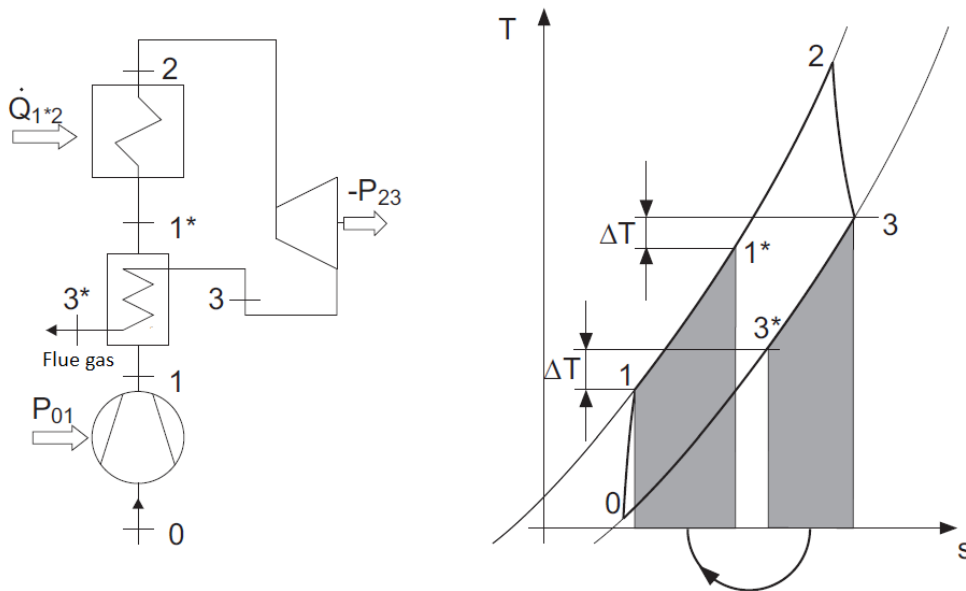


Figure 3.8: The recuperator enables the utilization of the heat the working fluid on the low pressure side of the cycle to heat the medium before it enters the boiler [32].

$T_3 - T_1$ is the maximum achievable temperature utilization and $T_{1*} - T_1$ is the actual achieved temperature increase.

Additional Turbine and Compressor Stages

Another method to increase the efficiency of the cycle is to add more stages turbine stages, hence increasing the thermodynamic mean temperature, or to add additional compressor stages in order to decrease the required compressor work. These configurations increase the exergetic efficiency of the cycle, but also increase the investment costs of the plant and its complexity. The mentioned additions to the cycle are illustrated in Fig. (3.9).

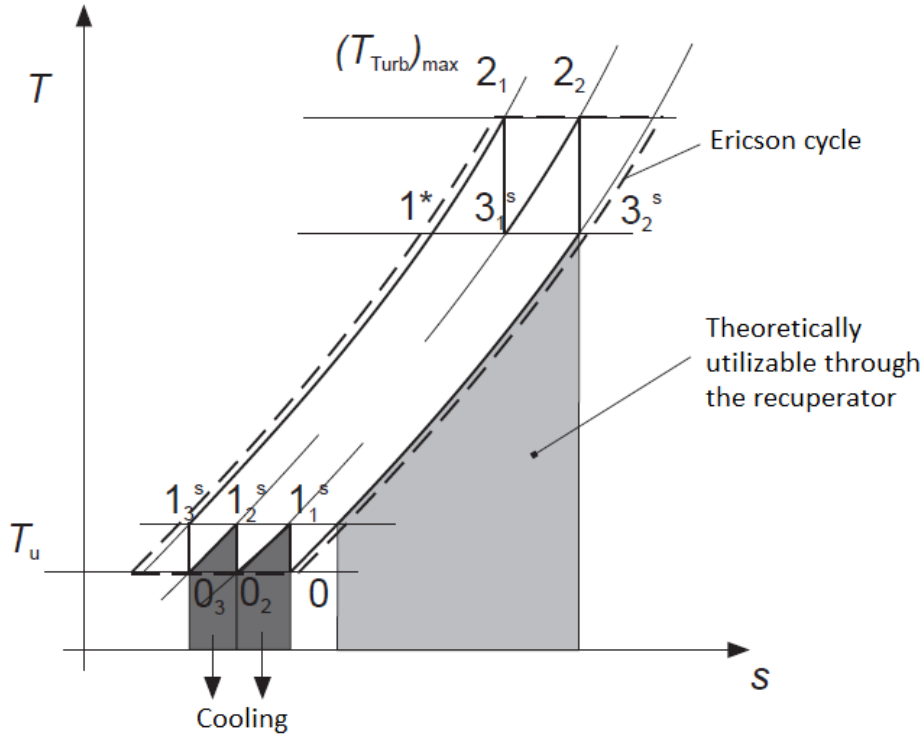


Figure 3.9: The ideal Ericson cycle is attempted to be approached by the addition of a recuperator and multiple compression and expansion stages [32].

3.2 Thermodynamic Cycles with CO_2 as Working Fluid

The supercritical power cycle takes advantage of the real gas behavior of the CO_2 in order to achieve high thermal efficiency. The main improvement of the sCO_2 cycle in comparison to the steam cycle is the reduced compressor work that results from the compressor work reduction due to property changes in the region of the critical point. Also because of the low critical temperature, it is possible to use water at ambient temperatures as a coolant. The advantages of CO_2 can be summed up as [34]:

- sCO_2 cycles achieve high efficiencies at low temperatures.
- The high operating pressure enables smaller size components, Fig. (3.10).
- Well known thermodynamic properties.
- Stability.

- Non-toxicity.
- Non-flammable.
- Low critical temperature.
- High power density.
- Low surface tension (reduced effects of cavitation in the machinery).
- Abundance.
- Low molecular leak due to higher molecular mass.
- Low cost.

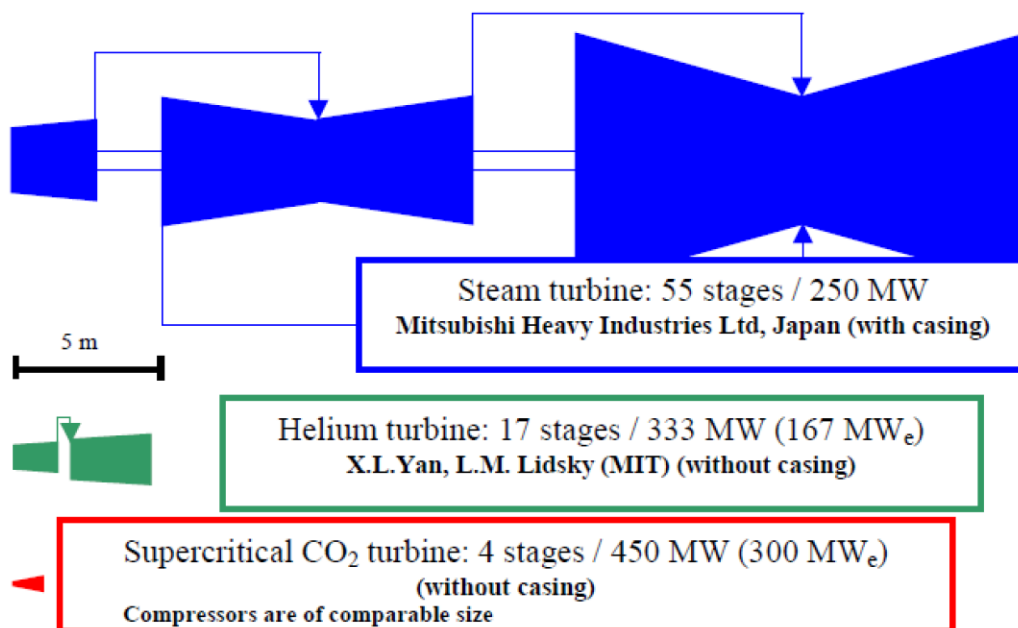


Figure 3.10: Size comparison of a steam, a helium and a carbon dioxide turbine [35].

3.2.1 Properties of CO_2

Compression near the critical point requires less compressor input work. This is caused by a rapid increase of the CO_2 density at a pressure level slightly above the critical pressure. The change of the compressor work is illustrated in Fig. (3.11). The red curve represents the required work to compress the fluid from various inlet pressure points to a compressor outlet pressure of 200 bar. Also the produced turbine work between the same pressure points is drawn for a comparison. It can be seen that the working fluid behaves almost like an ideal gas in the region of the turbine and that the highest net work is achieved for the inlet pressure of about 77 bar [34].

Another mentionable property of CO_2 is the strong dependency of the heat capacity on the pressure and temperature as already shown in Fig. (2.17). This leads to the fact that a pinch point problem can occur somewhere within the heat exchanger and not just on the cold or hot end. In order to minimize exergy losses a detailed analysis of the heat exchangers is necessary

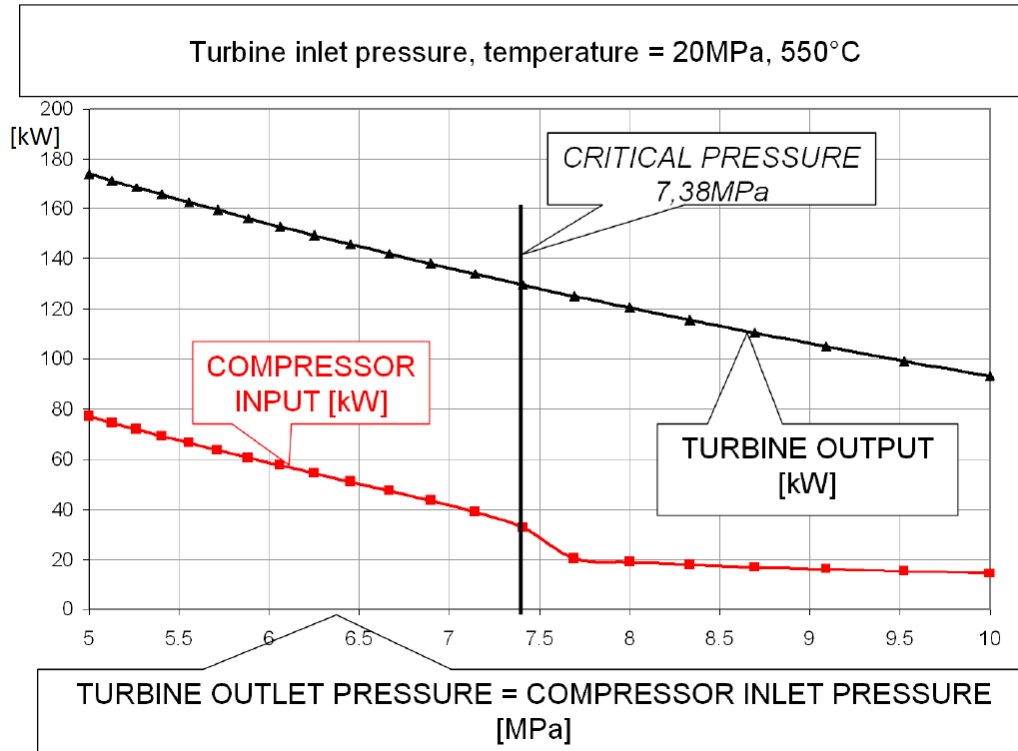


Figure 3.11: Comparison of the turbine and compressor work of CO_2 [35].

to prevent a pinch point problem. A T - s diagram, displaying all states of carbon dioxide is shown in Fig. (3.12).

Real Gas Behavior

In comparison to water or helium, carbon dioxide is characterized by a significant change of its compressibility factor. This leads to the beneficial behavior in the region of the critical point, the compressibility factor Z is defined as:

$$Z(p, T) = \frac{pv}{RT} \quad (3.9)$$

Where v is the specific volume in $[\frac{m^3}{kg}]$, p the pressure in $[bar]$, T the temperature in $[K]$ and R the specific gas constant in $[\frac{J}{kgK}]$. In the case that $Z = 1 = constant$, equation (3.9) represents the ideal gas law.

The specific compressor work w_V in a closed gas cycle can be calculated as:

$$w_V = \int_{p_0}^{p_1} v dp = \int_{p_0}^{p_1} \frac{ZRT}{p} dp \quad (3.10)$$

As can be seen in equation (3.10), lower values of the compressibility factor lead to a reduction of the compressor work. Especially in the vicinity of the critical point, where the compressibility factor is $Z \approx 0.25$. The working ranges of the turbine and compressor as a function of the compressibility factor can be seen in Fig. (3.13).

Therefore it is advisable to place the compressor entry point near to the critical point. On the other hand the specific turbine work between the same pressure levels as the compressor is calculated as:

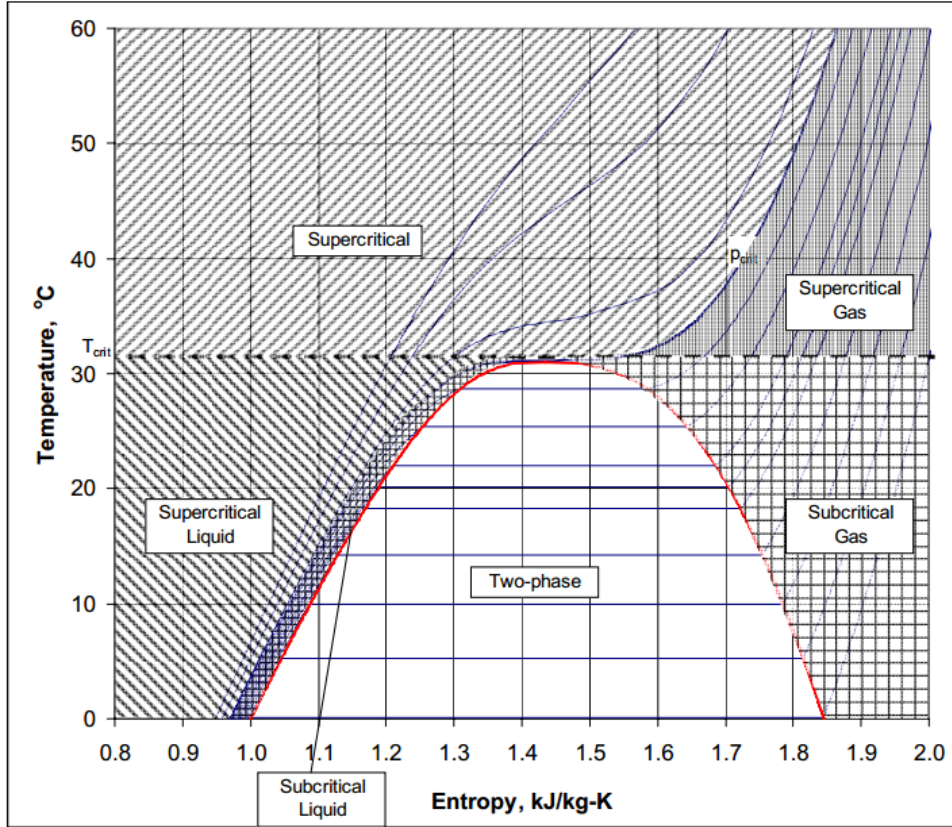


Figure 3.12: $T - s$ diagram of carbon dioxide displaying all conditions near the critical point [36].

$$w_T = \int_{p_1}^{p_0} v \, dp = \int_{p_1}^{p_0} \frac{ZRT}{p} \, dp \quad (3.11)$$

So that higher higher efficiency values can be achieved, the turbine should be placed in a region with higher compressibility factor. This is the case with CO_2 because the turbine works at levels with $Z \approx 1$.

3.3 SandTES

Large scale Thermal Energy Storage (TES) can deliver valuable contributions for balancing the volatile supply of renewable energy with demand. The price of the storage material itself exhibits the major part of the investment costs making its selection crucial. Many solid powders are low cost products and well suited storage materials. They offer good values of thermal capacities (ρc_p) and are easy to handle or transport. Their melting point is far above industrial interest making them applicable in the full temperature range of industrial interest.

In the *SandTES* concept, a storage system currently under development at the Technical University of Vienna, powders are used as storage material in an active thermal energy storage concept. In active TES concepts the primary heat transfer medium and the storage medium are transported through a heat exchanger. This enables a steady state operation, high efficiency and design flexibility (almost unlimited range in the ratio power/energy). The *SandTES* concept

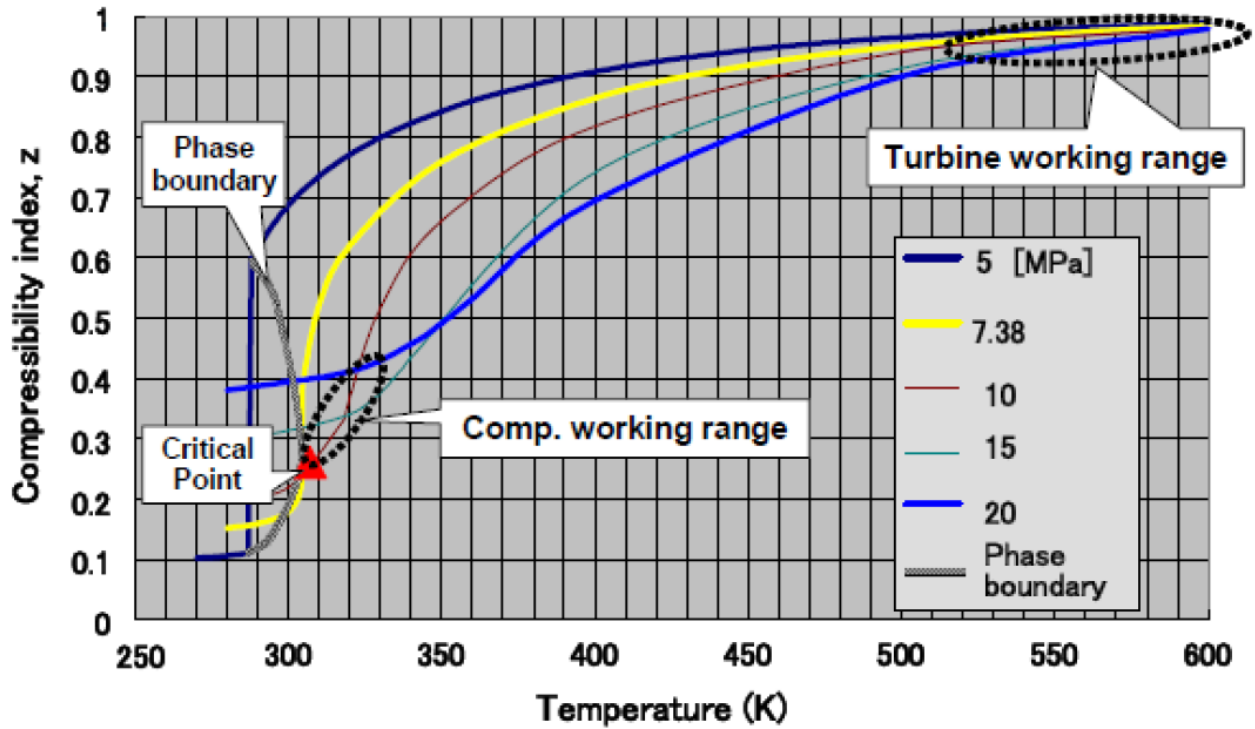


Figure 3.13: Compressor and turbine work range as a function of the compressibility factor and temperature [37].

applies fluidization technology to transport powders through a heat exchanger in stationary fluidization regime [38].

The *SandTES* active fluidized bed thermal energy storage system applies a fluidized bed heat exchanger to transfer heat between any Heat Transfer Fluid (*HTF*) and the storage medium sand. The concept consists of a stationary fluidized bed with an internal tube bundle heat exchanger, two sand bunkers and auxiliary devices handling the storage medium sand (conveyors) and delivering the air enabling the fluidized bed (blowers). An illustration of the *SandTES* concept is shown in Fig. (3.14).

In charging mode the sand enters the fluid bed heat exchanger at the left-side coming from the cold bunker in Fig. (3.14). The hot heat transfer fluid is flowing inside the tube bundle of the heat exchanger countercurrent to the sand. Heat is transferred from the hot medium to the cold sand and the internal energy of the sand is increased. The heated sand exits the heat exchanger on the right side and is transported to the hot bunker, while the cooled heat transfer fluid exits the fluidized bed heat exchanger at the left side of Fig. (3.14). The usage of fine sand ($80 - 100 \mu\text{m}$) keeps fluidization air mass flows low and maximizes the sand side heat transfer coefficient. The heat transmission coefficient is also influenced by the velocity of heat transfer fluid inside the tubes of the heat exchanger. The hot sand can be easily stored in huge hoppers with external and/or internal isolation. For the discharge of a *sandTES* unit, the flow directions of sand and the heat transfer fluid are altered in respect to the charge mode [39].

The advantages of the *SandTES* concept can be summed up as [40]:

- Low exergy losses at the heat transfer due to the countercurrent heat exchange.
- Sand is a cheap, non-toxic and a sustainable storage medium.

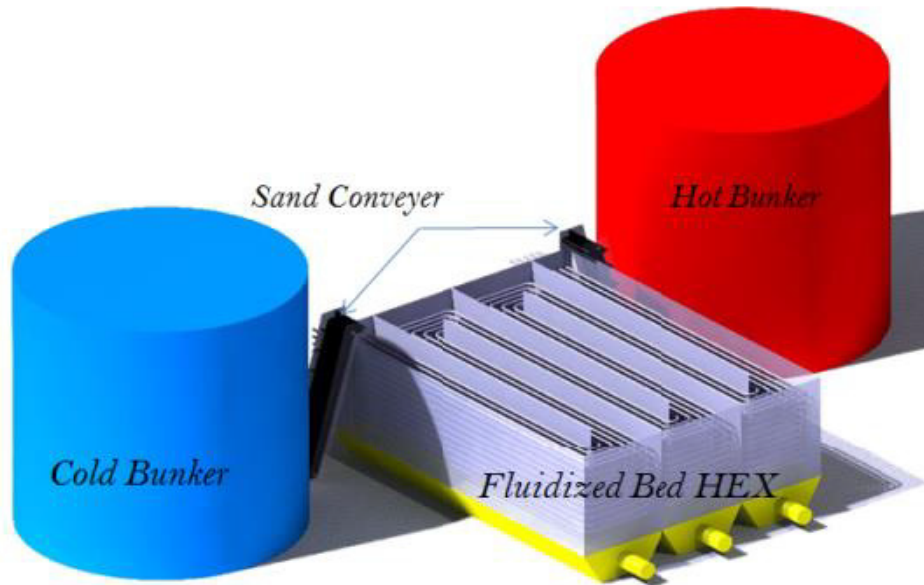


Figure 3.14: Illustration of the *SandTES* concept [38].

- The sand has a lower thermal conductivity in the non-fluidized state, meaning that the storage losses are very low. On the other hand when fluidized the thermal conductivity of the sand is very high.
- Very high melting point of the sand.
- High energy density due to high storage temperature levels.
- The charge and discharge temperatures remain constant after reaching the operational temperature level.
- Very big storage units possible.
- It can be combined with many energy storing concepts.

Chapter 4

Simulation

Several *ETES* systems will be presented and analyzed in this chapter. Firstly the used software is introduced. Then the simple *ETES* configuration featuring a heat pump and a simple Brayton cycle will be examined. Some suggested methods that attempt to increase the roundtrip efficiency follow. Finally the option to utilize and store waste heat and the addition of a transcritical CO_2 Rankine cycle to cool the working fluid are presented.

4.1 Software

In order to perform the simulations for this thesis many process simulation tools like *IPSEpro*, *EBSILON* or *gPROMS* were considered. The chosen software should already have programmed the required unit operations and a thermodynamic property database of CO_2 or at least provide the ability to model all needed components from scratch.

Another important option would be the ability to implement models programmed in other software tools. The *SandTES* project is currently programmed in *MATLAB* hence a link with this software would provide higher flexibility and reduce the modeling effort. A possible solution to this matter would be the software tool *CAPE OPEN* which provides a link among several process simulation software and other programs like *MATLAB*. Although this option exists for *gPROMS* the required add-on is fee-based. *IPSEpro* does not support this link, *SimTech* considered this option but hasn't implemented it into their product.

It was then decided to focus on the process simulations, meaning the utilization of *SandTES* and not the creation of a solid model because of the many parameters that would have had to be taken under consideration, like fluidization values or properties of the sand, that have no impact to the *ETES* system. Therefore *IPSEpro* was chosen as the appropriate software since it provides almost all units and a database of carbon dioxide. The *SandTES* unit is either represented by a heat sink or a heat source, since no other properties are of relevance to the present work.

4.1.1 IPSEpro

IPSEpro [41] is a set of software modules for creating process models and for utilizing these models throughout the lifecycle of process plants. *IPSEpro*'s modules can be used to:

- Calculate heat balances and predict design and off-design performance.
- Verify and validate measurements during acceptance tests.

- Monitor and optimize plant performance on-line.
- Plan modifications and upgrades of existing plants.

Unlike with other programs, *IPSEpro* users are not restricted to predefined models and model libraries. This makes *IPSEpro* a good tool for creating proprietary model libraries.

The core of *IPSEpro* embeds a highly flexible modeling system for calculating heat balances and for simulating processes. *IPSEpro* goes far beyond the capabilities of other available heat balance programs. The Model Development Kit introduces a unique level of flexibility by allowing the creation of new component models or create completely new model libraries.

IPSEpro can also be used for quick process assessments, detailed engineering, design, retrofitting, repowering, and acceptance testing. Its component-level flexibility and component-by-component approach allows to model virtually any type of system.

IPSEpro covers as the entire lifecycle of a process plant from conceptual design to plant operation. There are great advantages of using with *IPSEpro* a single software solution rather than isolated products throughout the lifecycle of a plant. Overall advantages in using *IPSEpro*:

- Short implementation time.
- Users need not to be computing specialists.
- A uniform environment for a wide range of problems.
- New components are easily integrated in an existing system.
- The user can concentrate on the physical background of his/her problem.
- State-of-the-art numerical methods.
- Comfortable graphical user interface without extra costs.
- Low maintenance costs.

The modeling of a turbine or a compressor that calculates the compression or expansion work as in equations (3.10) and (3.11) is not suited with *IPSEpro*, due to the fact that it uses for all state-changes enthalpy differences and because values like the compressibility factor are not included in its database.

Due to the fact that *IPSEpro* uses for all state-changes enthalpy-differences, the creation of a model using for its calculations turbine or compressor work which need values like the compressibility factor or the ability to calculate integrals is not suited for the purpose for this software. Also the missing option to code substance-databases that are not included in the provided libraries, forces the user to elude to another medium to simulate the heat transfer. In this work all heat exchangers are implemented using the media *CO₂-Water* instead of the actual *CO₂-Sand* pairing. The values of the water streams are of no significance for the outcome and should be regarded as a means to an end.

The *SandTES* reactor is simulated as a simple boiler during its discharging phase, when it is heating the heat transfer fluid, and as a *CO₂-Water* heat exchanger, simulating a heat sink in the charging mode, when the heat transfer medium heats the Sand.

4.1.2 EES

EES [42] is a general equation-solving program that can numerically solve thousands of coupled non-linear algebraic and differential equations. The program can also be used to solve differential and integral equations, do optimization, provide uncertainty analyses, perform linear and non-linear regression, convert units, check unit consistency, and generate publication-quality plots. A major feature of *EES* is the high accuracy thermodynamic and transport property database that is provided for hundreds of substances in a manner that allows it to be used with the equation solving capability.

4.1.3 REFPROP

REFPROP [43] is an acronym for REference fluid PROPERTIES. This program, developed by the National Institute of Standards and Technology, calculates the thermodynamic and transport properties of industrially important fluids and their mixtures. These properties can be displayed in tables and plots through the graphical user interface. For this work the NIST standard reference database 23, version 9.1 was used.

4.1.4 CAPE-OPEN

Although the *CAPE-OPEN* effort [44] was not actually used for this work, it was an option that was thoroughly investigated at the beginning, hence it will be presented here briefly. *CAPE-OPEN* stands for Computer Aided Process Engineering - freely available standard specification and it is a set of interface definitions pertaining to interoperability of *CAPE* software:

- Unit Operations.
- Thermodynamics.
- Chemical Compounds (databases).
- Numerics (solvers, sequential modular tools).
- Generic (identification, collections, parameter, life time utilities, error handling, persistence...).

CAPE-OPEN defines an interface set for interactions with thermodynamics and unit operations. The interface set is independent of the simulation application or the unit operation model or the thermodynamic model. This is called a socket-and-plug architecture where the simulation application represents the socket, in which unit operation models and thermodynamic models can plug in. Each socket and plug is responsible for providing their own implementation of the *CAPE-OPEN* interfaces. As a result, for each socket and plug, only one single interface implementation has to be developed and maintained in order to achieve interoperability between all sockets and plugs. This is illustrated in Fig. (4.1). Compared to a scenario where unit operation models or thermodynamic models require a specific interface to each simulation application, the use of *CAPE-OPEN* clearly reduces the effort of software development and maintenance. Currently, the use of unit operation models and thermodynamic models via *CAPE-OPEN* is supported in most commercially available chemical flowsheet simulators.

CAPE-OPEN is currently maintained by *CAPE-OPEN Laboratories Network, CO-LaN* which is also responsible for updating and publishing the *CAPE-Open* specifications. Its members are operating companies, software vendors, academic institutions and other interested parties.

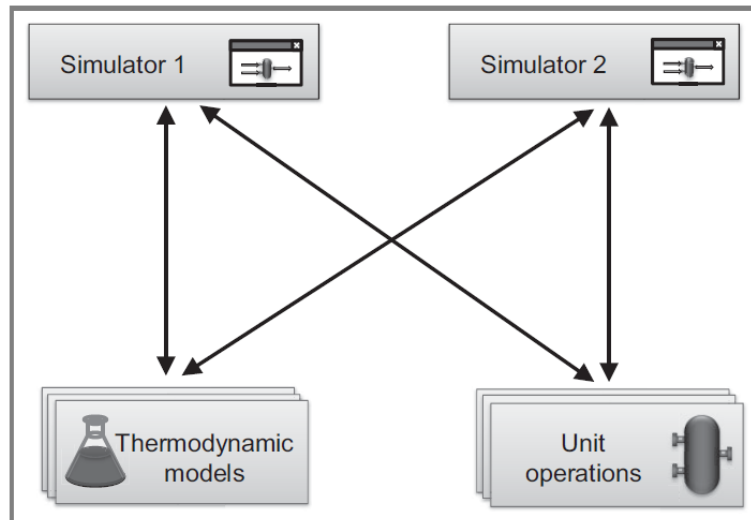


Figure 4.1: Interoperability. Every thermodynamic model and every unit operation can be used in multiple simulation applications. Consequently, every simulation application may select from a variety of unit operations and thermodynamic models [44].

4.2 *ETES* Utilizing Supercritical CO_2 Cycles

In this section several different concepts of *ETES* using supercritical cycles are presented. First the simplest layout combining a high-temperature heat pump and a Brayton cycle is examined. An improved configuration featuring a second turbine stage in the charging cycle follows in order to take advantage of the increase of the specific heat capacity of CO_2 below $150^\circ C$. As a final example a novel concept using an isothermal expander is proposed and analyzed.

In order to achieve an independent stand-alone plant for energy storage two *SandTES* units are required. A high-temperature *SandTES* (*HT-SandTES*) operating at the high-pressure side of the charge cycle, receiving the heat of the heat pump and a low-temperature *SandTES* (*LT-SandTES*) heating the fluid at the low-pressure side of the charge cycle. The *LT-SandTES* is charged by the discharge cycle via the heat at the outlet of the turbine. Because of this necessity, it is not possible to implement a recuperator to the configuration in order to improve the thermal efficiency of the discharge cycle.

An analysis of the temperature-profiles of the sand and the CO_2 , depicted in Fig. (4.2) showed that at temperatures above $350^\circ C$ the temperature-difference between the two media increases leading to high exergy-losses. Therefore the temperature-range from the saturation curve up to $350^\circ C$ was selected for the simulations. The rapid changes of the temperature-differences at the edges of the chosen temperature-range are attributed to the vast change of the specific heat capacity of both media in that region.

In order to make an objective comparison in all presented configurations the electricity generated in the generator of the turbine of the discharge cycle is set to $5 MW$. All mass flows are determined by this setting and by the fact that the stored heat in the *HT-SandTES* and *LT-SandTES* units have to be the same for the *charge* and *discharge* cycles. The potential heat loss can be attributed to the insulation which for the purposes of this work has been neglected, but is not expected to exceed a few percent.

Also it is pursued that the medium at the outlet of the turbine in the charge cycle does not enter the two-phase area. Therefore an indicator measuring the steam quality has been set to

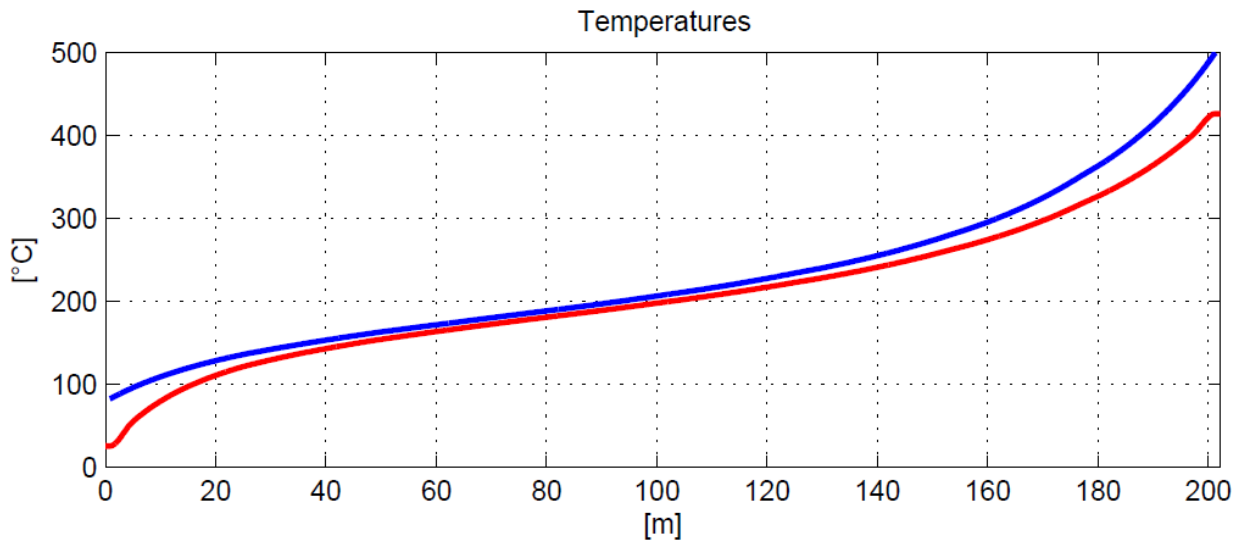


Figure 4.2: Temperature profiles of *Sand* in red and the heat transfer fluid (CO_2) in blue over the length of the heat-exchanger for fluid temperature-values up to $500^\circ C$.

values equal or superior to 1. Actually steam quality values above 1 are thermodynamically not defined, though *IPSEpro* uses this value to show that the current state of the medium is beyond the saturation curve (also negative values are possible which indicate that the medium exists only in the liquid state).

4.2.1 Simple Heat Pump and Brayton Cycle Configuration

The simple *ETES* is illustrated in Fig. (4.3). On the bottom left side of the plot the heat transfer fluid gets compressed to the high-pressure side of the cycle where it charges the *HT-SandTES* unit. Despite the fact that in the operational area of the *HT-SandTES* outlet the temperature is relatively low and the compressibility factor of the CO_2 is low as well a turbine is installed in order to retrieve some expansion work and to improve the roundtrip efficiency. At the turbine outlet a phase indicator is placed to ensure that the gas is not expanded into the two-phase-region. Then the gas has to be heated again to get back to its original state before it enters the compressor so that the cycle is closed. This happens in two steps. First a water-storage unit is used so that the *LT-SandTES* unit does not have to heat the heat transfer fluid from a very low temperature. This option enables the use of a smaller *SandTES* unit making the whole configuration cheaper. Also the changes of the specific heat capacity of the CO_2 in this temperature region can be better approached by the water-storage since many cheap water tanks operating at different temperature levels and with varying mass flows can minimize the exergy-loss. Then the medium is heated up to the compressor entry point by the *LT-SandTES* unit completing the cycle.

On the right side a simple Brayton cycle for discharge is shown. The *HT-SandTES* unit charged in the previously described cycle, now discharges heating the CO_2 on the high pressure side of the cycle. The turbine then expands the gas producing the electricity via a generator. At the low-pressure side, the still warm gas charges the *LT-SandTES* and the water-storage units that were used to heat the heat transfer fluid during the charge cycle. Finally the gas enters the compressor in the vicinity of the critical point where the compressibility factor is at its minimum achieving an improvement of both the roundtrip efficiency and the thermal efficiency of the discharge cycle.

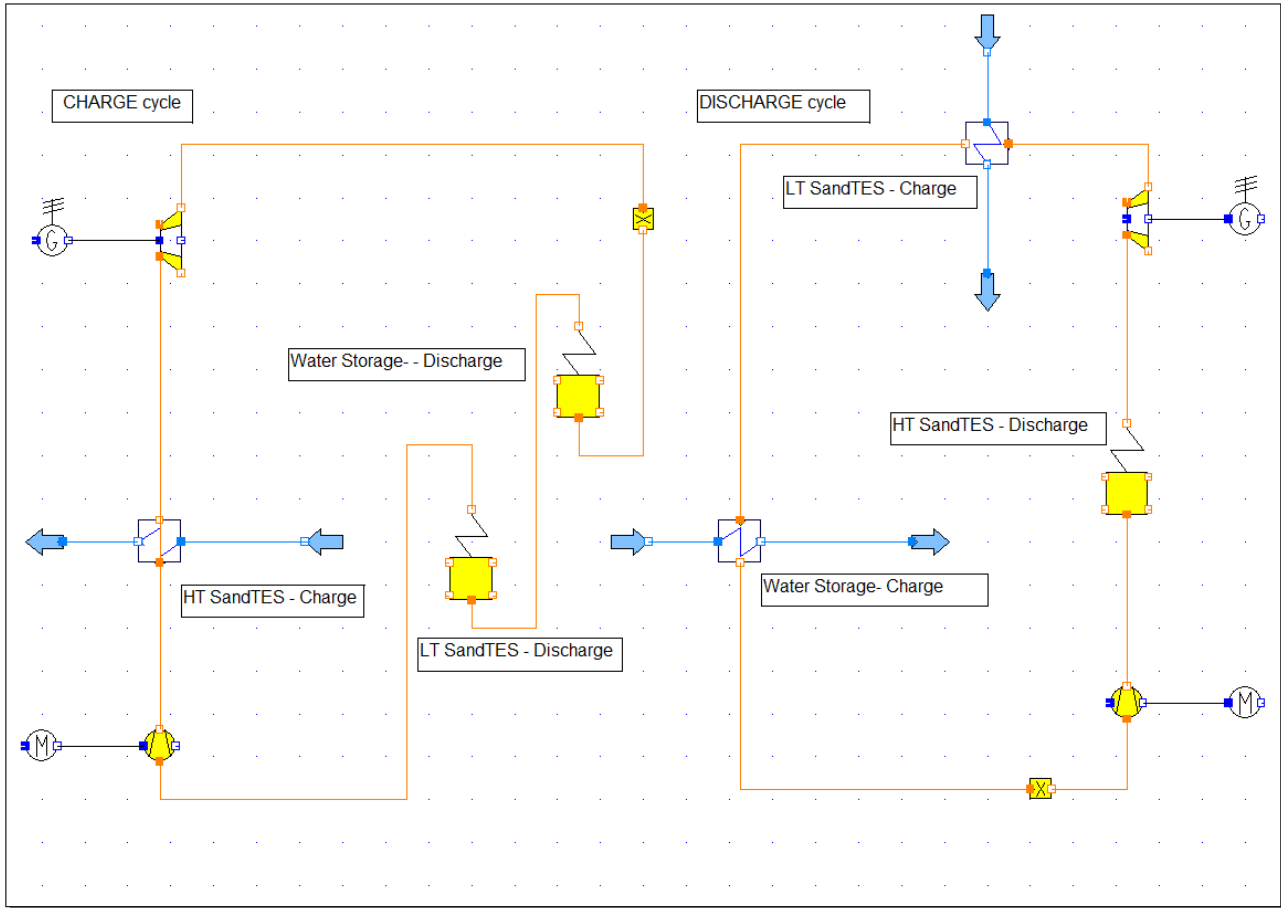


Figure 4.3: Layout of the simple *ETES* configuration in IPSEpro, charging cycle (heat pump) on the left side and discharging cycle on the right side of the screen.

Simulation of Different Sizes of the Heat Exchanger

Before actually being able to start with the parameter study of the CO_2 in different configurations, the optimum geometry and heat-transfer area of the heat exchanger had to be determined. Three cases were considered, named small, medium and large heat exchanger. In the small configuration the heat-transfer area is $A_{HEX}^s = 1029 m^2$, in the medium $A_{HEX}^m = 1369 m^2$ and in the large $A_{HEX}^l = 1700 m^2$.

As can be seen in the blue line of the top right corner of Fig. (4.4)¹ illustrating the large case where the heat transfer medium charges the *SandTES* unit and Fig. (4.5). The *SandTES* unit heats the CO_2 from an initial temperature value of $350^\circ C$ up to $285^\circ C$. The resulting temperature difference that occurs is $\Delta T^l = 65^\circ C$, while for the medium case it is $\Delta T^m = 88^\circ C$ and for small $\Delta T^s = 101^\circ C$ (the green connections in these flowsheets describe the required parameters for the fluidization and are of no relevance for the present work). This means that with increasing heat exchanger-area the exergy losses drop due to a lower temperature difference during heat transfer as can be seen in Fig. (4.6).

Despite the increase of the roundtrip efficiency, the differences between the different cases are about 2% meaning that other parameters like investment costs for larger units, land space etc. have to be taken into account in order to find the most suitable solution. For the purposes

¹The plots are taken from the active fluidization storage *SandTES* project currently under research at the Institute of Energy Systems and Thermodynamics of the Technical University of Vienna

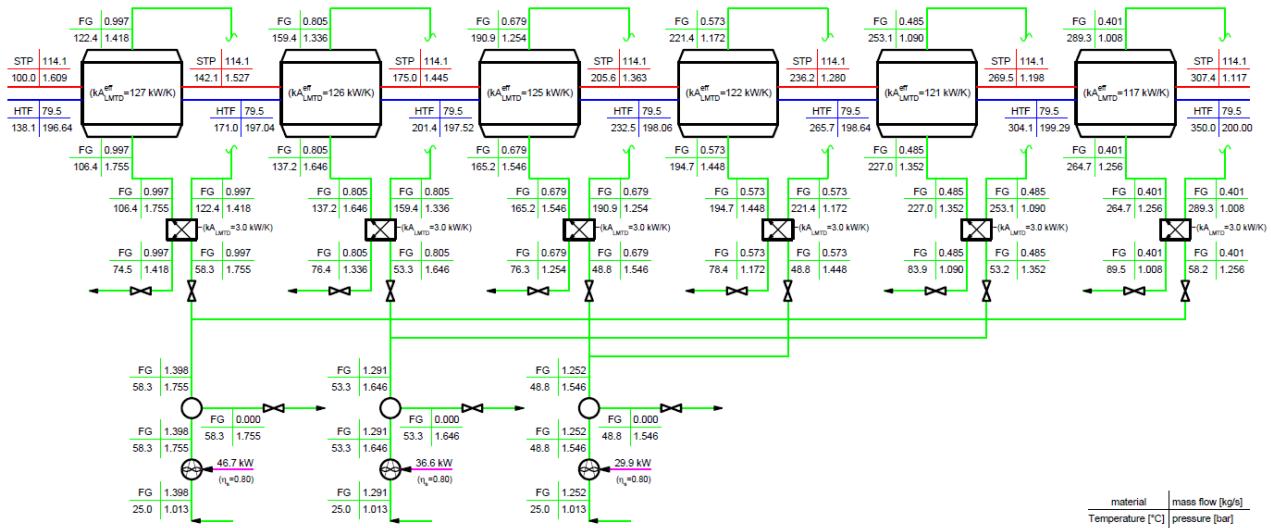


Figure 4.4: Overview of the temperature curves of sand (red) and the heat transfer fluid (blue) in the large configuration during the charging mode.

of this work the large case will be examined since it produces the higher efficiency.

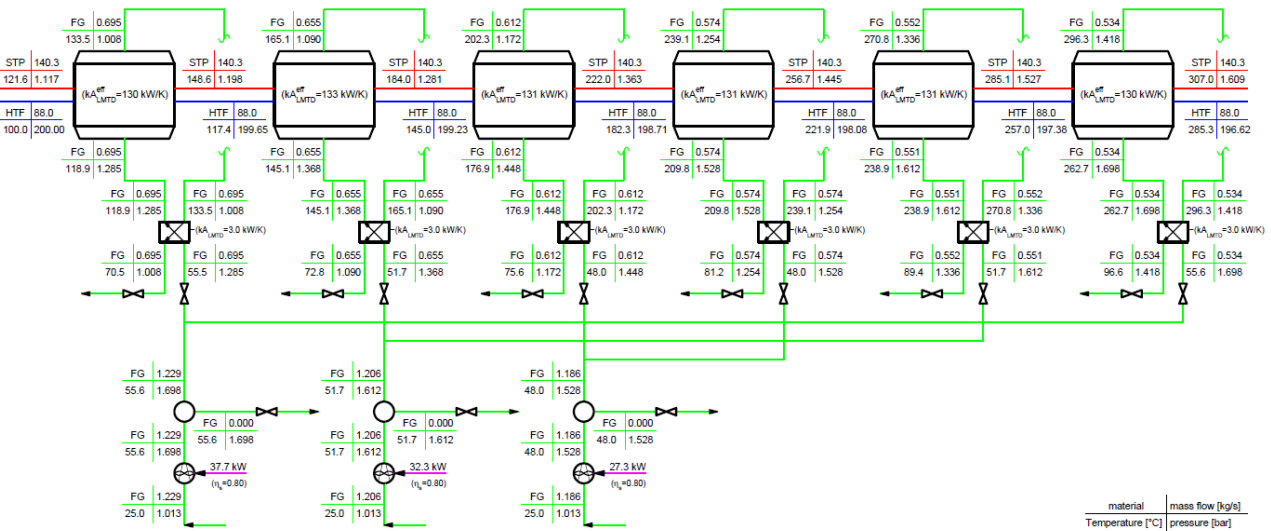


Figure 4.5: Overview of the temperature curves of sand (red) and the heat transfer fluid (blue) in the large configuration during the discharging mode.

Variation of the Compressor Outlet Pressure and Inlet Point

Since the variation of the maximum temperature of the discharge cycle is set due to the limitations provided by the *SandTES* unit, the optimization of the system can only be altered by the variation of the compressor outlet pressure and the inlet point of the compressor. For this point, most previous analyses have been limited to supercritical conditions, therefore other options will be investigated, such as a transition from supercritical to subcritical conditions.

For the first parameter study the roundtrip efficiency will be examined while the compressor outlet pressure varies from 150 – 250 bar. The entry point of the compressor will be set right at

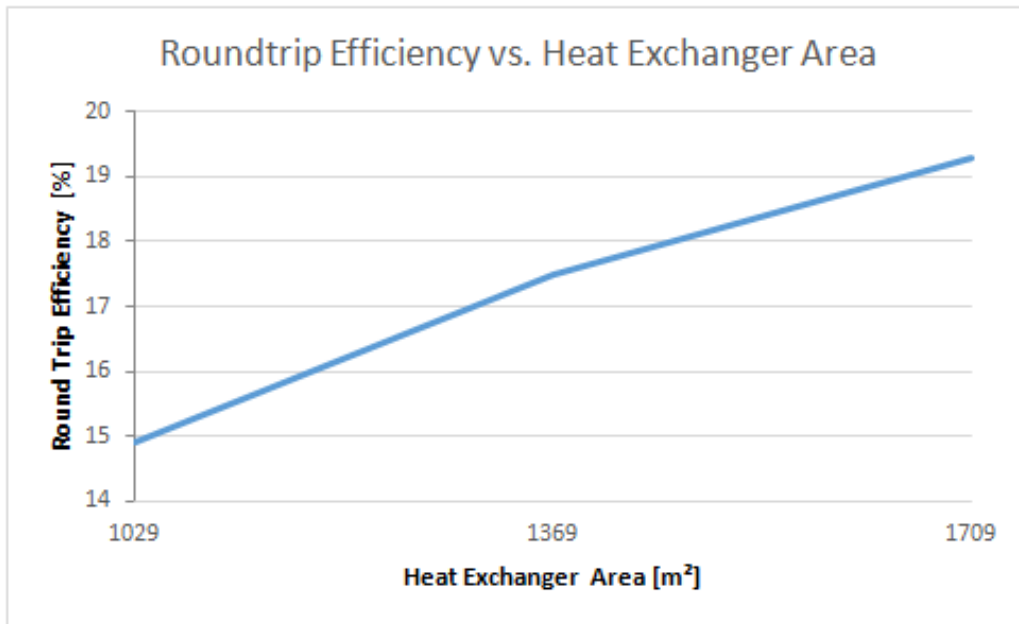


Figure 4.6: Change of the roundtrip efficiency for the different *SandTES* cases.

the critical point, where a minimum of the compressibility factor occurs and the charge cycle will operate at a high pressure side at 200 *bar*. Also the pressure range is selected in such a way that the vapor content at the outlet of the charge turbine is not exceeding the value of $x = 0.95$ in order to avoid erosion on the turbine blades.

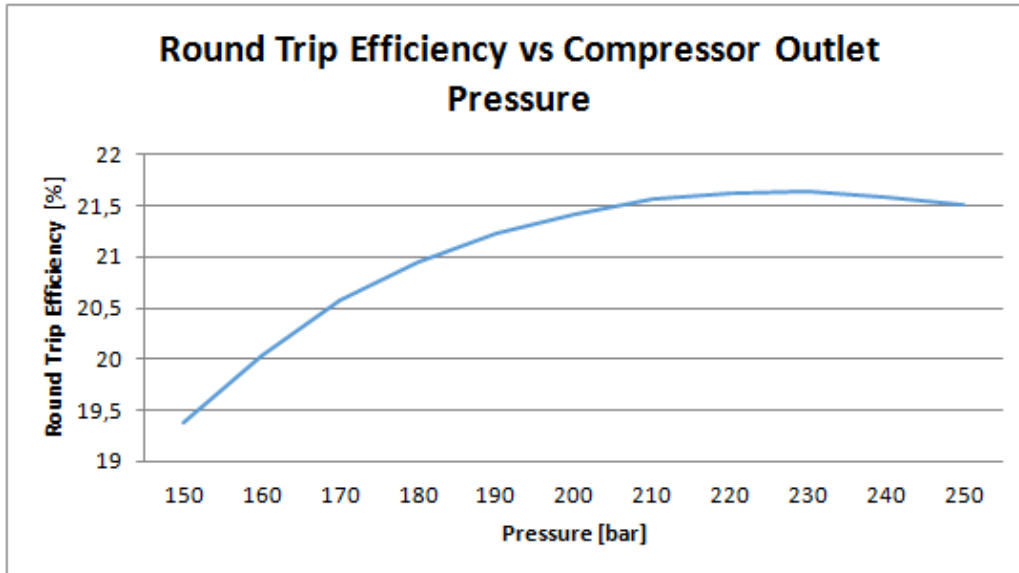


Figure 4.7: Change of the roundtrip efficiency for various compressor outlet pressures.

As can be seen in Fig. (4.7) the roundtrip efficiency increases with ascending compressor pressure outlet. This behavior is expected since at a higher turbine inlet pressure and with a constant state at the turbine outlet the pressure ratio rises. The fact that is worth to mention in this result is that approximately above 200 *bar*, the roundtrip efficiency does not increase with the same rate like until 200 *bar*. This means that at higher values the payoff of the pressure increase gets lower and lower. This behavior has also been observed in other studies, hence the

pressure should be set at 200 *bar* in order to achieve an optimum trade-off between roundtrip efficiency and the system components. This is mainly because above about 200 *bar* the isobaric lines are closer to each other than before, resulting in smaller ascending enthalpy differences.

In order to examine the influence of the compressor work dependency on the compressibility factor near the critical point to the roundtrip efficiency, a parameter study was performed along the saturation curve starting from 35 *bar* up to the critical point. The same conditions as in the previous example are applied to the charge cycle while the compressor outlet pressure is set to 200 *bar*.

The resulting curve is illustrated in Fig. (4.8). An increase in the roundtrip efficiency is discernible. Although, this behavior has to be attributed more to the increase of the turbine pressure ratio than the actual change of the compressibility factor in this region. Although also a decrease in the slope of the curve can be seen. This indicates that when approaching the critical point and therefore lower values of the compressibility factor the smaller compressor work affects the roundtrip efficiency.

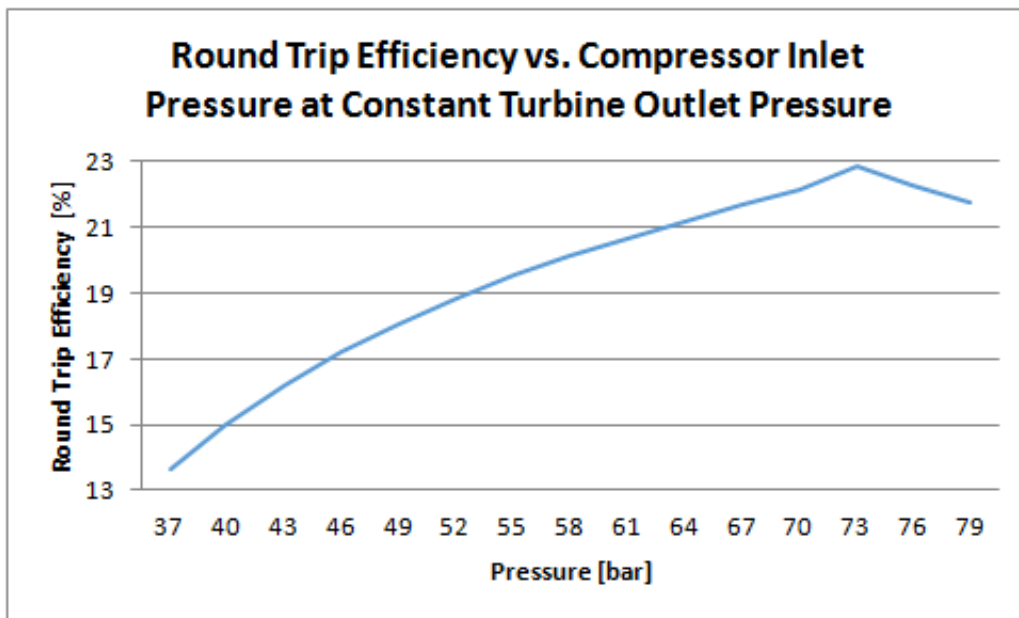


Figure 4.8: Change of the roundtrip efficiency for various compressor inlet pressures levels at constant outlet pressure.

In order to make a more objective approach, another parameter study but this time at constant pressure ratio should be performed so that clearer conclusions can be made about this property of CO_2 . Again the compressor inlet point is set at the saturation curve starting at 35 *bar*. The compressor pressure ratio is set to 2.7 meaning that the inlet pressure of the turbine varies. The results are shown in Fig. (4.9). This time the curve has the opposite curvature. This means that the slope of the curve increases as the inlet point approaches the critical point showing that the drop of the compressibility factor has an impact on the system. A maximum can again be seen at the region of the critical point after which the roundtrip efficiency drops again due to the increase of the compressibility factor and the higher pressure levels that are reached. As already mentioned above about 200 *bar* the isobaric lines are nearer to each other than before resulting in smaller ascending enthalpy differences.

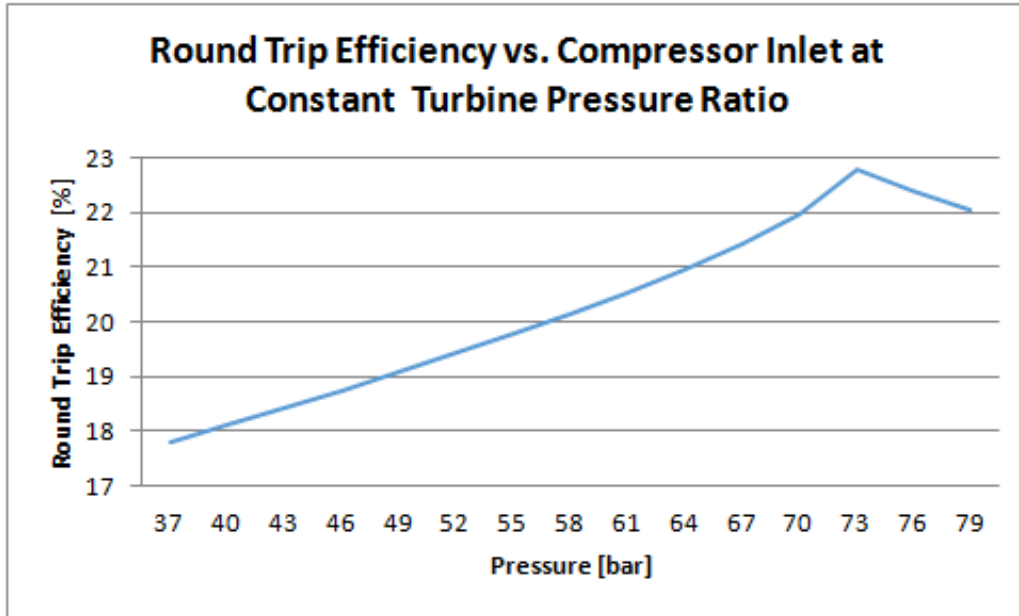


Figure 4.9: Change of the roundtrip efficiency for various compressor inlet pressures at a constant turbine pressure ratio.

4.2.2 Implementation of a Second Turbine in the Charge Cycle

In this section the implementation of a second turbine stage in the charge cycle will be tried out and the results will be analyzed. The idea is that the additional turbine stage operating between values with a higher compressibility factor as can be seen in Fig. (3.13), should improve the roundtrip efficiency. On the other hand the increase of the specific heat capacity mitigates this effect. The T - s diagram of Fig. (4.10) shows the working area of the second turbine and the isenthalpic curves in this region.

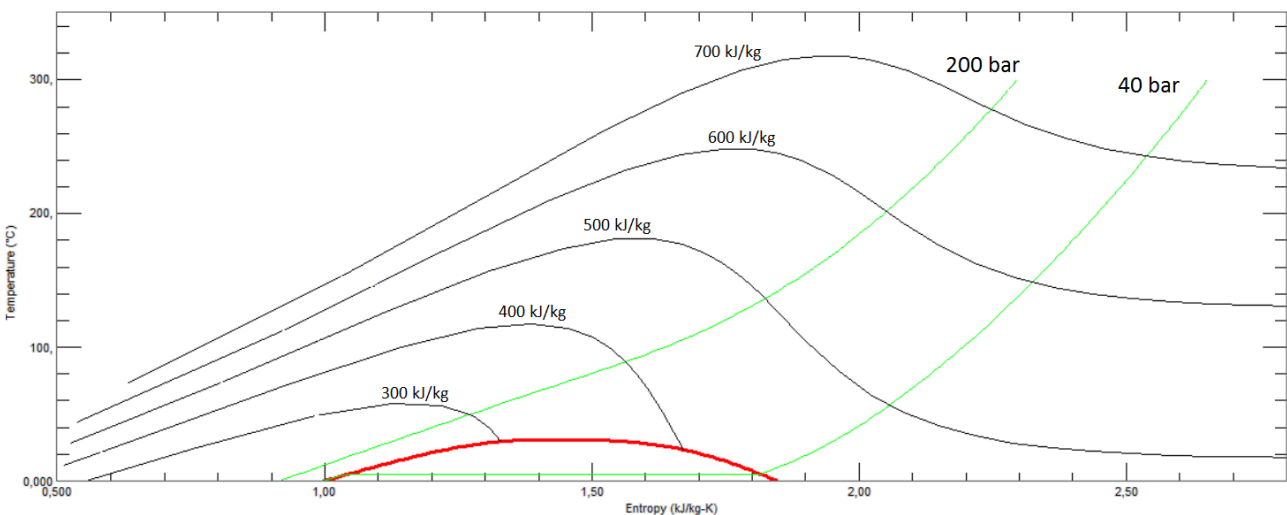


Figure 4.10: Temperature vs. entropy plot with the saturation (red), isobaric (green) and isenthalpic curves (black), (source: REFPROP).

In order to avoid the high exergy losses due to the rise of the specific heat capacity of the CO_2 in the interval below $200^\circ C$ the temperature difference of the heat transfer CO_2 -sand should be kept constant via the reduction of the mass flow.

The heat flow is proportional to the temperature difference, the specific heat capacity and the mass flow. So in order to keep it steady, with the same temperature difference, the mass flow has to be reduced because of the increasing heat capacity. The superfluous mass flow can be redirected into a second turbine and hence mitigating the exergy loss and producing more electricity.

The flowsheet of the charge cycle can be seen in Fig. (4.11). Here the *HT SandTES* is divided into 2 stages. In the first stage the whole mass flow of the heat transfer fluid is used to heat the sand and in the second stage a portion of the mass flow is extracted achieving a constant temperature difference.

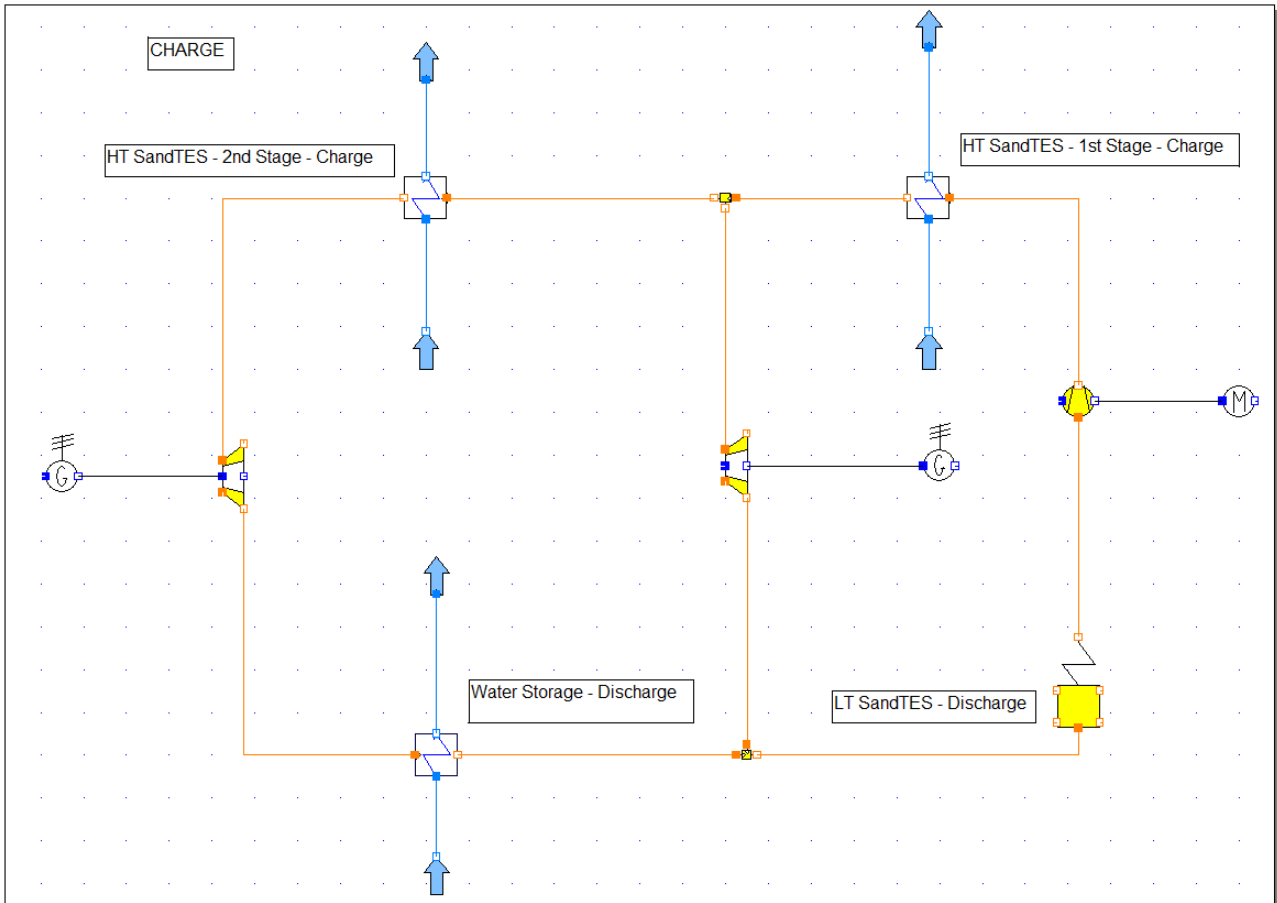


Figure 4.11: Flowsheet of the charge cycle in an *ETES* system utilizing the increase of specific heat capacity of CO_2 at temperatures below $150^\circ C$ in *IPSEpro*.

Since it is not possible to program the properties of the sand in *IPSEpro* the calculations regarding the recovered roundtrip efficiency have been performed in *EES* as follows:

Up to $200^\circ C$ the temperature difference between the CO_2 and the sand is roughly constant at about $\Delta T = 25^\circ C$ as can be seen from Fig. (4.4). After that point, the temperature difference rises. So in order to keep the heat flow constant:

$$\dot{Q} = \dot{m} * c_p * \Delta T \quad (4.1)$$

Regarding the increase of c_p , \dot{m} has to be adapted. The following values can be taken from the *VDI-Heat Atlas*: $c_p(\theta = 200^\circ C, p = 200 \text{ bar}) = 1,383 \frac{kJ}{kg * K}$, $c_p(\theta = 150^\circ C, p = 200 \text{ bar}) =$

$1,632 \frac{kJ}{kg \cdot K}$ and $c_p(\theta = 100^\circ C, p = 200 \text{ bar}) = 2,367 \frac{kJ}{kg \cdot K}$. So a mean specific heat capacity for this interval at $p = 200 \text{ bar}$ can be calculated as:

$$c_{pm} = \frac{c_p(\theta = 200^\circ) + c_p(\theta = 150^\circ) + c_p(\theta = 100^\circ)}{3} = 1.794 \frac{kJ}{kg \cdot K} \quad (4.2)$$

This means that in this area, the proportion of the mean specific heat capacity c_{pm} in relation to the heat capacity $c_p(\theta = 200^\circ C, p = 200 \text{ bar})$ is:

$$\frac{c_{pm}}{c_p(\theta = 200^\circ C, p = 200 \text{ bar})} = 1.297 \quad (4.3)$$

Now assuming that the temperature difference as well as the heat flow stay constant, the relation of the mass flow $\dot{m}_{(\theta=100-200^\circ C)}$ in the interval ($\theta = 100 - 200^\circ C$) to the initial mass flow \dot{m}_{init} can be calculated as:

$$\frac{\dot{m}_{init}}{\dot{m}_{(\theta=100-200^\circ C)}} = \frac{c_p(\theta = 200^\circ C, p = 200 \text{ bar})}{c_{pm}} = \frac{1}{1.297} = 0.771 \quad (4.4)$$

Hence only:

$$\dot{m}_{(\theta=100-200^\circ C)} = \frac{\dot{m}_{init}}{1.297} = 0.771 * \dot{m}_{init} \quad (4.5)$$

is required to charge the *HT-SandTES* in the interval $\theta = 100 - 200^\circ C$. The remaining 22.9% of the mass flow can be redirected into the second turbine. Assuming that the fluid enters the turbine at $200^\circ C$ and 200 bar , and exits at $95^\circ C$ (in order to meet exactly the temperature of the other portion of the fluid that is heated by the water storage, so that no entropy of mixture occurs) and 32 bar (these are the same values as in the configuration in the previous chapter so that an realistic comparison can be made), the power produced by the generator connected to the turbine can be calculated as:

$$P = \dot{m}_{split} * \eta_{Tmech} * \eta_{Gen} * (h_{(\theta=200^\circ C, p=200 \text{ bar})} - h_{(\theta=95^\circ C, p=32 \text{ bar})}) \quad (4.6)$$

Now replacing the mass flow with that from equation (4.5) calculated value and assuming the following efficiencies: $\eta_{Tmech} = 0.9$ and $\eta_{Gen} = 0.99$ and also with the enthalpy values from *REFPROP*, the additional specific work can be calculated as:

$$\frac{P}{\dot{m}_{init}} = 0.229 * 0.9 * 0.99 * (597.79 \frac{kJ}{kg} - 548.26 \frac{kJ}{kg}) = 10.11 \frac{kJ}{kg} \quad (4.7)$$

In the previous chapter the required mass flow to charge the *HT-SandTES* was $\dot{m}_{init} = 111.3 \frac{kg}{s}$ so the additional power produced via the implementation of a second turbine is:

$$P = \dot{m}_{init} * 10.2 \frac{kJ}{kg} = 111.3 \frac{kg}{s} * 10.11 \frac{kJ}{kg} = 1.13 \text{ MW} \quad (4.8)$$

At this point the 22.9% of the mass flow that gets split has to be subtracted from the calculation of the first turbine. This one operates between 200 and 32 *bar* as well but between 138 and $-2^\circ C$. With the same efficiencies as the second turbine and with the enthalpy values acquired again from *REFPROP* is calculated as:

$$P = 0.229 * 111.3 \frac{kg}{s} * 0.9 * 0.99 * (502.87 \frac{kJ}{kg} - 434.6 \frac{kJ}{kg}) = 1.55 \text{ MW} \quad (4.9)$$

As a matter of fact the impact of the higher compressibility factor gets overshadowed by the change of the specific heat capacity. The additional produced power is 1.13 MW while the lost is 1.55 MW , worsening the output by 0.42 MW .

Therefore the second turbine stage is not beneficial for the roundtrip efficiency. Of course via the mass flow splitting, less CO_2 needs to be heated by the water storage which is charged in the *discharge* cycle. So the heat not needed to charge the water storage unit could be used for another purpose like providing the heat source for an ORC cycle. But again the gains would be small while the configuration of the system would get more complex and expensive.

4.2.3 Supercritical *ETES* with an Isothermal Expansion

A limiting factor for the previous described supercritical *ETES* concepts is that a second *SandTES* unit is required to provide the necessary heat on the low pressure side of the *charge* cycle. This unit is charged by the low pressure side of the *discharge* cycle therefore not allowing the potential use of a recuperator in this cycle. This fact limits the thermal efficiency of the cycle and therefore more heat is required to warm up the working fluid up to the turbine inlet temperature.

A possible solution to this problem would be the implementation of an isothermal expander instead of a turbine in the *charge* cycle. In this way, the temperature of the charge cycle would not go below the outlet temperature of the *SandTES* unit, since no isentropic expander is used. After the isothermal expansion the fluid would be right at the compressor inlet point, closing the cycle.

The option of an isothermal expander has already been proposed by Kim et al. [9] and was described in chapter (2.3.2). The expander model for the ideal isothermal expansion is based on the following equations.

The specific heat input q_T between input (index 1) and output (index 2) is calculated as:

$$q_T = T * (s_2 - s_1) \quad (4.10)$$

While the specific expansion work w_t is:

$$w_t = q_T - (h_2 - h_1) \quad (4.11)$$

The power P_T produced by the generator, depends on the mass flow through the expander \dot{m} and a efficiency coefficient η_{isothT} to approximate a real expansion:

$$P_T = \dot{m} * \eta_{isothT} * w_t \quad (4.12)$$

The configuration in *IPSEpro* is illustrated in Fig. (4.12). The compressor entry point in the *discharge* cycle is again set near the critical point where less input work is required and the power produced by the generator attached to the turbine in the *discharge* cycle is set to 5 MW . The mass flows of the two cycles are combined in such way, so that the heat stored in the *SandTES* unit in the *charge* cycle is the same as the discharged heat in the *discharge* cycle.

Two different discharging cycles will be analyzed and compared, these are:

- A Brayton cycle with a recuperator and
- a re-compression cycle.

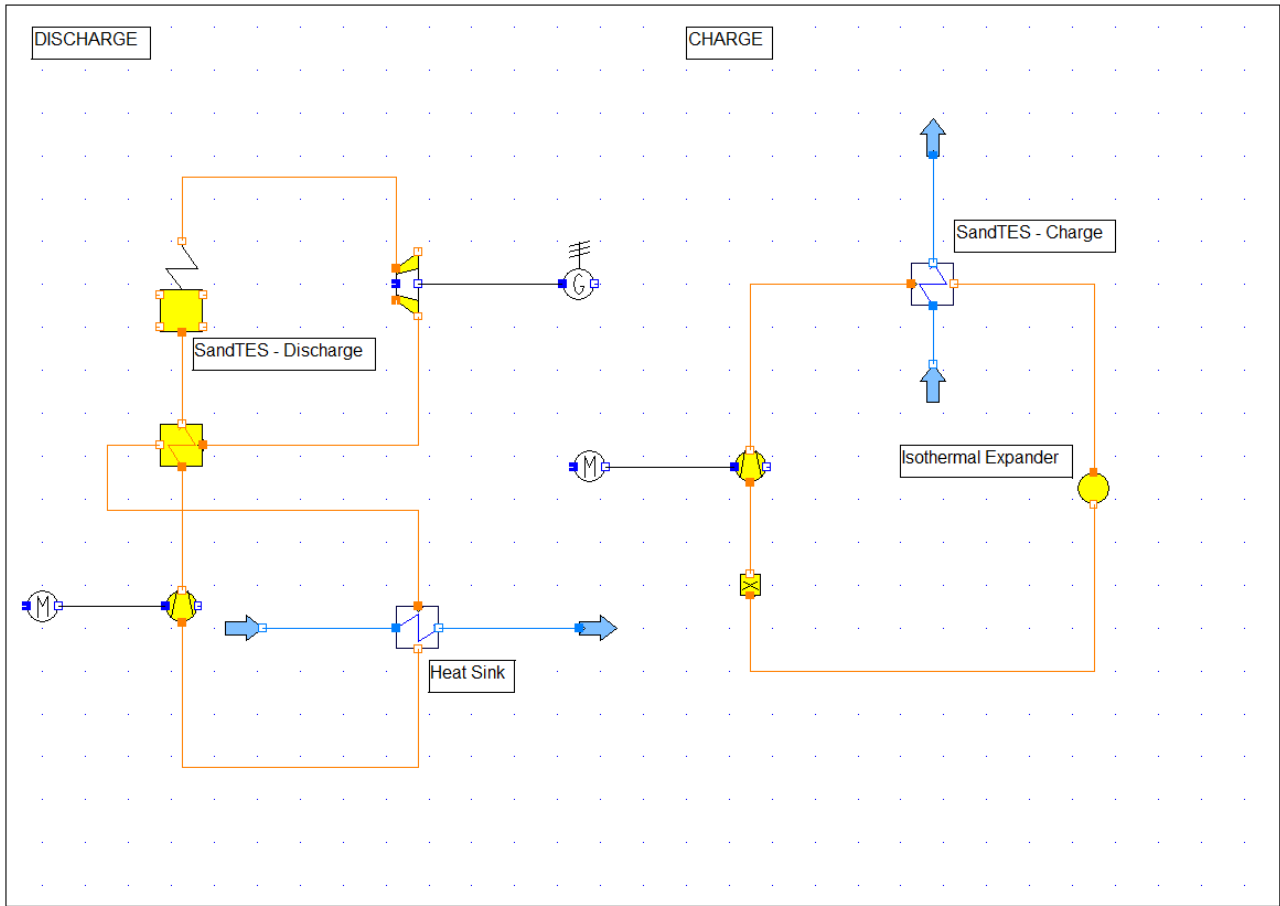


Figure 4.12: Layout of the isothermal *ETES* cycle with a Brayton cycle with a recuperator in *IPSEpro*.

For all cycles the turbine as well as the compressor efficiencies are set to $\eta_T = \eta_C = 0.9$, a temperature difference of $\Delta T = 10^\circ\text{C}$ is assumed on the low temperature side of the recuperator, the compressor inlet temperature is set to 32°C (so that the two phase region is avoided) and all pressure losses are neglected. The turbine inlet pressure is set to 200 bar , while the turbine pressure ratio is varied. The efficiency of the isothermal expander will be assumed at $\eta_{isoT} = 0.7$. All used *discharge* cycles as well as some more are thoroughly presented by Dostal in [34].

While the *discharge* cycle will vary, the *charge* cycle will stay the same operating at a high pressure level of 200 bar , while the compressor inlet temperature has to be 138°C as it follows from the conditions of the *SandTES* unit.

Simple Brayton Cycle

This cycle is the simplest gas cycle used for energy production. It consists of a compressor, turbine, a heat source (in this case a *SandTES* unit) a heat exchanger and a cooling unit. In general the thermal efficiency of this cycle is not high, however a comparison with other cycles will highlight the contribution of each arrangement to the efficiency. The layout can be seen in Fig. (4.13).

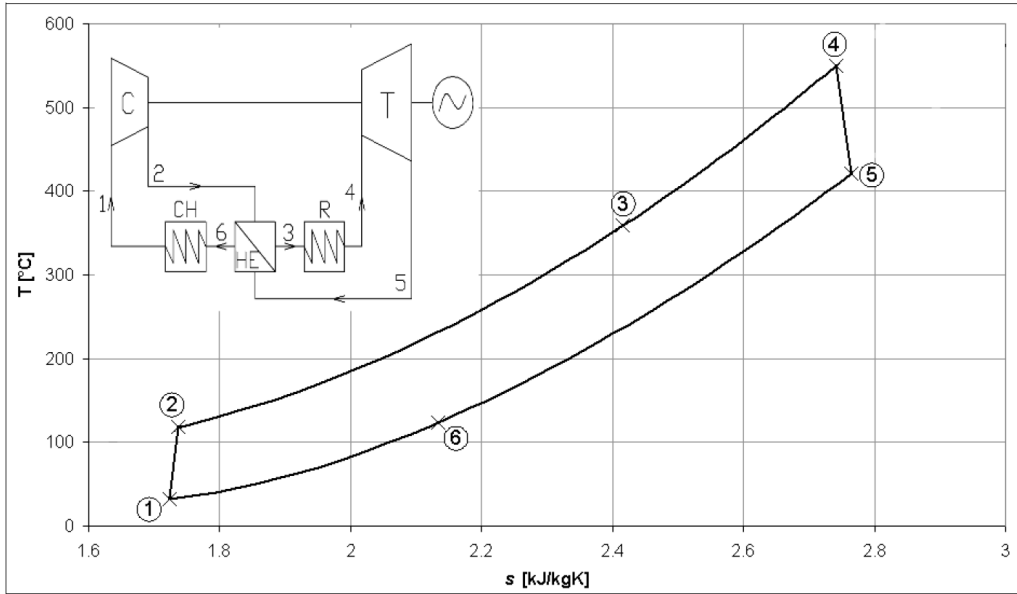


Figure 4.13: The simple Brayton cycle with a recuperator [34].

Re-compression Cycle

This cycle shown in Fig. (4.14), introduces a second compressor, while two recuperators are used, one operating at temperatures above and the other below approximately 150°C .

Before cooling, the flow is split into two streams. One passes the recompression compressor and the other flows through the cooler to the main compressor. The flows, having the same pressure and temperature, are mixed again at the outlet point of the recompression compressor. Hence the pinch point problem is avoided due to the lower mass flow at the high pressure side of the low temperature recuperator. This means that the specific heat capacity is equal on both sides. This system rejects less heat and therefore the thermal efficiency of the cycle is improved.

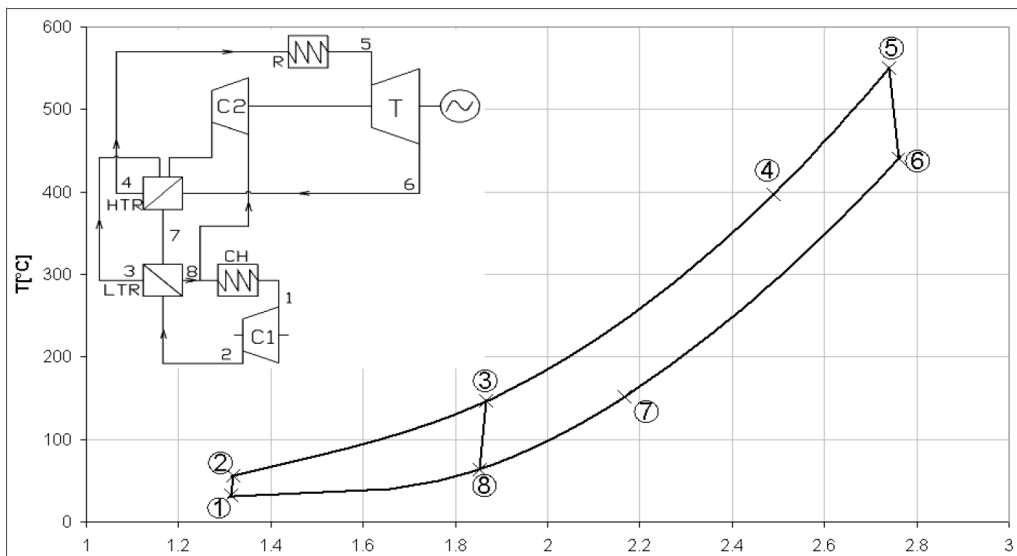


Figure 4.14: The re-compression cycle [34].

Analysis and Comparison

The results of the analysis are presented in Fig. (4.15). The simple Brayton cycle results in a higher roundtrip efficiency up until a turbine pressure ratio of about 2.3. The maximum occurs at a turbine pressure ratio of 1.5, although the mass flow required at this point is extremely high due to the fact that the enthalpy differences are low. As already mentioned the power output of the *discharge* cycle has been set to 5 MW. This means that by changing the pressure ratio the mass flow of the *charge* cycle changes, while the *SandTES* inlet temperature in the *discharge* cycle depends on the outlet pressure of the turbine. Hence the lower the pressure, less heat can be recovered via the recuperator.

On the other hand, the recompression cycle utilizes this fact via the mass flow splitting to achieve a higher recuperator efficiency. This phenomenon gets amplified at lower pressure levels (at higher turbine pressure ratios) since the low temperature recuperator will always be able to heat the medium up to a set value. The high temperature recuperator will then be able, with equal mass flows on the two sides, to heat the medium up to higher temperature levels.

The simulations performed on this cycle had to be stopped at a turbine pressure ratio of 2.5 because at this point the set mass flow is not sufficient to be heated via the low temperature recuperator. With further adjustment to the mass flow split even higher turbine pressure ratios are possible further increasing the roundtrip efficiency of the configuration.

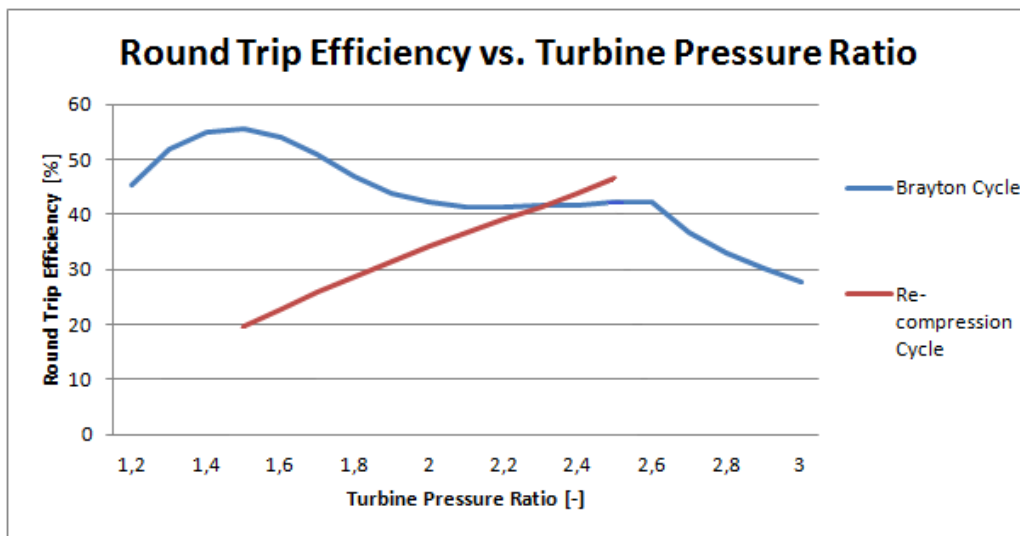


Figure 4.15: Comparison of the roundtrip efficiency of the two proposed discharge cycles for an isothermal *ETES* system.

In the previous analysis the mass flow fraction of the split to the whole mass flow was kept constant at 0.3. In order to further illustrate the impact this setting has onto the roundtrip efficiency, another study was performed by varying the mass flow at a constant turbine pressure ratio of 2.4. At this value the previously proposed layouts have about the same efficiency, therefore the results can show how the mass flow variation further improves the cycle.

At higher mass split fractions a lower portion is heated via the low temperature heat exchanger. This means that at the high temperature heat exchanger, where the difference of the specific heat capacity between the two pressure levels is much lower, more heat can be recovered. This means that less heat needs to be provided by the *SandTES* unit. Accordingly the mass flow of the *charge* cycle drops hence reducing the compressor work input.

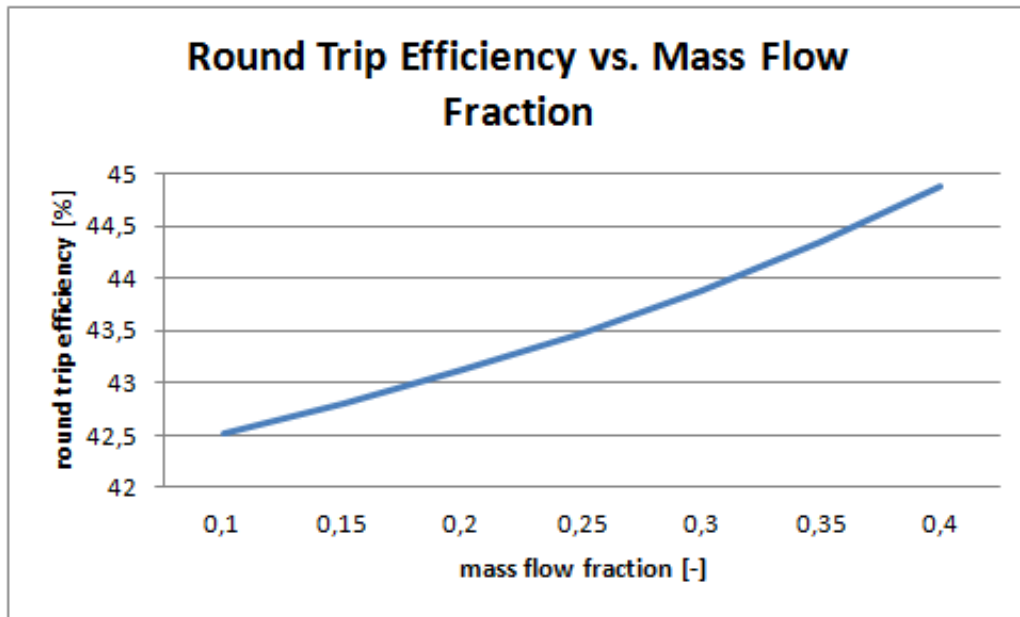


Figure 4.16: Roundtrip efficiency vs. mass flow split fraction of an isothermal *ETES* system for a constant turbine pressure ratio.

The results are presented in Fig. (4.16). The frame has been set to 0.15 – 0.5 since outside of this interval the minimum temperature requirements for the heat exchangers are no longer fulfilled. It can be seen that the roundtrip efficiency rises with higher mass flow fractions, this is mainly due to the higher efficiency of the high temperature recuperator that occurs.

4.3 Combined Heat and Energy Storage

It was shown in the previous sections that the limiting factor of supercritical CO_2 *ETES* systems is that heat is required in order to warm up the working fluid on the low pressure side of the *charge* cycle. An option to reduce this problem is the implementation of an isothermal expander as shown in chapter (4.2.3).

Another option, that combines electrothermal energy and waste-heat recovery and storage would be to utilize the potential waste heat to warm up the working fluid in the *charge* cycle or to use it in addition to the heat provided by the *SandTES* unit. In this way, both the roundtrip efficiency would rise and the waste heat would be recovered. On the other hand the system would no longer be site independent but would rely on the availability of some kind of waste heat.

At first the Brayton cycle utilizing the waste heat will be analyzed. The heat input is assumed to be $10 MW_{th}$ at about $300^\circ C$. This temperature level was chosen as all previous simulations were performed for this case. The waste heat will just decrease the required heat input of the *SandTES* unit, hence decreasing the required mass flow in the *charge* cycle.

The other option would be to use the waste heat instead of the *LT-SandTES* unit to heat up the working fluid on the low pressure side of the *charge* cycle. With this configuration it would be possible to add a recuperator into the configuration. Finally, the increase in the efficiency of the cycle will be compared with the independent *ETES* systems presented in section (4.2.1).

4.3.1 Utilizing Waste Heat in Addition to the Two SandTES Units

In this section it will be shown how the simple Brayton *ETES* system can be improved by the additional utilization of waste heat. The turbine inlet point will be set at 200 bar and 285 °C and the turbine pressure ratio is set to 2.7. The compressor *discharge* cycle is set in such a way that the two phase area is avoided.

The amount of added waste heat will just be subtracted from the needed input by the *HT-SandTES* unit resulting in a lower mass flow in the *charge* cycle, hence reducing the power needed for the compressor, which is the component that needs the most power input of the system.

Simulations show that the increase of the roundtrip efficiency of the system, without taking into account the waste heat input, is about 12.5 %. The efficiency of the basic *ETES* system rose with the addition of the waste heat to 35.1 %. These values occur at the predefined conditions for the waste heat parameters, in general the more heat available the more the efficiency of the system will increase.

4.3.2 Replacement of the *LT-SandTES* Unit with Waste Heat

In the previous example the waste heat was used as an addition to the heat input of the *HT-SandTES* unit. Now it will be used to replace the *LT-SandTES* unit at the low pressure side of the *charge* cycle, hence enabling the use of a recuperator in the *discharge* cycle.

As already mentioned, in order to provide the heat needed to warm up the working fluid in the *charge* cycle, if an independent system is pursued, the option of a recuperator must be relinquished in the *discharge* cycle, because the heat is needed to charge a second *SandTES* unit. This limitation can be remedied with the addition of another heat source, in this case waste heat.

These settings increase the roundtrip efficiency for about 8 % to 38.85 %. For the same parameters as in the simple *ETES* system, 8 MW_{th} are required in order to achieve an electricity production of 5 MW . This means that less heat is required than in the previous case. If the same heat input is assumed the turbine produces about 1.2 MW more output. Although, despite the increased energy output the roundtrip efficiency stay the same since it is not dependent on the output.

4.3.3 Comparison with an Independent *ETES* System

An overview of the results is given in Table (4.1). Both cases improve the roundtrip efficiency significantly. The replacement of the *LT-SandTES* unit improves the cycle by 8 % while an addition of 8 MW_{th} boosts the efficiency by about 12.5 %.

It would be also possible to combine the two cases, meaning that waste heat warms up the working fluid on the low pressure side of the *charge* cycle as well as reduces the required heat by the *HT-SandTES*. Such a configuration would lead, depending on the waste heat available, to even higher roundtrip efficiency values.

Other factors that could be taken under consideration are the fluctuating electricity price during night and day, in order not only to pursue the maximum electricity output but also to minimize the operational costs of the plant. Other cycles could be tried out including the recompression cycle proposed for the isothermal system, or the implementation of a second turbine stage in the *discharge* cycle.

Configuration	Roundtrip efficiency	Efficiency improvement compared with the simple <i>ETES</i> system
Simple <i>ETES</i> System without recuperator	22.64 %	–
Heat input reduction by waste heat ($8 MW_{th}$)	35.1 %	12,46 %
Replacement of the <i>LT-SandTES</i> via waste heat	30.85 %	8,21 %

Table 4.1: Overview of the improvement of the roundtrip efficiency of the simple Brayton *ETES* system through the utilization of waste heat.

4.4 Improvements through the Addition of a Transcritical CO_2 Cycle

In the previous flowsheets that make use of a recuperator, the working fluid enters the cooler at about 74 bar and 104°C . Under these circumstances it would be possible to use this energy flow as the heat source for an *ORC*. There are many working fluids that could be used for the *ORC*, but since this work focuses on CO_2 this medium will be used despite its possible drawbacks in the heat exchange and the fact that its critical point is located at a relatively low temperature level. Because of the low critical temperature and high operating pressure, the cycle is not a real Rankine cycle since at the high pressure side the fluid transfer from the liquid directly to the vapor phase. A cycle like this is called a transcritical *ORC*.

The turbine outlet point is set at 34.85 bar , that is the pressure at which in the two phase area the CO_2 has a temperature of 0°C and so that no condensation occurs. In this way an ice storage unit can be used as a heat sink to condensate the working fluid until the pump entry. The maximum turbine inlet pressure that can be achieved is 135 bar , beyond that point the provided heat is not enough to heat the working fluid of the *ORC*. On the other hand the minimum entry pressure is set at 80 bar so that the working fluid does not enter the two phase region (the critical pressure is at 73.75 bar). For all cases the mass flow of the primary cycle is set to $1 \frac{\text{kg}}{\text{s}}$ and the mass flow in the *tORC* varies because of the changing enthalpy difference but stays in the region of about $0.55 \frac{\text{kg}}{\text{s}}$.

The produced electrical power is shown in Fig. (4.17). As expected the produced power increases at a higher turbine pressure ratio. Though the curve is not linear, its slope decreases as the pressure rises. This is attributable to the decreasing mass flow of the *ORC* on the one hand but mainly to the increase of the specific heat capacity in this temperature range.

For the further simulations the turbine inlet pressure is set to 130 bar since at this point both an acceptable heat exchanger efficiency and a high work output occur. The two systems that can be improved by this additional cycle are the Brayton cycles with a recuperator. Both have exactly the same cooler entry point at 74 bar and 104°C but different mass flows. The mass flow of the isothermal *ETES* system is $71.32 \frac{\text{kg}}{\text{s}}$ while the mass flow of the system utilizing waste heat instead of a *LT-SandTES* unit is $87.54 \frac{\text{kg}}{\text{s}}$.

Since the mass flow is higher, it would be assumed that the isothermal cycle would be less improved than the cycle utilizing waste heat, but due to the higher work input in this cycle both systems are improved for about the same amount. The efficiency of the isothermal cycle improves to 57.39% at an additional production of 1.33 MW . The efficiency of the system using waste heat improves to 52.07% at an added 1.63 MW . Despite the fact that about 0.3 MW

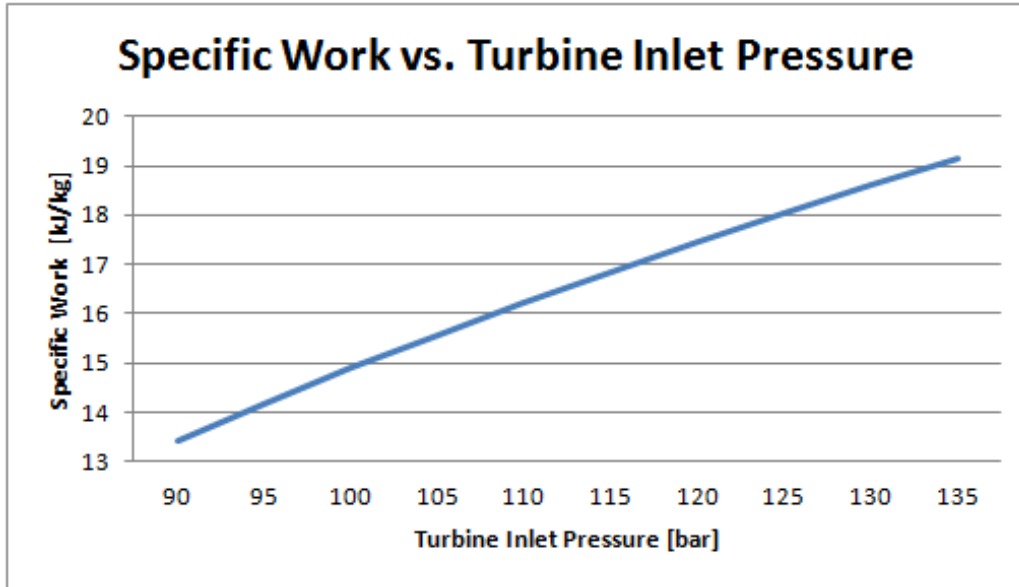


Figure 4.17: Produced power by the *tORC* cycle vs. turbine inlet pressure for $1 \frac{kg}{s}$ mass flow in the primary cycle.

more are added to the output both efficiencies increase by about 20%. This means that the higher power output provided by the *tORC* gets mitigated by the increased compressor work in the cycle that utilizes waste heat. An overview of the results is given in Table (4.2). this outcome shows again that an isothermal *ETES* system can provide higher efficiencies than all other cycles proposed.

Configuration	Roundtrip efficiency	Efficiency improvement	Additional power output
Isothermal <i>ETES</i> System	57,39%	20,61%	1.33 MW
Cycle utilizing waste heat	52.07%	21,22%	1.63 MW

Table 4.2: Overview of the improvement of the roundtrip efficiency of the *ETES* with a recuperator through the addition of a transcritical Rankine CO_2 cycle.

4.5 Summary and Outlook

A plethora of electrothermal energy storage systems utilizing supercritical CO_2 were presented in this thesis. The most simple configurations, like the simple Brayton cycle without a recuperator yielded round trip efficiencies of about 22%, while the maximum achieved efficiency was provided by the isothermal *ETES* system with an additional organic Rankine cycle amounted to about 58%. These values are quiet low in relation to the other proposed configurations presented in chapter (2). Although operating an *ETES* system at higher temperature levels seems promising, the high exergy losses that occur in the heat transfer keep the round trip efficiency to low values.

The most promising and realistic at the present day application of the proposed *ETES* systems would be the combination of an *ETES* system with waste heat recovery. This configuration yields high round trip efficiency values and does not require an isothermal expander,

which exists only on theoretical basis. The *TES* unit would make the site more independent regarding it's electricity requirement, reduce waste heat and the site emissions.

The major limiting factor of this work was the heat transfer between the carbon dioxide and the sand of the *Sand-TES* unit. Modeling different sand-types is not possible in *IPSEpro* therefore either another sand with a better thermal matching should be chosen or the thermal properties of different sand-types should be implemented in a model in *IPSEpro*. Of course other thermal storage units could also be examined.

The aim of this work was to develop many different *ETES* concepts with the same parameters, like maximum turbine inlet temperature, turbine power output or compressor ratio, in order to achieve an objective comparison between each system. Another approach could be the sole optimization of one of the presented cycles so that the optimal operational behavior is found.

List of Figures

1.1	World energy-related carbon dioxide emissions, 1990-2040 (billion metric tons) [1].	1
1.2	Comparison of various energy storage technologies in terms of power capacity and discharge time [3].	2
1.3	Efficiency and cost bands of the proposed <i>ETES</i> system as a function of power rating [5].	3
2.1	Working principle of a electrothermal energy storage system during charging mode [3].	5
2.2	Working principle of a electrothermal energy storage system during discharging mode [3].	6
2.3	Maximum roundtrip efficiency of a <i>ETES</i> system as a function of r_{bw} and $\eta_{C/E}$ [9].	8
2.4	Flow diagram during charging and discharging of Cahns proposed system [12]. .	9
2.5	Flow diagram during charging and discharging of Wolfs proposed system [12]. . .	10
2.6	Thermal conductivity (green) and dynamic viscosity (red) of Argon over temperature (Source: Engineering Equation Software, F-Chart Software).	11
2.7	Overview of the storage principle proposed by Desrues et al. during charging mode (left) and discharging mode (right) [16].	12
2.8	Storage efficiency as a function of T_1 , the polytropic efficiency η at ambient temperatur and at a thermal compression ratio of 1.55 [16].	12
2.9	Simplified schematic of the <i>PHEES</i> system developed by Isentropic Ltd. [18]. . .	13
2.10	Thermodynamic efficiency of <i>PHEES</i> and <i>PCES</i> . Roundtrip efficiency as a function of the storage temperature. The lower abscissa represents the nondimensional temperature ratio, the upper abscissa represents dimensional temperature for the case of an ambient temperature of $T_0 = 20^\circ C$. T_1 is the temperature of the hot storage and Ψ the roundtrip efficiency calculated according to [21]. . . .	15
2.11	Bad and good match between the cycle and heat sources/sinks. Bad match (upper two cases) reduces the roundtrip efficiency. Good match is on the lower two frames for sensible heat storage (left) and latent heat storage (right) [5]. . .	16
2.12	Schematic of the charging (left) and discharging (right) configuration of an <i>ETES</i> system [5].	17
2.13	Process flow diagram of the base case configuration design of an <i>ETES</i> plant [24].	18
2.14	Process flow diagram of the optimum design <i>ETES</i> plant with the maximum roundtrip efficiency [25].	18
2.15	Process flow diagram of a design solution with inter-cooling between thermal engine turbine stages [25].	19
2.16	Optimal Pareto fronts according to [22].	20
2.17	Variation in the isobaric specific heat of CO_2 in the operating temperature range depending on the CO_2 pressure [9].	22

2.18	Schematic of <i>ETES</i> cycle during charging mode utilising both low- and high-temperature sources, charging mode (left) and discharging mode (right) [23]. . .	22
2.19	T-s diagram of an <i>ETES</i> system utilising both low- and high-temperature sources, generation mode [23].	23
2.20	Schematic of an isothermal <i>ETES</i> system with a transcritical CO_2 cycle, charging mode (left) and discharging mode (right) [9].	24
2.21	Base reference cycle of isothermal <i>ETES</i> systems with a transcritical CO_2 cycle [9].	24
2.22	Cascaded system for charging with an ammonia cycle for low temperature compression and water as the working fluid for high temperature compression. Single fluid (water) Rankine cycle for discharging [31].	25
3.1	Schematic and $T - s$ diagram of a simple steam power plant. The working fluid (water) passes through the two phase area, this means that it can absorb high amounts of heat at very low temperature differences [32].	27
3.2	Schematic and $T - s$ diagram of an improved simple steam power Rankine cycle through re-heating [32].	29
3.3	Schematic and $T - s$ diagram of the improved steam Rankine power cycle through feedwater preheating via mass flow splitting [32].	29
3.4	Working principle of an <i>ORC</i> with (right) and without (left) recuperator [33]. .	30
3.5	$T - s$ diagram of a few typical organic fluids and of water [33].	32
3.6	Schematic of a closed (left) and an open (right) gas power cycle [32].	34
3.7	Exergy losses in a gas power cycle. The entropy increases in the two adiabatic machines due to the irreversibility of the processes. The exergy difference from point 3 to point 0 is waste, because the heat is released to the environment [32].	35
3.8	The recuperator enables the utilization of the heat the working fluid on the low pressure side of the cycle to heat the medium before it enters the boiler [32]. . .	35
3.9	The ideal Ericson cycle is attempted to be approached by the addition of a recuperator and multiple compression and expansion stages [32].	36
3.10	Size comparison of a steam, a helium and a carbon dioxide turbine [35].	37
3.11	Comparison of the turbine and compressor work of CO_2 [35].	38
3.12	$T - s$ diagram of carbon dioxide displaying all conditions near the critical point [36].	39
3.13	Compressor and turbine work range as a function of the compressibility factor and temperature [37].	40
3.14	Illustration of the <i>SandTES</i> concept [38].	41
4.1	Interoperability. Every thermodynamic model and every unit operation can be used in multiple simulation applications. Consequently, every simulation application may select from a variety of unit operations and thermodynamic models [44].	45
4.2	Temperature profiles of <i>Sand</i> in red and the heat transfer fluid (CO_2) in blue over the length of the heat-exchanger for fluid temperature-values up to $500^\circ C$.	46
4.3	Layout of the simple <i>ETES</i> configuration in IPSEpro, charging cycle (heat pump) on the left side and discharging cycle on the right side of the screen.	47
4.4	Overview of the temperature curves of sand (red) and the heat transfer fluid (blue) in the large configuration during the charging mode.	48
4.5	Overview of the temperature curves of sand (red) and the heat transfer fluid (blue) in the large configuration during the discharging mode.	48

4.6	Change of the roundtrip efficiency for the different <i>SandTES</i> cases.	49
4.7	Change of the roundtrip efficiency for various compressor outlet pressures.	49
4.8	Change of the roundtrip efficiency for various compressor inlet pressures levels at constant outlet pressure.	50
4.9	Change of the roundtrip efficiency for various compressor inlet pressures at a constant turbine pressure ratio.	51
4.10	Temperature vs. entropy plot with the saturation (red), isobaric (green) and isenthalpic curves (black), (source: <i>REFPROP</i>).	51
4.11	Flowsheet of the charge cycle in an <i>ETES</i> system utilizing the increase of specific heat capacity of CO_2 at temperatures below $150^\circ C$ in IPSEpro.	52
4.12	Layout of the isothermal <i>ETES</i> cycle with a Brayton cycle with a recuperator in <i>IPSEpro</i>	55
4.13	The simple Brayton cycle with a recuperator [34].	56
4.14	The re-compression cycle [34].	56
4.15	Comparison of the roundtrip efficiency of the two proposed discharge cycles for an isothermal <i>ETES</i> system.	57
4.16	Roundtrip efficiency vs. mass flow split fraction of an isothermal <i>ETES</i> system for a constant turbine pressure ratio.	58
4.17	Produced power by the <i>tORC</i> cycle vs. turbine inlet pressure for $1 \frac{kg}{s}$ mass flow in the primary cycle.	61

List of Tables

3.1	Advantages of organic Rankine cycles and steam Rankine cycles	33
4.1	Overview of the improvement of the roundtrip efficiency of the simple Brayton <i>ETES</i> system through the utilization of waste heat.	60
4.2	Overview of the improvement of the roundtrip efficiency of the <i>ETES</i> with a recuperator through the addition of a transcritical Rankine CO_2 cycle.	61

Bibliography

- [1] U.S. Energy Information Administration, “International energy outlook 2013.”
- [2] European Environment Agency, “Trends and projections in Europe 2013: Tracking progress towards Europe’s climate and energy targets until 2020.”
- [3] Y.-M. Kim, “Novel concepts of compressed air energy storage and thermo-electric energy storage,” *PhD Thesis, Ecole polytechnique federale de Lausanne*, 2012.
- [4] M. Haider and A. Werner, “An overview of state of the art and research in the fields of sensible, latent and thermo-chemical thermal energy storage,” *e & i Elektrotechnik und Informationstechnik*, vol. 130, no. 6, pp. 153–160, 2013.
- [5] M. Mercangöz, J. Hemrle, L. Kaufmann, A. Z’Graggen, and C. Ohler, “Electrothermal energy storage with transcritical CO₂-cycles,” *Energy*, vol. 45, no. 1, pp. 407–415, 2012.
- [6] J. Yang, “China’s wind sector lost \$1.6 billion in 2012,” <http://www.windpowermonthly.com/article/1168216/chinas-wind-sector-lost-16-billion-2012>.
- [7] H. Trabish, “Why aren’t those wind turbines turning? : Greentech media,” <http://www.greentechmedia.com/articles/read/why-arent-those-wind-turbines-turning>.
- [8] L. Bird, J. Cohran, and X. Wang, “Why those wind turbines aren’t turning,” <http://newenergynews.blogspot.co.at/2014/06/todays-study-why-those-wind-turbines.html>, 2014.
- [9] Y.-M. Kim, D.-G. Shin, S.-Y. Lee, and D. Favrat, “Isothermal transcritical CO₂-cycles with tes (thermal energy storage) for electricity storage,” *Energy*, vol. 49, pp. 484–501, 2013.
- [10] F. Marguerre, “Das thermodynamische Speicherverfahren von Marguerre: Ein Beitrag zur Spitzenstromerzeugung und zur Senkung der Stromverteilungskosten,” *Escher-Wyss Mitteilungen*, vol. 6, no. 3, pp. 67–76, 1933.
- [11] B. Weissenbach, “Thermal storage power station for peak-load generation near to consumers,” *BRENNST.-WARME-KRAFT*, vol. 33, no. 12, pp. 479–482, 1981.
- [12] R. Cahn, “Thermal energy storage by means of reversible heat pumping,” *US patent 4,089,744*, 1978.
- [13] B. M. Wolf, “Verfahren zur speicherung und rückgewinnung von energie.”
- [14] J. Ruer and T. Desrues, “Pumped heat energy storage,” <http://www.keynergie.com/articles/paper%20phs-paper.pdf>.

- [15] “Isentropic ltd - isentropic - pumped heat electricity storage,” <http://www.isentropic.co.uk/>.
- [16] T. Desrues, J. Ruer, P. Marty, and J. F. Fourmigué, “A thermal energy storage process for large scale electric applications,” *Applied Thermal Engineering*, vol. 30, no. 5, pp. 425–432, 2010.
- [17] T. Desrues, *Large scale Thermal Energy Storage of Electricity*. PhD thesis.
- [18] J. Howes, “Concept and development of a pumped heat electricity storage device,” *Proceedings of the IEEE*, vol. 100, no. 2, pp. 493–503, 2012.
- [19] A. White, G. Parks, and C. N. Markides, “Thermodynamic analysis of pumped thermal electricity storage,” *Applied Thermal Engineering*, vol. 53, no. 2, pp. 291–298, 2013.
- [20] J. D. McTigue, A. J. White, and C. N. Markides, “Parametric studies and optimisation of pumped thermal electricity storage,” *Applied Energy*, 2014.
- [21] A. Thess, “Thermodynamic efficiency of pumped heat electricity storage,” *Physical Review Letters*, vol. 111, no. 11, 2013.
- [22] M. Morandin, M. Mercangöz, J. Hemrle, F. Maréchal, and D. Favrat, “Thermoeconomic design optimization of a thermo-electric energy storage system based on transcritical CO₂-cycles,” *Energy*, vol. 58, pp. 571–587, 2013.
- [23] Y.-M. Kim, C. G. Kim, and D. Favrat, “Transcritical or supercritical co₂ cycles using both low- and high-temperature heat sources,” *Energy*, vol. 43, no. 1, pp. 402–415, 2012.
- [24] M. Morandin, F. Maréchal, M. Mercangöz, and F. Buchter, “Conceptual design of a thermo-electrical energy storage system based on heat integration of thermodynamic cycles – part a: Methodology and base case,” *Energy*, vol. 45, no. 1, pp. 375–385, 2012.
- [25] M. Morandin, F. Maréchal, M. Mercangöz, and F. Buchter, “Conceptual design of a thermo-electrical energy storage system based on heat integration of thermodynamic cycles – part b: Alternative system configurations,” *Energy*, vol. 45, no. 1, pp. 386–396, 2012.
- [26] D. Fudenberg and J. Tirole, *Game theory*. Cambridge, Mass.: MIT Press, ©1991.
- [27] S. A. Wright, A. Z’Graggen, J. Hemrle, “Control of a supercritical co₂ electro-thermal energy storage system,”
- [28] R. Fuller, J. Hemrle, L. Kaufmann, “Turbomachinery for a supercritical co₂ electro-thermal energy storage system,”
- [29] Michele, “Feasibility study of an electrothermal energy storage in the city of Zurich,” *22nd international conference on electricity distribution*.
- [30] Sachan Anurag, “Study of the integration of district heating and cooling with an electro-thermal energy storage system,” *Master Thesis, Ecole polytechnique federale de Lausanne*, 2012.
- [31] W. D. Steinmann, “The chest (compressed heat energy storage) concept for facility scale thermo mechanical energy storage,” *Energy*, vol. 69, pp. 543–552, 2014.

- [32] “Isentropic - energy storage systems,” <http://www.isentropic.co.uk/Energy-Storage-Systems#PHES>.
- [33] Sylvain, “Sustainable energy conversion through the use of organic rankine cycles for waste heat recovery and solar applications,” *University of Liege*, 2011.
- [34] M. Kuhlanek and V. Dostal, “Supercritical carbon dioxide cycles: Thermodynamic analysis and comparison,” <http://stc.fs.cvut.cz/history/2009/sbornik/Papers/pdf/KulhanekMartin-319574.pdf>.
- [35] V. Dostal, “A supercritical carbon dioxide cycle for next generation nuclear reactors,” *PhD thesis, Massachusetts Institute of Technology*, 2004.
- [36] Nuclear Engineering Division, “Performance improvement options for the supercritical carbon dioxide brayton cycle,” *Argonne national laboratory*, 2007.
- [37] H. Hasuike, T. Yamamoto, T. Fukushima, T. Watanabe, M. Utamura, and M. Aritomi, “Test plan and preliminary test results of a bench scale closed cycle gas turbine with supercritical co,” in *ASME Turbo Expo 2010: Power for Land, Sea, and Air*, pp. 485–492, June 14–18, 2010.
- [38] K. Schwaiger, M. Haider, M. Hämmerle, D. Wünsch, M. Obermaier, M. Beck, A. Niederer, S. Bachinger, D. Radler, C. Mahr, R. Eisl, and F. Holzleithner, “sandtes – an active thermal energy storage system based on the fluidization of powders,” *Energy Procedia*, vol. 49, pp. 983–992, 2014.
- [39] M. Haider, K. Schwaiger, F. Holzleithner, and R. Eisl, “A comparison between passive regenerative and active fluidized bed thermal energy storage systems,” *Journal of Physics: Conference Series*, vol. 395, 2012.
- [40] M. Haemmerle, “Anwendungsmöglichkeiten der Hochtemperatur Sand-Wärmespeicherung zur Flexibilisierung des Strommarktes,” *Presentation 13. Symposium Energieinnovation*.
- [41] SimTech, “Ipsepro,” <http://www.simtechnology.com/CMS/index.php/ipsepro>, 19.04.2015.
- [42] F. Chart Software : Engineering Software, “EES: Engineering Equation Solver,” <http://www.fchart.com/ees/>, 19.04.2015.
- [43] US Department of Commerce, “Nist,” <http://www.nist.gov/srd/nist23.cfm>, 2014.
- [44] J. van Baten and M. Pons, “Cape-open: Interoperability in industrial flowsheet simulation software,” *Chemie Ingenieur Technik*, vol. 86, no. 7, pp. 1052–1064, 2014.